Interaction of microorganisms with sheet silicates

Dissertation

zur Erlangung des akademischen Grades
doctor rerum naturalium (Dr. rer. nat.)

vorgelegt dem

Rat der Chemisch-Geowissenschaftlichen Fakultät
der Friedrich-Schiller-Universität Jena

seit 1558

von M. Sc. Wafaa M. H. A. Zidan

geboren am 15. Juni 1978 in Giza / Egypt

Gutachter:

Prof. Dr. Reinhard Gaupp
Institute of Geosciences, Faculty of Chemistry and Earth sciences,
Friedrich Schiller University, Jena, Germany

Prof. Dr. Erika Kothe
Institute of Microbiology, Faculty of Biology and Pharmacy,
Friedrich Schiller University, Jena, Germany

Tag der öffentlichen Verteidigung: 24.05.2013

„Und euch ist vom Wissen nur wenig gegeben“

Der Edle Koraan, Al- Israa, 85

“And you have not been given from knowledge except a little”

The Holly Quran, Al- Israa, 85

" وَمَا أُوتِيتُم مِّن الْعِلْمِ إِلاَّ قَلِيلاً "

القرآن الكريم ، سورة الإسراء ، ٨٥

Zusammenfassung

Um die Wechselwirkung zwischen Mikroorganismen und Schichtsilikate zu untersuchenwurden Nontronit (NAu-2) und Klinochlor (CCa-2) in Pulverform kleiner 2 µm mit zwei Mikroorganismen *Streptomyces acidiscabies* und *Schizophyllum commune* in flüssigen Kulturmedien zwei Monate inkubiert. NAu-2 ein quellfähiges Mineral ist, wo hydratisierte Ionen in die Zwischenschicht eingelagert werden. Dadurch weiten sich die Minerale auf und die Mineraloberflächen sind Lösungsprozessen und mikrobiellem Angriff ausgesetzt. Im Gegensatz dazu ist CCa-2 kein quellfähiges Mineral. Aufgrunddessen ist NAu-2 anfälliger für mikrobielle Auflösung als der CCa-2. XRD-Spektren zeigen, dass keine Veränderung in der Struktur der CCa-2 auftreten, während NAu-2 unter mikrobiellem Einfluss amorph wurde. *S. acidiscabies* Stamm produziert organische Säuren, EPS (extrapolymere Substanzen), Enzyme, Siderophore und Melanin. Die zeitgleiche Produktion dieser Biomoleküle könnte der Grund dafür sein, dass *S. acidiscabies* Stamm nicht nur bei der Freisetzung einige Elemente aus beiden Mineralen effizienter war als *S. Commune* Stamm, sondern auch beim Indizieren des Rückgangs von Flächennormalen von polierten CCa-2-Stücken. VSI-Bilder zeigten, dass sich die Oberfläche der polierten CCa-2-Stücke unter dem Einfluss von *S. acidiscabies* Stamm veränderte und einen maximalen Verlust von 2,6 μm^3 pro 1 μm^2 verursachte. Diese mikrobielle Alteration war effektiver als die Veränderungen infolge von chemischer organischer und anorganischer Säurebehandlung. Dies deutet daraufhin, dass weder Protonierung noch Chelatbildung allein verantwortlich waren. Wahrscheinlich war der Actinobacteriumstamm in der Lage, die CCa-2-Oberfläche durch die Ausscheidung von organischen Säuren zusammen mit Siderophoren zu verändern, wodurch beide Produkte innerhalb EPS-Biofilme aufkonzentriert wurden. Direkter Kontakt könnte essentiell für die Entstehung von Lösungsspuren und Vertiefungen sein. Aufgrund der sehr kurzer Kolonisationszeit durch *S. commune* Stamm entstand keine Alteration der polierten CCa-2-Stücke. Der Einfluss der Minerale führte zu morphologischen Veränderungen der Mikroorganismen. Pelletstrukturen traten auf, die bei *S. acidiscabies* Stamm mit CCa-2 stark verkrustet Mineralflocken und glatte Hyphen auf. Im Falle von NAu-2 waren mikrobielle Pellets ohne eine Spur von Mineralflocken, aber die Hyphen waren leicht verkrustet. *S. commune* Stamm war nicht fähig Pellets unter dem Einfluss von CCa-2 zu bilden und in Anwesenheit von NAu-2 Mineralen wurden Pellets mit nur 0.25 g Masse gebildet. Während andere Pilzstämme (*Ceratocystis polonica* und *Alternaria brassicola*), die Melanin produzieren, Pellets mit 1 g NAu-2 gebildet haben. Mit Hilfe der FTIR-Spektroskopie konnte gezeigt werden, dass *S. acidiscabies* Stamm EPS in höheren Konzentrationen produzierte, wenn Minerale anwesend waren als bei der Inkubation in reinem Minimalmedium. Ester von

langkettigen Fettsäuren in der Form von Triglyceriden können auch vorliegen, was durch TEM festgestellt wurde. Die räumliche Verteilung der FTIR-Banden von Spektren, die an *S. acidiscabies* Stamm-Proben, die mit NAu-2 beimpft wurden, aufgenommen wurden, zeigen, dass EPS (Polysaccharide und Proteine), innerhalb der Pellets für mineralische Befestigung lokalisiert wurden. Bei der Inkubation von *S. acidiscabies* Stamm mit CCa-2, ist die Phosphatester-Bande bei 1245 cm^{-1} der Fettsäureester fehlgepaart, was daraufhin deutet, dass Phospholipide kein Hauptbestandteil der Probe sind. Ihre Verteilung auf den Rändern der Pellets, was mit Mg angereichert CCa-2 ist, zeigen, dass es ein starker Magnesium-Chelator ist. CCa-2 induzierte weder bei *S. acidiscabies* noch bei *S. commune* Stämme die Produktion von extrazellulären Proteinen. Im Gegensatz dazu produzierten beide Stämme in Anwesenheit von NAu-2 einige extrazelluläre Proteine, welche durch das Bradford-Assay nachgewiesen wurden.

Abstract

To study the interaction between microorganisms and sheet silicates, nontronite (NAu-2), and chlinochlore (CCa-2) as a powder form less than 2 µm were incubated with two microorganisms; *Streptomyces acidiscabies* and *Schizophyllum commune* strains in liquid culture flasks for two months. CCa-2 is a non swelling mineral, while NAu-2 is a swelling mineral, where hydrated ions incorporate into the mineral interlayer. Consequently, the mineral expands and additional mineral surfaces are more exposed to solution and microbial attack. That is why NAu-2 was more susceptible to microbial dissolution than the CCa-2. X-ray diffraction (XRD) spectra showed that there was no change at all in the structure of CCa-2, while NAu-2 became amorphous to X-rays. *S. acidiscabies* E13 strain produces some organic acids, exo-polysaccharides (EPS), enzymes, siderophores, and melanin. The production of some of these biomolecules together at the same time might be the main reason that the *S. acidiscabies* strain was more efficient not only in releasing some elements from both minerals than the *S. commune* strain, but also in inducing some surface normal retreats of CCa-2 polished pieces. Vertical scanning interferometry (VSI) images showed that the *S. acidiscabies* strain altered the surface of small polished pieces of CCa-2, and caused a maximum loss of 2.6 μm^3 per 1 μm^2. *S. acidiscabies* was also the most effective in comparison to chemical acid treatments regardless organic or non-organic, which indicated that neither protonation nor chelation alone could be the mechanisms for the *S. acidiscabies* strain to perform such normal surface retreats over the CCa-2. Most probably the actinobacterium strain was able to alter the CCa-2 mineral surface, by the excretion of some organic acids together with siderophores, where both products were concentrated within EPS biofilms. Direct areal contact might be essential also for such dissolution and etch pits formations, as *S. commune* strain has left the surface of the mineral after colonizing it for a very short time. Therefore, the fungus strain hasn't caused any effect over the small polished CCa-2 pieces. Microbial pellets formed by the *S. acidiscabies* strain with CCa-2 had heavily encrusted mineral flakes and smooth hyphae, while in case of NAu-2, no trace for many mineral flakes but the hyphae were almost encrusted. *S. commune* strain wasn't able to form microbial pellets with any amount of CCa-2, and formed pellets with only 0.25 g of the NAu-2 minerals. While other fungal strains (*Ceratocystis polonica* and *Alternaria brassicola*) which produce melanin have formed microbial pellets with 1 g of NAu-2. FTIR showed that *S. acidiscabies* strain has produced in the presence of the two minerals some EPS with concentrations higher than what is present in the strains grown alone in the minimal medium. Esters of long chain fatty acids in the form of triglycerides might be present too as they were detected by TEM. Maps showing spatial distribution of some FTIR bands for the *S.*

acidiscbaies strain inoculated with NAu-2 have shown that EPS (polysaccharides and proteins), were localized inside the pellets for mineral attachment. While when the *S. acidiscabies* strain was incubated with CCa-2 the phosphate ester band at 1245 cm^{-1} mismatched the spatial distribution of fatty esters, which indicated that phospholipids were not a major component in the sample, however their distribution on the edges of the pellets with the rich Mg CCa-2 mineral showed that they are a potent magnesium chelator. CCa-2 haven't induced neither *S. acidiscabies* nor *S. commune* strains to produce any extracellular proteins, while with NAu-2 both strains have produced some extracellular proteins in the liquid culture medium, which was measured by the Bradford assay.

Content

Kurzfassung..... I

Abstract..... III

List of Figures..... IX

List of Tables…….. XII

List of Abbreviations..... XIII

1. Introduction…..... 1

1.1. Motivation and goals…….. 2

2. Review of literature…….. 4

2.1. Microbe- mineral interactions……. 4

2.2. Mechanisms of microbial interaction ……..... 5

2.2.1. Oxidation reduction reactions……..... 5

2.2.2. Proton and ligand effect……... 6

2.2.3. Other mechanisms…….. 6

2.3. The importance of silicate minerals…….. 7

2.4. Sheet silicates used in this study……. 9

2.4.1. Smectite group: nontronite (NAu-2)……...…… 9

2.4.1.1. Effect of microorganisms on smectite…….. 11

2.4.2. Chlorite group: Clinochlore (CCa-2)…….. 13

2.4.2.1. Effect of microorganisms on chlorite…… 15

2.5. Methods for studying microbe mineral interaction……..... 16

2.5.1. Atomic Force Microscopy (AFM)……. 16

2.5.2. Vertical Scanning Interferometry (VSI)…… 17

2.5.3. Fourier Transform Infrared Spectromicroscopy (FTIRS)……. 19

2.5.3.1. The FT-IR theory…….. 21

2.5.3.2. Synchrotron Radiation FTIR (SR-FTIR) …..... 25

2.5.3.3. Limitations…… 26

2.5.3.4. Future perspectives……..... 28

3. Materials and methods…… 29

3.1. Liquid culture flask Experiments……..... 29

3.1.1. Silicate minerals as a powder material…….. 29

3.1.2. Strains and culture media…… 30

3.1.3. Sterilization……... 31

3.1.4. Inoculate preparation…….…….... 31

3.1.5. Sampling……... 32

3.1.6. XRD…….. 32

3.1.7. Raman spectroscopy……. 33

3.1.8. SEM of microbial pellets……..... 33

3.1.9. Bradford protein assay…….……. 34

3.1.10. FTIR ……..... 34

3.1.10.1. FTIR spectromicroscopy……..……... 34

3.1.10.2. Attenuated Total Reflectance (ATR-FTIR)……. 35

3.2. Solid agar plate experiments……... 35

3.2.1. Polished minerals…… 35

3.2.2. Sterilization……... 36

3.2.3. Adding inoculants……. 36

3.2.4. Addition of organic and inorganic acids……... 36

3.2.5. Removal of microorganisms……. 37

4. Results……..…….. 37

4.1. Liquid culture flask Experiments……. 37

4.1.1. ICP-OES……..... 37

4.1.2. pH measurements…….. 39

4.1.3. XRD…….…….. 40

4.1.4. Raman spectroscopy…….. 42

4.1.5. SEM of microbial pellets……... 43

4.1.6. Bradford protein assay……... 44

4.1.7. FTIR spectromicroscopy……..... 45

4.1.8. ATR-FTIR……..... 47

4.1.9. SEM of sheet silicates…… 49

4.2. Solid agar plate experiments…… 51

4.2.1. Atomic force microscopy (AFM)……..... 51

4.2.2. Vertical scanning interferometry (VSI)……... 52

4.2.3. SEM of sheet silicates……..... 55

5. Discussion…… 59

5.1. Liquid culture flask Experiments…….. 59

5.1.1. ICP-OES……..... 59

5.1.2. pH measurements…….. 60

5.1.3. XRD……... 60

5.1.4. Raman spectroscopy……...……... 61

5.1.5. SEM of microbial pellets ……..... 61

5.1.6. FTIR ……..... 64

5.1.7. ATR-FTIR ……...…….. 67

5.1.8. SEM of sheet silicates……... 67

5.2. Solid agar plate experiments…….. 68

5.2.1. AFM……... 68

5.2.2. VSI…… 68

5.2.3. SEM of sheet silicates……... 69

6. Summary and Conclusions……. 70

7. References……. 74

Acknowledgment…….. 87

Selbständigkeitserklärung..... 91

Curriculum Vitae..... 92

List of figures

(Fig. 1) Crystal structure of Nontronite…… 9

(Fig. 2) XRD peaks of the <0.2 µm size fractions of NAu-2, spacing is in Å..... 10

(Fig. 3) Normalized infrared spectra in the OH-deformation region of the initially unaltered Garfield nontronite..... 10

(Fig. 4) Idealized crystal structure of chlorite…… 13

(Fig. 5) X-ray diffraction pattern of randomly oriented pretreated ripidolite from 2 to 65° 2 theta……..…… 14

(Fig. 6) The IR spectra in the region 8 to 25 µm for (a) sheridanite, ; (b) ripidolite; (c) clinochlore; and (d) penninite…….. 15

(Fig. 7) Schematic image of an atomic force microscope…….……. 16

(Fig. 8) VSI device with a schematic diagram ……..... 18

(Fig. 9) Basic components of FT-IR spectrometer…….…… 22

(Fig. 10) A representative FT-IR absorbance spectrum (4000-1000 cm^{-1}) of a colony of a Gram-negative bacterium, *Salmonella enterica*……..... 23

(Fig. 11) Schematic diagram of Fourier transform infrared (FTIR) spectromicroscopy experimental setup……... 25

(Fig. 12) Illustration of the advantage provided by using a synchrotron source for infrared microscopy…… 26

(Fig. 13) Temperature controlled sample holder for aqueous cell suspensions based on compression of a polymeric spacer between two optical windows……... 28

(Fig. 14) CCa-2 polished sterilized pieces on solid agar plates incubated with; *S. acidiscabies* (A, B, C) and *S. commune* (D, E, F)……..... 36

(Fig. 15) ICP-OES measurements of samples taken from flasks containing CCa-2 inoculated with both strains *S. acidiscabies* and *S. commune* …….…… 38

(Fig. 16) pH of *S. acidiscabies* with; CCa-2 (A), with NAu-2 (B), and growing alone in MM (C). pH of negative controls; CCa-2 (D), and NAu-2……..... 39

(Fig. 17) XRD for autoclaved and non-autoclaved NAu-2 (air dried and glycolated)…. 40

(Fig. 18) XRD for air dried NAu-2 incubated with *S. commune* and *S. acidiscabies*….. 40

(Fig. 19) XRD for glycolated NAu-2 incubated with both strains *S. commune* and *S. acidiscabies*…… 41

(Fig. 20) XRD spectrum of CCa-2 (air dried) before and after incubation with both strains (*S. acidiscabies* and *S. commune*)…….. 41

(Fig. 21) Raman images showing NAu-2 flocs when incubated with; *S. acidiscabies* (A), but no NAu-2 flocs with *S. commune* (B)…….. 42

(Fig. 22) Clinochlore over XRD holder when incubated with; *S. acidescabies* (A) and without treatment (B)…… 42

(Fig. 23) Microbial pellets of *S. acidiscabies* incubated with CCa-2 (A, B), mineral flakes are present (C) and the hyphae are smooth (D) ……. 43

(Fig. 24) *S. commune* with 0.25 g NAu-2 (A), mineral flakes appearing perpendicular to the hyphae (B)……... 44

(Fig. 25) Color of the dye has changed with NAu-2 only and not with CCA-2 when both minerals were inocubated with *S. commune* (A)…….. 45

(Fig. 26) FT-IR spectra of samples collected from consecutive stages of *S. acidicscabies* growth culture with NAu-2 and CCa-2…….……. 46

(Fig. 27) ATR-FTIR for the O-H stretching region of the NAu-2 incubated with *S.acdiscabies* and *S. commune* and their negative control……... 48

(Fig. 28) ATR-FTIR for the O-H deformation, and Si-O stretching region for NAu-2 incubated with *S. acidiscabies* and *S. commune* and their negative control….. 49

(Fig. 29) CCa-2 before incubation with scale bar; 2 µm (A), and 300 nm (B)…… 49

(Fig. 30) CCa-2 after incubation with *S. commune* with scale bar; 2 µm (A), and 200 nm (B)……..... 50

(Fig. 31) CCa-2 after incubation *S. acidescabies* with scale bar; 3 µm (A) and 200 nm (B)…….. 50

(Fig. 32) NAu-2 before incubation with scale bar; 2 µm (A), and 200 nm (B)…… 50

(Fig. 33) NAu-2 after incubation with *S. commune* with scale bar; 2 µm (A), and 200 nm (B)…… 50

(Fig. 34) NAu-2 after incubation *S. acidescabies* with scale bar; 2 µm (A), and 200 nm (B)……..... 51

(Fig. 35) AFM images for very rough CCa-2 polished piece before any treatment……. 51

(Fig. 36) AFM images for sharp edged CCa-2 particles before incubation (A) and for roundish edged particles after incubation with *S. acidiscabies* (B)……... 52

(Fig. 37) *S. commune* left the surface of CCa-2 after colonizing it for just few days….. 52

(Fig. 38) VSI image for CCa-2 polished pieces incubated with *S. commune* …….. 53

(Fig. 39) 3-D VSI image for surface normal retreat induced by *S. acidiscabies* in the unmasked (reacted) part (A), smoothness and roughness of masked and reacted surfaces are represented by different histogram heights (B)…… 53-54

(Fig. 40) VSI image for CCa-2 polished piece treated with HNO_3, the histogram analysis showing a single peak indicating no divergence due to surface retreat……... 54

(Fig. 41) VSI image for CCa-2 polished piece treated with oxalic acid, no difference in surface roughness between masked and unmasked surfaces…... 55

(Fig. 42) VSI image for CCa-2 polished piece treated with citric acid, the two arrows indicate no change in surface topography……..……. 55

(Fig. 43) SEM images for smooth surfaces(A) and a rough one contains a hole(B),(C) and (D) are element map distribution for Fe, Al, and Mg in the form of veins or spots respectively…….. 56

(Fig. 44) CCa-2 surfaces after inorganic acid treatment with; HNO_3 (A), and H_2SO_4 (C) with element mapping for both acids respectively (B &D)…… 57

(Fig. 45) Hyphen of *S. commune* appears over a rough surface in addition to the element mapping…… 58

(Fig. 46) SEM images showing *S. commune* colonizing CCa-2 polished piece, some of the fungal hyphen were removed gently by a tweezer (A)...…… 58

(Fig. 47) Melanin protects fungi from different environmental stress…….. 63

(Fig. 48) Melanin produced by *S. acidiscabies* when inoculated with NAu-2……. 64

(Fig. 49) TEM image for *S. acidiscabies* with NAu-2, showing many lipid vacuoles among the hyphen……. 65

(Fig. 50) Maps acquired at 25 µm intervals across *S. acidiscabies* incubated with NAu-2…… 66

(Fig. 51) Maps acquired at 25 µm intervals across *S. acidiscabies* incubated with CCa-2……. 66

List of tables

Table (1) Different experiments performed using different analysis techniques…….. 3

Table (2) Assignment of functional groups associated with major vibration bands in mid IR spectra of bacteria……. 24

Table (3) Major oxide chemistry for the < 0.2 μm size fraction of NAu-2 and CCa-2…. 30

Table (4) Band assignments cm^{-1} for IR spectral features in smectites……..... 47

List of Abbreviations

AQDS	anthraquinone-2,6-disulfonate
AFM	atomic force microscopy
ATR-FTIR	attenuated total reflectance - Fourier transform infrared
CCD	charge coupled device
CYM	complex yeast media
DLaTGS	deuterated lanthanum triglycine sulphate
DMRB	dissimilatory metal reducing bacteria
DOM	dissolved organic matter
DTA	differential thermal analysis
DTT	dithiothreitol
EDX	energy dispersive X-ray spectroscopy
FTIRM	fourier transform infrared microspectroscopy
EPS	extracellular polysaccharides
FA	fulvic acid
FIB	Focused ion beam
FPA	focal plane array
ICP-OES	inductively coupled plasma - optical emission spectrometry
LB	Luria broth agar plate
MCT	mercury cadmium telluride
MM	minimal medium
Nd:YAG	neodymium-doped yttrium aluminum garnet
PTFE	polytetrafluoroideethylene
PBS	phosphate buffered saline
SEM	scanning electron microscopy
SR-FTIR	synchrotron radiation fourier-transform infrared
SDS	sodium dodecyl sulfate
SPP	sodium pyrophosphate
TAG	Triacylglycerol
TM-AFM	tapping mode atomic force microscopy
TEM	Transmission electron microscopy
TR- FTIR	time resolved fourier-transform infrared
TCA	trichloroacetic acid
VSI	vertical scanning interferometer
XRD	X-ray diffraction
XRF	X-ray fluorescence
XPS	X-ray photoelectron spectroscopy

1. Introduction

The microbe-mineral interface serves as a starting point for examining the role of microbial organisms in large-scale geochemical transformations. From the Earth's science perspective exists a long-standing appreciation of the key roles where microbial organisms have been intimately and quantitatively involved in elemental cycling and mineralogical transformations over geological time scales. The research training group (alteration and element mobility at the microbe-mineral interface) is focusing on the respective role of microorganisms in weathering, reactive transport and mineralization mechanisms. Many studies within the research training group have been conducted at the former uranium mining site, Ronneburg, in eastern Thuringia, Germany, where the banks of the stream in this area are characterized by exceedingly high concentrations of heavy metals as a consequence of the permanent inflow of acid mine drainage water over several decades (Geletnekyetal., 2002) and where the strain *Streptomyces acidiscabies* E13 which is used in this study was isolated. The effects of released heavy metals, such as uranium on ground water, soils, microorganisms and plants was examined and it was found that most heavy metals are bound to Fe- and Mn-oxides (Grawunder *et al.,* 2009) and that reductive microbial processes did not have a major impact on metal retention at this site (Burkhardt *et al.,* 2009). The multi-component system black slates including fine phyllosilicate minerals (e.g. muscovite and chlorite), were found to occur also at the same site. Such slates enriched in organic matter (OM) are considered the most important crustal reservoirs of organic carbon. It has been estimated that weathering of black slates causes about 12% of the estimated annual CO_2 flux from oxidative weathering of sedimentary rocks (Jaffe *et al.,* 2002). Oxidative weathering of OM in sedimentary rocks contributes significantly to the global cycling of carbon (Berner, 2003; Petsch *et al.,* 2005). As limited knowledge exists for fungal-induced corrosion on multi-component rocks like fine-clastic sediments that have particles or pieces of rock (clasts) in them, such as claystones and shales or slates, Siegel (2010) performed a study which focused on the change of surface morphology and chemistry in weathering black slates of different oxidation states due to fungal activity. For continuous investigation of the former work which have been started within the research training group, this study focuses on the surface alteration and weathering processes of fine silicate minerals like chlorites which were present in the black slates, that were found in the former uranium site. Rothhardt (2012) focused on the microbial influence on the alteration of organic coatings on sand grains, and because the aqueous phase is the link between microbes and minerals, further study will

focus on dissolved organic matter (DOM) in aqueous systems to learn more about degradation processes in biogeochemical cycles.

1.1. Motivation and goals

It is important to understand how microbial cells interact with minerals and how they extract and utilize metals found in the surrounding minerals, as well as to know what effect these minerals might have on microorganisms in return. One goal of this work was to study the interaction between two filamentous microorganisms; the filamentous bacterium (*Streptomyces acidiscabies* E13), and the filamentous fungus (*Schizophyllum commune* 12–43,) with two sheet silicates; clinochlore (ripidolite) CCa-2 and nontronite (NAu-2), and to know which effect do each side of this relationship have on the other side.

The formation of etch pits by microorganisms on mineral surfaces are of interest as potential biosignatures. However, quantifying the effects of colonization on mineral surfaces is not easy. Barker *et al.* (1998) and Rogers *et al.* (1998) have detected etch pits on feldspars near attached microbial colonies. Fisk *et al.* (1998) observed remnants of cells within etched channels on basaltic glass and found the etchings consistent with microbial weathering. Similarly, Furnes *et al.* (2004) found tubular and segmented etchings that were likely microbial in origin on formerly glassy basalts. Irregular etchings on hematite particles were detected by Maurice *et al.* (1996) and on muscovite surfaces after incubation with bacteria in laboratory and field experiments by Maurice *et al.* (2002). Etch pits were detected on surfaces where colonies have been removed by Thorseth *et al.* (1995) and Bennett *et al.* (1996). In this study small polished CCa-2 pieces were used to determine the change in the surface topography of these polished pieces caused by the two microorganisms. As the input of inorganic anthropogenic acids is an obvious source of soil acidification in addition to the major sources of organic acids derived by decomposition of organic substances and root exudates, we wanted to determine also the effect of organic and inorganic acids on CCa-2 surface alteration in comparison with the microbial effect. To achieve such a goal, polished CCa-2 surfaces were analysed by atomic force microscopy (AFM), vertical scanning interferometer (VSI), and scanning electron microscopy (SEM) after the removal of the two microbial strains using 2% SDS.

Understanding the mechanisms controlling bacterial adhesion at mineral surfaces is critical for addressing environmental phenomena associated with the fate and transport of bacterial cells. These processes are central to both contamination and remediation of soil and groundwater supplies. Measuring how microorganisms interact with their environments through their wide

range of metabolic capabilities is essential to understand the roles of microbial activity in soil or sediment environments. However, these measurements should be made in well-controlled experiments that simulate microbial viability and functionality under in situ conditions. This is important because microorganisms are very sensitive to their immediate environments and the microbes themselves alter associated sediments and environmental materials as a consequence of metabolic activity (Ehrlich, 1998; Newman and Banfield, 2002). That is why this study focused on FT-IR spectomicroscopy as a tool to detect some of the chemical changes induced by the two different microorganisms as an expressed reaction when exposed to the sheet silicates CCa-2 and NAu-2. Table 1 shows the different experiments, which were performed using different analysis techniques to achieve our goals.

Table (1) different experiments performed using different analysis techniques

Experiment type	Minerals used	Strains / treatment used	Analysed part	Analysis used
Liquid culture exp.	NAu-2, CCa-2	*S. acidiscabies* *S. commune*	Liquid part	ICP-OES, pH, Bradford assay.
			Soild part	XRD, SEM, ATR-FTIR, Raman spect.
			Biological part	FTIR, SEM
Solid agar plate exp.	CCa-2	*S. acidiscabies* *S. commune*	Surfaces of the mineral	AFM , VSI, SEM
		Organic acids Inorganic acids		

As minerals were sterilized by autoclaving, it was important to test first if autoclaving had any effect on our mineral' structure by doing the XRD anaylsis after autoclaving. Whether minerals have induced the two microbial strains to produce extracellular proteins in the minimal medium or not, this was tested by the Bradford assay. The importance of melanin in protecting microorganisms from different unfavourable environmental conditions like the release of heavy metals from the two minerals was tested by using two funagal strains (*Ceratocystis polonica* and *Alternaria brassicola*) which are producing melanin and compare their growth with the growth of the fungus strain *S. commune* which doesn't produce this melanin.

2. Review of literature

2.1. Microbe-mineral interactions

Microbe-mineral interactions lie at the heart of the Geomicrobiology, as minerals and rocks are the most fundamental earth materials with which microbes interact at all scales. Microbial interaction with mineral surfaces is commonly found in soils, sediments and ground waters. This interaction can significantly alter microbial activity (Van Loosdrecht *et al.,* 1990), the ecological distribution of bacteria, biomineralization, weathering of minerals, and biodegradation of pollutants (Van Schie and Fletcher, 1999). Microorganisms modify the rates and mechanisms of chemical and physical weathering and clay growth, thus playing fundamental roles in the dissolution of silicate structure in the rock weathering process, in the genesis of clay minerals, and soil and sediment formation (Banfield *et al.,* 1999). The presence of clay minerals can be a typical symptom of biogeochemically-weathered rocks (Barker *et al.,* 1998). There are many reasons for microorganisms to colonize mineral surface; first, when one or more of the essential nutrients is depleted in the environments, essential macro- or micronutrients can be found in many minerals (Bennett *et al.,* 1996; Grantham and Dove, 1996; Rogers *et al.,* 1998; Kalinowski *et al.,* 2000), so it is not strange to know that microbially mediated mineral dissolution is usually incongruent, which means that certain elements are removed preferentially relative to others (Dong, 2012). Bennett *et al.* (1996) found that the progression of mineral weathering may be influenced by a mineral's nutritional potential, with microorganisms destroying only beneficial minerals and leaving a residuum of "useless" minerals. Rogers and Bennett (2004) found that interaction is restricted to only those surfaces that offer nutritional value to the native microbial consortium. Minerals serve also as

energy sources for microbial metabolism, like the coupling of organic carbon oxidation to the dissimilatory reduction of Fe and Mn (Lovely and Phillips, 1988; Nealson and Myers, 1992). Mineral colonization is a general response to a range of environmental stresses where surface attachment offers protection as well as synergistic **relationships** with other cells might occur (Dawson *et al.,* 1981; Kjelleberg and Hermansson, 1984).

2.2. Mechanisms of microbial interaction

When individual microbes discover the advantages of living on mineral and rock surfaces because of sufficient supplies of nutrients and protection from lethal environmental stress and predation, they tend to produce signal molecules to attract other organisms to gradually build a community called "biofilm" (Harrison *et al.,* 2005). Biofilms might contain proteins, lectins, and polysaccharides, which help microorganisms to attach to mineral surfaces as Thorseth *et al.* (1995) and Barker *et al.* (1998) have found. Once a biofilm community is established, minerals and rocks undergo weathering, and some minerals dissolute, other precipitate, and some other undergo transformation. Weathering of minerals usually occurs via release of organic acids and other ligands (such as siderophores), oxidation of reduced minerals, and reduction of oxidized minerals. These mechanisms will be explained in details. Fungi have been found to excrete higher concentrations of more effective chelating agents than, for example, bacteria (Palmer *et al.,* 1991). However, bacteria are more abundant and exist in extreme environments that fungi cannot tolerate.

2.2.1. Oxidation reduction reactions

Oxidation-reduction reactions are common in nature, and are believed to be a primary mechanism for the weathering of rocks and minerals (Walker, 1949), and in determining the properties of clays, soils, and sediments. Although reduction of structural Fe in clay minerals within soils and sediments is thought to be mediated primarily by the enzymatically catalyzed activity of indigenous microorganisms (Gates *et al.,* 1993), most research has focused on chemical mechanisms of structural Fe reduction in clay minerals. The reduction of structural Fe in smectite is mediated abiotically, by reaction with dithionite, or hydrazine, which are not likely to play a significant role in clay mineral reduction in natural environments. These inorganic chemical reductants are likely to be minor components of soils. Structural Fe can be reduced also biotically, by Fe-reducing bacteria, which are ubiquitous in soils and sediments

and are likely to be the dominant mediator of redox cycling of Fe in the environment. It is important to determine the relative reducibility of Fe (III)-bearing oxides and clay minerals by iron-reducing microorganisms (Jaisi *et al.* 2007 b).

2.2.2. Proton and ligand effect

Adsorption of H^+-ions on mineral surfaces enhances the hydrolysis of X-O (X = Si, Al, Fe, Mg) bonds and consequently the detachment of X into solution. Organic electrolytes, especially organic acids - like citric, oxalic and gluconic acids, produced mainly by fungi, and formic, acetic, lactic, pyruvic, succinic, 2-ketogluconic and some other acids produced by bacteria - accelerate the dissolution of feldspar at mildly acidic pH by surface complexing of metals that speed the breakdown of metal-oxygen bonds, which is considered the rate-limiting step (Hiebert and Bennett, 1992; Bickmore *et al.,* 2001). For several bacteria, dissolution of silicates results from complexation of cationic components by 2-ketogluconate. Microbes may also excrete ligands such as ferric iron-complexing siderophores produced by bacteria and fungi, and lobaric and physolic acids produced by lichens, which promote rock weathering (Ehrlich, 1998). However, Golubev *et al.* (2006) have tested the effect of pH and nine organic ligands on smectite dissolution and found by using XRD, FT-IR, and XPS no major change in structure, surface chemical composition or specific surface area as a function of pH, ligand concentration, and duration of experiments.

2.2.3. Other mechanisms

Bacteria have also been shown to accelerate the dissolution of silicates in some cases by the production of hydroxyl anion, extracellular polysaccharides (**EPS**), and enzymes (Hiebert and Bennett 1992; Welch and Ullman 1993; Vandevivere *et al.* 1994). Metabolic agents may be excreted into the bulk phase but may also involve adhering organisms and biofilms on surfaces of silica or silicates resulting in etching (Bennett *et al.,* 2001). All organisms can affect mineral weathering reactions by producing CO_2 and the formation of the the weak carbonic acid H_2CO_3 can also result in solubilization of silicates (Sanz-Montero *et al.*, 2009; Gadd, 2010). Alkaline conditions can mobilize silicon from silicates, ammonia production from urea hydrolysis is one of the bacterial mechanisms (Ehrlich & Newman, 2009). At high pH, Si surface sites are deprotonated and therefore carry negative charge, detachment of silicon appears to control overall silicate dissolution rates (Brady and Walther, 1989). According to Palmer *et al.* (1991)

and Gadd (2010) the role of microbially produced organic acids in the weathering process is probably greater through chelation than through acidification because, under in situ conditions, relatively high amounts of organic acids can be produced while little acidification occurs. Many bacteria excrete organic acids, and the type of acid produced usually being a function of the nature of the limiting nutrient. Incomplete oxidation of a carbon substrate in an oxic environment has been referred to as overflow metabolism (Tempest and Neijssel, 1992). Bacteria producing these different acids under specific growth limitations have various physiological advantages. For example, the production of gluconate (or 2-ketogluconate), which is common in many bacteria, may be used to generate energy at a high rate. Other common by-products of overflow metabolism include, e.g., pyruvate, acetate, or 2-ketoglutarate. These metabolites can also enhance dissolution of silicate minerals like what Vandevivere *et al.* (1994) have singled out that the partial oxidation of glucose to organic acids was the predominant mechanism by which the non-proliferating bacteria enhanced feldspar dissolution at neutral pH. The rate and extent of Fe mineral reduction by bacteria has been shown to be different according to experimental conditions such as the type of microorganisms and clay minerals, microbe/clay mineral concentration ratio, ferric iron content and layer charge, clay particle size (surface area), interlayer composition of clay minerals, presence or absence of electron shuttle, solution chemistry (pH, aqueous chemical composition), and temperature (Dong *et al.,* 2009). There are several mechanisms by which iron-reducing bacteria deliver electrons to solid Fe (III), some species require direct contact with Fe (III) oxides to reduce them like *Geobacter* species., while other species like *Shewanella* do not require direct contact, because they can produce chelators to solubilize Fe (III) in minerals and release electron-shuttling compounds (Lovley *et al.,* 2004; Dong *el al.*, 2009).

2.3. The importance of silicate minerals

Silicates are the largest class of minerals, comprising 30% of all minerals and making up 90% of the Earth's crust (Ehrlich, 1998). They are formed in rocks and soil when silicon dioxide is combined with oxides of magnesium, aluminium, calcium and iron. Silicate minerals are unstable and they break down to form clays. Clay minerals play an important role in environmental processes such as nutrient cycling, plant growth, contaminant migration, organic-matter maturation, and petroleum production (Stucki *et al.,* 2002; Kim *et al.,* 2004; Stucki, 2006). For example, the low hydraulic conductivity and high sorption capacity of some clay minerals which might prevent or delay possible radionuclide migration make the use of

bentonite (a rock containing mostly smectite) a promising material for designing barriers for nuclear waste disposal (Bauer *et al.,* 2001; Ferrage *et al.,* 2007). Arnold *et al.* (1998) have also revealed that the weathering of a phyllite containing significant amounts of an Fe-rich ripidolite chlorite resulted in the formation of small quantities of a poorly crystalline Fe oxide hydroxide, which dominated the sorption process of uranyl (VI) on phyllite. It is also known that the weathering of Ca- and Mg-bearing silicates controls CO_2 uptake from the atmosphere (Berner, 1992), and thus the climate of the earth at the long-term scale according to the following equation: $CO_2 + 2H_2O + CaAl_2Si_2O_8 \longrightarrow Al_2Si_2O_5(OH)_2 + CaCO_3$. Iron is the fourth most abundant element in the Earth's crust next to oxygen, silicon and aluminium, so it's abundant in clays and clay minerals should be no surprise (Stumm and Sulzberger, 1992). The changes in the oxidation state of the structural iron in clay minerals control their physical and chemical properties in natural environments such as clay particle size (flocculation), dispersion, swelling, hydraulic conductivity, specific surface area, cation and anion exchange and fixation capacity, layer charge, layer stacking order, magnetic exchange interactions, octahedral site occupancy, surface acidity, reduction potential, and also affects the surface chemistry of the clay and its reactivity toward organic and inorganic contaminants (Stucki *et al.,* 2002; Kim *et al.,* 2004; Stucki 2006; Stucki and Kostka 2006; Jaisi *et al.,* 2007a). Fe (II) sorbed and/or precipitated on Fe (III)-containing minerals (e.g., goethite, lepidocrocite, or amorphous ferric iron hydroxide) was found to be highly reactive with respect to reduction of contaminants (Ernstsen, 1996; Cervini-Silva *et al.,* 2000). Rates and extents of degradation of pesticides had increased in the presence of reduced smectites compared to oxidized and reduced–reoxidized counterparts (Xu *et al.,* 2001). Jaisi *et al.* (2008) found that the surface-complexed Fe^{2+} is the most reactive among different Fe^{2+} species associated with NAu-2 in reduction and immobilization of groundwater contaminants. According to Stucki and Kostka (2006) the reduction of structural Fe (III) to Fe (II) tends to decrease the surface area, interlayer spacing, water swellability, and hydraulic conductivity of clay minerals. In general, reduction increases the negative layer charge and cation exchange capacity, while the interlayer cations become less exchangeable. Biological cycling of iron is of particular significance because it is sometimes a limiting nutrient in the world ocean. Microbial reduction of Fe^{3+} coupled to the oxidation of organic matter in sediments is an important regulator of ocean chemistry and of carbon cycling (Canfield *et al.,* 1993). The transformation of smectite-to-illite is considered to be one of the most important mineral reactions during sediment diagenesis of mudstones and shales, as the degree of the smectite to illite reaction is linked to the maturation, migration and trapping of hydrocarbons. "Smectite illitization" is often used as an index for the generation of petroleum and natural gas.

2.4. Sheet silicates used in this study

In this study two sheet silicates were used; a dark brown-yellowish nontronite (NAu-2) which belongs to the smectite group, its origin is South Australia; and a very light green whitisch clinochlore (ripidolite is the old name) (CCa-2) which belongs to the chlorite group, and its origin is from Flagstaff Hill, El Dorado County, California, USA.

2.4.1. Smectite group: nontronite (NAu-2)

Smectites may be either dioctahedral or trioctahedral, depending on whether the octahedral layer is filled with two out of three positions with a trivalent cation or fully filled with a divalent cation. The dioctahedral smectites can be divided into two principal groups (a) aluminium smectites and (b) the the iron-rich varieties including ferruginous smectites and nontronites (Frost *et al.*, 2002). Nontronite is a swelling, dioctahedral, smectite-group 2:1 clay mineral, and thus contains two tetrahedral sheets per octahedral sheet (Fig. 1). In the case of the ferruginous smectites the theoretical structural formula can be written as: $(M^{++}{}_{x/2}\cdot nH_2O)$ $(Fe^{3+}{}_4)$ $(Si_{8-x}Al_x)$ O_{20} $(OH)_4$, where M is the interlayer cation, and Ca^{2+} was assumed to be the dominant exchangeable cation (keeling *et al.*, 2000). Tetrahedral sites are predominantly filled by Si ions but substitutions of Al, and occasionally of Fe^{3+} can occur. The dioctahedral sheet of nontronite is composed mainly of Fe^{3+}, although some substitution by trivalent Al^{3+} and divalent Mg^{2+} does occur. The octahedral sheet has two different sites denoted M1 and M2. M1 is the trans octahedron with OH groups located at opposing corners whereas M2 is the cis octahedron with the two OH groups located on the same edge (Fig. 1). Only two of the three octahedral positions per half unit cell (2 M2 + M1) are occupied, which can be either the two M2 sites (trans-vacant), or the M1 and one of the two symmetrically independent M2 sites (cis-vacant).

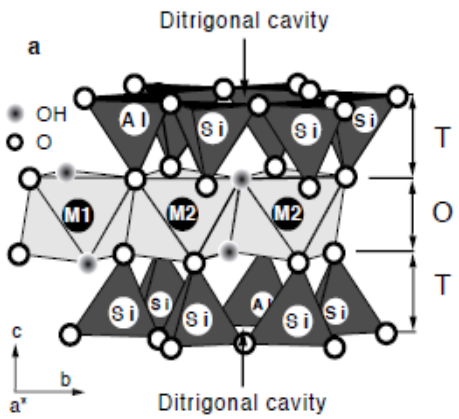

(Fig. 1) Crystal structure of Nontronite

Smectite clays are formed and most stable at low temperature and pressure, which are the typical conditions in soils and surficial sediments. As soils and sediments are buried at depths of 2000-4000 m, smectite clays undergo alteration to illite-smectite mixed layer clays, and at greater depths the mixed layer clay is altered to illite through K adsorption in interlayer positions, or even to chlorite if Mg is abundant (Zhang *et al.,* 2007 b). Nontronites are the product of low-temperature hydrothermal alteration of primary minerals, biotite, and amphibole. Figure 2 shows XRD peaks for NAu-2 in addition to another Nontronite (NAu-1).

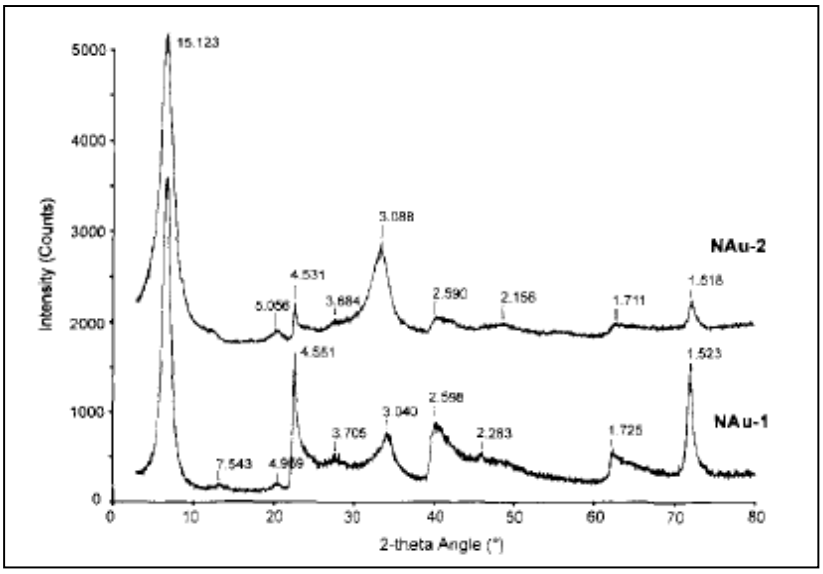

(Fig. 2) XRD peaks of the <0.2 µm size fractions of NAu-2, spacing is in Å (Keeling *et al.,* 2000).

The effects of Fe oxidation state on the infrared (IR) spectra of dioctahedral smectite were studied by Fialips *et al.* (2002 b). Deformation bands belonging to M-O-H (with M = Mg, Al, or Fe) in the unaltered (unreduced) and reduced samples are shown in (Fig. 3). The overall decrease in intensity of the M-Fe-OH-deformation bands (550 - 950 cm^{-1}) upon reduction reflects the progressive loss of OH groups.

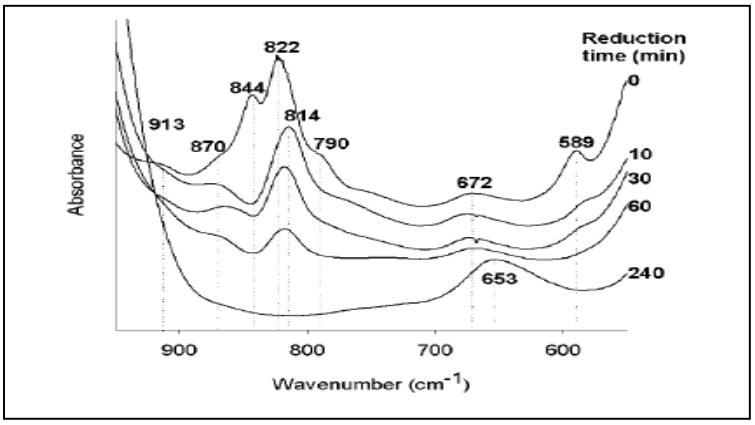

(Fig. 3) Normalized infrared spectra in the OH-deformation region of the initially unaltered Garfield nontronite and of the samples reduced during 10 to 240 min. with buffered sodium dithionite (Fialips *et al.,* 2002 a).

The varying positions of these bands upon reduction are generated by changes in the cationic environment surrounding the remaining OH groups as more Fe^{3+} is reduced to Fe^{2+}. The infrared and thermal gravimetric data done by Komadel *et al.* (1995) revealed that the structural OH content of reduced-reoxidized clay is about 15 to 20 % less than in the original (oxidized) sample, indicating that the structure remains partially dehydroxylated even after reoxidation.

2.4.1.1. Effect of microorganisms on smectite

Smectites have been shown to be more reducible than other clay minerals, likely due to their high layer expandability, low layer charge, and high surface area. According to differences in crystal chemistry of minerals, nontronite was the most easily reduced, and then chlorite, and finally illite was the least bioreduced (Dong *et al.,* 2009). Recent studies have shown that bacteria are capable of reducing the structural Fe (III) in smectite which serves as an electron acceptor under anaerobic conditions for respiration and growth (Gates *et al.,* 1993, 1998; Kostka *et al.,* 1996, 1999 a, b; Kim *et al.,* 2003, 2004; Stucki and Kostka, 2006; Seabaugh *et al.,* 2006; Jaisi *et al.,* 2005, 2007a, b; Dong *et al.,* 2009). Microbial reduction of Fe (III) can take place through two mechanisms: solid-state reduction, and dissolution-precipitation. In solid state reduction, changes in the clay structure are small and fully reversible upon reoxidation of reduced smectites (Gates *et al.* 1996; Favre *et al.* 2002; Lee *et al.,* 2006; Kashefi *et al.,* 2008). In contrast, some other studies have proofed the occurrence of microbial dissolution of nontronite (Dong *et al.* 2003; Furukawa and O'Reilly 2007; Kim *et al.* 2004; Li *et al.* 2004; Zhang *et al.* 2007a), and they observed the dissolution textures of smectites and the formation of biogenic products (Si, siderite, vivianite, and illite). According to Vodyanitskii (2007), solid-phase reduction of structural Fe (III) is specific to weakly ferruginous phyllosilicates, while reduction dissolution occurs for highly ferruginous phyllosilicates where NAu-1 has altered and amorphous Si globulas were formed at the surface of celleular polymers and bacterial cells. Kim *et al.* (2004) demonstrated that the mesophilic Fe (III) reducing bacterium *Shewanella oneidensis* catalyzed the smectite-to-illite transformation via a dissolution-precipitation mechanism through reduction of structural Fe (III) at room temperature and 1 atmosphere within 14 days. The microbially mediated S-I reaction can qualitatively be written as: Ca-smectite + Al^{3+} + K^{+} → K-illite + SiO_2 + Fe^{2+} + Ca^{2+}. The S-I reaction requires external K and Al sources (Eberl *et al.,* 1993; Drief *et al.* 2002) because smectite usually has a much lower amount of K and Al, but a higher amount of iron than illite. The possible source of K and Al in natural environments may be from feldspar and/or mica

dissolution. Li *et al.* (2004) found that X-ray diffraction, transmission electron microscopy, and energy dispersive spectroscopy have revealed significant changes in the structure and composition of NAu-2 during its alteration by bacterial sulfate reduction. Jaisi *et al.* (2005) tested the control of Fe (III) site occupancy on the rate and extent of microbial reduction of Fe (III) in nontronite, and their results revealed that Fe (III) in the tetrahedral and the *trans*-octahedral sites was bioreduced. The the *cis* octahedral Fe (III) remained relatively unchanged, which was similar to what Vodyanitskii (2007) has found too. Dong *et al.* (2009) found that when the extent of reduction is small (<30 %), the smectite structure remains stable, but above this threshold, it becomes unstable and the clay mineral may dissolve, with the formation of secondary mineral phases such as amorphous silica, siderite, vivianite, and illite, depending on the specific experimental conditions. Lee *et al.* (2006) found that when the levels of bacterial reduction are up to ~1 mmole Fe/g clay of Fe-bearing smectites, this results in changes of the clay structure, but the changes are largely reversed upon reoxidation. Jaisi *et al.* (2007 b) found that the more expandable nontronite structure (i.e., low layer charge) allows easier access of electron donor and cell shuttling compounds to the Fe (III) centers in the structure, leading to a higher extent of Fe (III) reduction. O'Reilly *et al.* (2005) wanted to test whether the reduction occurs while Fe is still in the clay structure or after Fe is released into the aqueous phase, and found that the nontronite (NAu-1) dissolution precedes microbial reduction of Fe. Vodyanitskii (2007) reached also to same result and found that microbial reduction of crystallized nontronite NAu-1 developed in the following stages: (1) nontronite transformation into a low-ordered clay mineral and deferruginated aluminosilicates, and the formation of either Fe (III) precipitates or dissolved Fe (III) particles from the released Fe (III); and (2) the subsequent microbial reduction of Fe (III). Fe (II) species at clay mineral surfaces can be formed by reduction of structural Fe (III) in the clay lattice and/or by surface complexation of dissolved Fe (II). The presence of Fe (II) on the surfaces of clay mineral is an important factor which may inhibit the reductive dissolution of clay because Fe (II) will be sorbed onto clay and bacterial surfaces, consequently blocking the electron transfer and hinder further bioreduction. However, Hyacinthe *et al.* (2008) supposed under their experimental conditions that electrons can be transformed from Fe (II) cations adsorbed to the mineral surface to Fe (III) centers within the interior of the mineral particles, and that strong metal binding groups in the cell wall of the iron-reducing microorganisms are present. These mechanisms prevent the sorbed Fe (II) cations from interfering with the transfer of electrons from the cells to Fe (III) centers at the mineral surfaces. Only at high levels of aqueous Fe (II) the electron uptake capacity of the Fe (III) minerals or the metal binding capacity of the cell wall will be saturated, upon which inhibition of the iron-reducing activity would be expected.

2.4.2. Chlorite group: Clinochlore (CCa-2)

The structure of the common chlorites consists of regularly alternating negatively charged tetrahedral-octahedral-tetrahedral (2:1 / TOT/ talc like) layers and positively charged brucite interlayer (Fig. 4). The tetrahedral layers in chlorites are distorted from their ideal configuaration by rotations of their tetrahedral, which results with other deviations in stronger hydrogen bond between (OH) ions of the brucite and oxygens of the talc layers (Deer *et al.*, 2009). In most chlorites there are 12 octahedral cations per $O_{20}(OH)_{16}$ and approximately equal amounts of Al in tetrahedral and octahedral sites, such minerals referred to as trioctahedral chlorites. In a small number of chlorite species, the number of octahedral cations per $O_{20}(OH)_{16}$ is ≤10, and these are described as dioctahedral chlorites. Extensive substitution of the Si^{4+} by Al^{3+} or occasionally by Fe^{3+} or B^{3+} occurs in the TOT sheet. Charge balancing cations are located in the hydroxyl sheets of the TOT or interlayer. These ions are typically Mg^{2+}, Fe^{2+}, Al^{3+} and Fe^{3+}, but important substitutions of Cr, Ni, Mn, V, Cu or Li may occur. The simplest classification of the chlorites is into Fe-rich types, known as chamosite, and Mg-rich types, known as clinochlore (Bayliss, 1975).

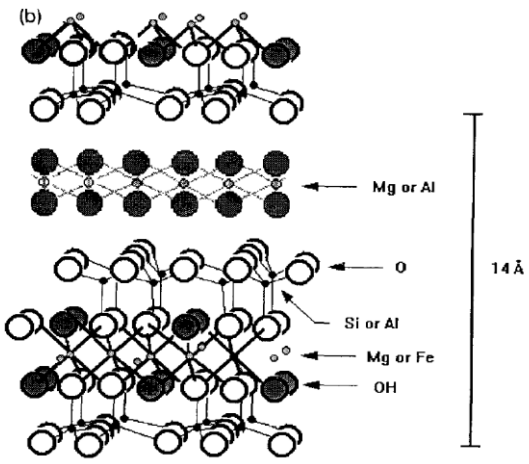

(Fig. 4) Idealized crystal structure of chlorite. An octahedral sheet of cations lies between two tetrahedral sheets of silicon and aluminium, and has a hydroxy-interlayer (Malmström *et al.,* 1996).

The Fe-rich examples occur most frequently in sandstones that were deposited at the transition between marine and non-marine environments and the presence of Fe-rich oolites in many samples suggests a link to the ironstone facies. The Mg-rich varieties tend to be found in aeolian or sabkha sandstones in close association with evaporites. They are probably replacements of Mg-rich smectites via the intermediate mineral corrensite. Platt (1993) found that chlorite is itself beneficial to hydrocarbon reservoir quality because it has resulted in the

preservation of primary porosity that is 5-10% higher than in adjacent sandstones where chlorite is absent. Gaupp *et al,* (1993) found that sandstones with porelining chlorite have the highest porosities of any sandstone in the studied region). Hillier (1994) found that pore-lining chlorites are often responsible for the preservation of porosity in deeply buried sandstones because they inhibit the formation of quartz overgrowths, but little is understood about when and how they form. Chlorites can be found in low- and medium-grade pelitic and mafic metamorphic rocks formed at temperatures up to about 400°C and pressures of few kilo bars. They are also common constituent of igneous rocks in which they have generally been formed by hydrothermal alteration of primary Mg- and Fe bearing minerals such as pyroxenes, amphiboles, biotite, and other ferromagnesian minerals (Nesse, 2000; Deer *et al.,* 2009). Furthermore they appear as a product of diagenesis in clay bearing sediments and sedimentary rocks. Most commonly, chlorites occur as fine-grained scaly or foliated massive aggregates, characterized by their green color, micaceous habit and cleavage, and by the fact that the folia, in contrast to micas, are not elastic (Deer *et al.,* 2009). Clinochlore is a trioctahedral, non swelling mineral, with chemical formula: $(Mg, Fe^{2+})_5 Al(Si_3 Al) O_{10}(OH)_8$. Figure 5 shows XRD pattern for ripidolite.

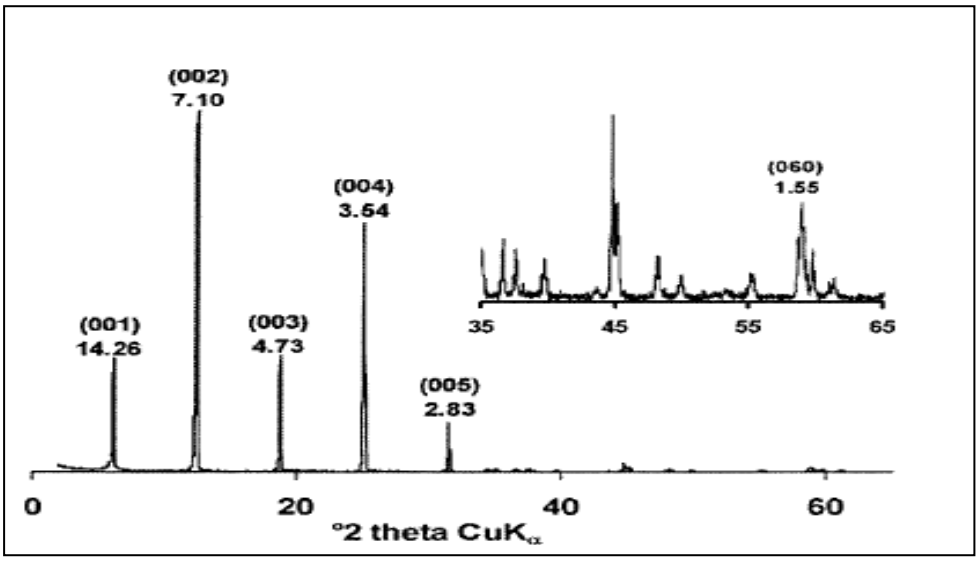

(Fig. 5) X-ray diffraction pattern of randomly oriented pretreated ripidolite from 2 to 65° 2 theta and enlargement of the 35 to 65° 2 theta area (125- to 38-µm fraction); spacing in Å (Hamer *et al.,* 2003).

Post and Plummer (1972) used Infra red spectroscopy (fig. 6) in addition to X-ray diffraction, and differential thermal analysis (DTA) to investigate the chlorite minerals of the Flagstaff Hill area in its preliminary stages as a fruitful area for information on the genesis, alteration, and weathering characteristics of the different chlorite minerals, and to consequently suggest the area as an adequate source for chlorite samples usable as reference standards.

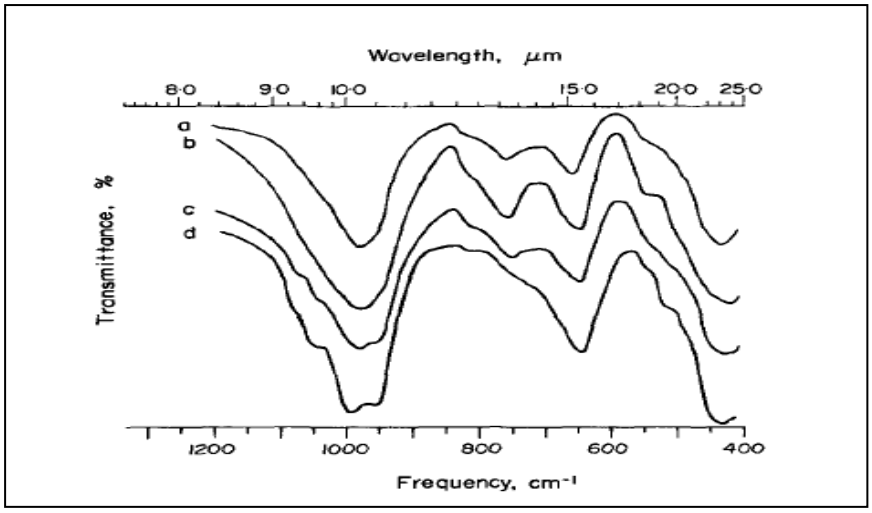

(Fig. 6) The IR spectra in the region 8 to 25 μm for (a) sheridanite, ; (b) ripidolite; (c) clinochlore; and (d) penninite.

2.4.2.1. Effect of microorganisms on chlorite

Jaisi *et al.* (2007a) assessed the role of biogenic Fe (II) in microbial reduction of Fe (III) in three clay minerals; nontronite, illite, and chlorite by *Shewanella putrefaciens* CN32. The order of the rate and extent of reduction was as follows: nontronite > chlorite > illite. Their opinion agreed with (Dong *et al.*, 2003; Jaisi *et al.*, 2005; Seabaugh *et al.*, 2006), that the amount and the crystal-chemical environment of Fe (III) in the structure as well as layer charge of the overall structure are likely to be the important factors controlling the extent of reduction. According to Dong *el al.* (2009), non-expandable structures of clay minerals (such as illite and chlorite) is bioreducible, but to a limited extent, this bioreduction is enhanced by the presence of electron shuttling compounds like humic acids and Anthraquinone-2,6-disulfonate (AQDS). However, most studies have tested the dissolution of chlorite chemically and not biologically. For example; Brandt *et al.* (2003) studied dissolution of preconditioned pH 2 chlorite with intermediate Fe-content macroscopically via mixed flow experiments as well as microscopically via atomic force microscopy (AFM) for several months. Hamer *et al.* (2003) studied the effect of organic (acetic, oxalic, citric) and inorganic (hydrochloric, nitric, sulfuric) acids on the dissolution of ripidolite at 25ºC over an acid concentration range of 0.03 to 10 mM. Krawczyk-Bärsch *et al.* (2004) studied the Fe-oxyhydroxide colloids formed from the simulated weathering of chlorite platelets in contact with water for 2 months. Lowson *et al.* (2005) studied the dissolution rates of an iron rich chlorite as a function of pH concentration for the pH range 3 to 10.5 and at 25°C.

2.5. Methods for studying microbe mineral interaction

2.5.1. Atomic Force Microscopy (AFM)

A major precise manner by which microbial activity influences mineral-surface reactions is required. AFM is a viable technique for imaging bacteria attached to mineral surfaces. However, sample preparation has proven to be crucial. Maurice *et al.,* (1996) found that an organic extractant used to separate bacteria from particle surfaces left a residue that could be considered by mistake as one of the dissolution features in AFM images. Atomic force microscopy (AFM) was developed in the mid of 1980s. (Binnig *et al.,* 1986; Hochella *et al.,* 1990) were the first who described its basic operation principles. In brief, a sample is mounted on the top of a piezoelectric scanner composed of materials such as lead-zirconium-titanite that permit movement with Å-level precision. The sample is scanned continuously in 2 dimensions (x-y) beneath a force-sensing probe consisting of a tip that is attached to or part of a cantilever. Z-direction (height) movements are also made by the scanner as required to compensate for changes in sample height or forces between the tip and the sample. Attractive or repulsive forces between the tip and the sample cause the cantilever to bend or deflect. This deflection can be monitored by a laser light (Fig. 7), which reflects off the back of the cantilever into a photodiode detector.

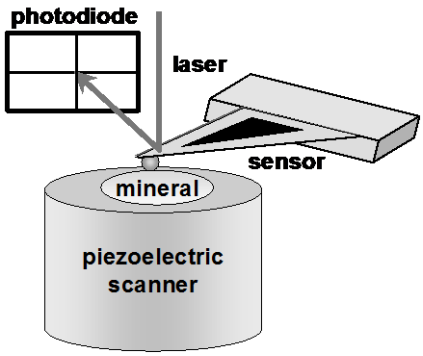

(Fig. 7) Schematic image of an atomic force microscope. A sample (mineral) is positioned on a piezoelectric scanner, which moves the sample in three dimensions relative to the sensor (i.e., cantilever). The cantilever deflects due to attractive or repulsive forces between itself and the sample. Deflection of the cantilever is monitored by reflecting a laser off the top and into a photodiode array. The cantilever often terminates by a tip, which can be activated with various substances such as functional groups or cells (shown as a sphere on the end of the sensor). (Lower *et al.,* 2001).

Contact mode AFM operates by scanning a tip attached to the end of a cantilever across the sample surface. In the contact AFM mode, the tip contacts the sample surface. In the Tapping mode (TM)-AFM, a scanning tip is attached to the end of an oscillating cantilever across the

sample surface, so it is excellent for imaging soft and easily deformable microbes and organic residues. AFM is a powerful high-resolution imaging technique capable of quantifying mineral-surface and microbial cell structure. However, it suffers from the artifacts caused by tip-sample interactions in addition to the limited field of view. Grantham and Dove (1996) used Fluid TM-AFM to investigate the effect of iron coatings on the interactions of *Shewunella putrefuciens* with silica glass surfaces (as analogues for quartz), and found that bacteria in nutrient-depleted solutions adhered to Fe-coated substrates more strongly than bacteria seeded in nutrient-rich solutions. Maurice *et al.* (1996) used AFM to study interactions between Fe (III)-(hydr) oxides and a *Pseudomonas* sp. soil microbe and found that reacted hematite and goethite particles showed no obvious dissolution features; however, a small fraction of hematite platelets were severely eroded. Bickmore *et al.* (2001) studied the behavior of two smectite minerals, hectorite (trioctahedral) and nontronite (dioctahedral) in situ in acid solutions, using atomic force microscopy. Naidja and Huang (2002) used AFM pictures along with XRD and FTIR data to show the protein– birnessite complex, and the coating of the mineral surfaces by the protein molecules as well as the changes in the protein conformation, resulting in the unfolding and flattening of the protein molecules after binding to the mineral surfaces. In situ AFM performed by Brandt *et al.* (2003) on the basal surfaces of a chlorite sample, which has been preconditioned at pH 2 for several months, indicated a defect controlled dissolution mechanism. Liu *et al.* (2003) investigated the bioleaching mechanism of pyrite by the indigenous *Thiobacillus thiooxidans* and the AFM images showed that the pyrite surface area positively correlated with the oxidation rate. Rosso *et al.* (2003) did AFM experiments to probe well characterized basal surfaces of hematite single crystals for dissolution features arising from controlled exposure to the dissimilatory metal reducing bacteria (DMRB) *Shewanella putrefaciens* and the images suggested that during anaerobic respiration the bacteria release a soluble agent or agents into the medium that causes facile dissolution of these unstable surface sites. Gazzè *et al.* (2012) investigated the effects of symbiotic ectomycorrhizal fungi on the topography of a chlorite mineral, using atomic force microscopy and have found primary channels of the order of a micron in width and up to 50 nm in depth chlorite. However contact took place for seven months in an axenic microcosm.

2.5.2. Vertical Scanning Interferometry (VSI)

A new imaging technique was required that can quantify any resulting changes in mineral-surface topography, while maintaining high spatial resolution with a large field of view, and a

large vertical scan range with fast data acquisition. VSI meets these requirements and enables the measurement of both local dissolution (etch pits) and global dissolution rates (surface normal retreat) (Davis and Lüttge, 2005). Interferometry is an optical technique which is used to measure surface topography with very high precision. Interferometers produce surface height maps by splitting a beam of light exiting a single source into two separate beams. One beam is reflected from the sample surface while the other is reflected from a reference mirror (Fig. 8). When the two beams are recombined, interference phenomena produce an interferogram consisting of fringes which reflect the topography of the sample surface. A charge coupled device (CCD) detector is used to register and feed the interferogram to a computer where phase-mapping programs produce a topographic image of the surface. VSI is a type of interferometry which is optimized for the wide dynamic range needed to image rough surfaces. It uses a white light illumination source, which allows large vertical scans (up to 100 µm with better than 2 nm resolution). Because interferometry measures relative surface height, changes in mineral surface topography must be measured relative to a reference surface. This is usually done by placing an inert mask on the surface. When measuring the average height difference between the reacted and unreacted surfaces, an absolute value of surface normal retreat can be determined. Davis and Lüttge (2005) used AFM and VSI as complementary techniques to indicate existence of a complex relationship between microbial surface

(Fig. 8) VSI device with a schematic diagram.

colonization of by *Shewanella oneidensis* MR-1 and carbonate mineral- surface dynamics. Buss *et al.* (2007) found by using AFM and VSI some biopits caused by siderophore-producing bacteria (*Bacillus* sp.) incubated with iron-silicate glass planchets chemically similar to

hornblende for 46 days. Waters *et al.* (2008) used VSI to investigate the initial stages of *Shewanella oneidensis* MR-1 attachment to glass, steel and aluminium surfaces, and they found that using VSI with some modifications to the analytical software may be a unique window for studying the bacterial/substrate interface that can be used for quantitative observations. Siegel (2010) quantified etch pits on black slate samples induced by fungal activity using VSI. The etch pits measured were 3 – 4 μm in width and 180 – 200 nm in depth, while more etch pits were found on graphite surfaces. Rothhardt (2012) found using VSI that *S. commune* strain has changed the topography of organically coated sand grains, and formed irregular etch pits within the average of 0.88 μm width, 4.22 μm long, and 0.63μm depth.

2.5.3. Fourier Transform Infrared Spectromicroscopy (FTIRS)

FTIRM is emerging as a spectroscopic probe and imaging tool for correlating molecular structure to biochemical dynamics and function. It is true that FTIR spectromicroscopy does not achieve nanoscale spatial resolution like fluorescence microscopy. However, it has the unique advantage of being a label-free method that can probe many biomolecules simultaneously. In addition, FTIR spectra are sensitive to many molecular properties of a sample, including chemical composition and molecular structure, therefore providing a wealth of complementary information. Since infrared light is nonionizing, there is a promising future for time-resolved imaging of living cells. FTIR-Spectroscopy has the advantage over other methods that it is minimally disturbing, thus reducing perturbation of the sample and consequently the introduction of experimental artifacts. FTIR spectroscopy and spectromicroscopy have proven to be useful in assessing the chemical changes involved in bacterial mineral interactions. Devasia *et al.* (1993) showed by FTIR that *Thiobacillus ferrooxidans* cells grown on sulfur, pyrite, and chalcopyrite synthesized proteinaceous new cell surface appendages to adhere to the solid mineral substrates. Such an appendage was absent in ferrous iron-grown cells as it is not required during growth in liquid substrates. Holman *et al.* (1999) showed by their spatially resolved synchrotron radiation FTIR spectromicroscopy that on magnetite, toxic Cr^{6+} is reduced to less mobile, less toxic, and stable Cr^{3+} only in the presence of the isolated microorganisms, and that reduction was accelerated during the simultaneous biodegradation of toluene. Parikh and Chorover (2006) examined the contribution of various bacterial surface functional groups to adhesion at hematite and ZnSe surfaces using attenuated total reflectance (ATR) FTIR. Their results indicated that both terminal phosphate/phosphonate and phosphodiester groups, either exuded from the cell or present as surface biomolecules, are involved in bacterial adhesion to Fe-oxides through

formation of innersphere Fe-phosphate/phosphonate complexes. Moreau *et al.* (2007) had demonstrated using synchrotron radiation fourier-transform infrared (SR-FTIR) micro-spectroscopy the intimate association of proteins with spheroidal aggregates of biogenic zinc sulfide nano-crystals, as an example of extracellular biomineralization. They suggested that microbially derived extracellular proteins can limit the dispersal of nanoparticulate metal-bearing phases, such as the mineral products of bioremediation, which may otherwise be transported away from their source by subsurface fluid flow. Ueshima *et al.* (2008) observed by FTIR that the presence of exopolysaccharides (EPS) produced by the bacterial species *Pseudomonas putida* does not significantly affect the extent of Cd removal from solution. The first application of FTIR spectromicroscopy to study the biochemical composition of algae was carried out by Giordano *et al.* (2001) when they examined the changes in the major cellular constituents of the diatom *Chaetoceros muellerii* in response to nitrogen starvation. Benning *et al.* (2004) ascertained by SR-FTIR the changes in the chemistry of cultured cyanobacterial filaments and their response to precipitation of amorphous silica from microbe/fluid/mineral interaction experiments that were done in situ and in vivo. Heraud *et al.* (2005) found from high quality (FTIR) spectra acquired from living *Micrasterias hardyi* cells, that nitrogen-starved cells re-supplied with N showed an increase in lipid in all positions measured across the cell over a 23 h period of re-supply, with the largest increases occurring in positions where the chloroplasts were observed. Hirschmugl *et al.* (2006) used SR- FTIR spectroscopy to follow and describe the changes occurring in the main macromolecular pools of the common freshwater euglenophyte *Euglena gracilis*, which were allowed to grow and age in batch cultures. This mimics, even if in a simplified way, the progressive depletion of external resources occurring in natural bloom conditions. Holman *et al.* (2009) used high-resolution (FTIR) spectromicroscopy to continuously follow cellular chemistry within living obligate anaerobes in order to understand the mechanisms which enable them to survive a sudden exposure to oxygen. Goff *et al.* (2009) demonstrated the capability of SR-FTIR spectromicroscopy to detect metabolite formation in single, living cells of the unicellular algae *Chlamydomonas reinhardtii*. Dean *et al.* (2010) found that FTIR spectra of freshwater microalgae *Chlamydomonas reinhardtii* and *Scenedesmus subspicatus* grown in N-limited media showed increasing lipid:amide I and carbohydrate:amide I ratios over time. Using FTIR-Focal Plane Array (FPA) imaging, Isenor *et al.* (2010) wanted to characterize the composition of *Curvularia protuberata* hyphae, and to compare a strain isolated from plants inhabiting geothermal soils with a non-geothermal isolate. It was determined that the protein content in some *C. protuberata* cells remains fairly constant throughout the length of a hyphae, whereas the mannitol is found at discrete, irregular locations. Finally, it is important to notice that the

information derived from FTIR spectromicroscopy is just like the tip of an iceberg. Because of the complexity of a biogeochemical system, this information alone is not sufficient for a systematic understanding of how intrinsic microorganisms interact with their surroundings. The use of multiple complementary biochemical, analytical, and imaging techniques is thus necessary.

As the (FTIRS) has been used for three months in the Swiss Light Source (SLS) at the Paul-Scherrer Institute in Villigen, Switzelrland, this tool is going to be explained in more details.

2.5.3.1. The FT-IR theory:

Mid-IR spectroscopy is a powerful, nondestructive, technique that provides chemical information on materials. (Parker, 1983; Tobin *et al.,* 2010). The technique is based on studying the interaction of infrared radiation with samples. When IR radiation is passed through a sample, some radiation is absorbed and the rest is transmitted. The infrared region (approximately 10-14000 cm^{-1}) of the electromagnetic spectrum is in turn conventionally divided into three spectral sub-regions, the near (4000-14000 cm^{-1}), mid-(400-4000 cm^{-1}), and far-IR (10-400 cm^{-1}). The mid-IR (400-4000 cm^{-1}) is the most commonly used region for molecular studies as all molecules possess characteristic absorption bands in this range. When IR radiation passes through a sample, specific wavelengths are absorbed causing the chemical bonds in the material to undergo vibrations such as stretching, and bending (Smith, 1996). The plot of the amount of light absorbed by the sample versus the frequency or wavelength of the absorbed light is called the infrared absorption spectrum of the sample. Absorption of an infrared photon requires that the interaction of molecules with incident light yields a change in the distribution of electric charge within molecules. Incoming infrared light will be absorbed by the molecule if the following two criteria are met: the frequency of the infrared light matches exactly the frequency of a vibrational mode, and the vibration causes an asymmetric change in the charge distribution within the molecule (i.e. it causes a change in the electric dipole moment of the molecule). Fourier Transform Infrared (FTIR) spectroscopy is a technique for measuring the spectrum of infrared light that allows simultaneous recording of all of the infrared frequencies. An optical device called an interferometer, usually a Michelson interferometer, with a beam splitter (a semi-reflecting film), a fixed mirror, and a moving mirror, is used to analyze the light spectrum (Fig. 9). The interferometer uses interference patterns to make accurate measurements of the intensity and wavelength of light. The

interferometer produces a plot, called an interferogram, which has all of the infrared frequencies "encoded" into it. The interferogram can be measured very quickly, usually on the order of one second or even faster. The measured interferogram signal cannot be interpreted directly in terms of molecular properties. Extracting molecular information requires a frequency spectrum (a plot of the absorption at each individual frequency).

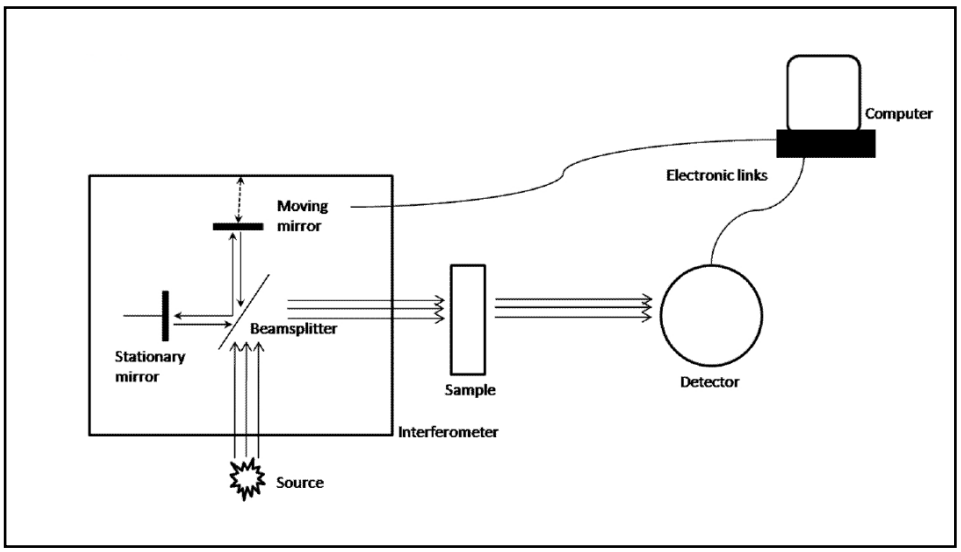

(Fig. 9) Basic components of FT-IR spectrometer

A means of "decoding" the individual frequencies is required. This can be accomplished via a well-known mathematical technique called the Fourier transformation, which converts the interferogram (intensity versus time spectrum), to an IR spectrum (intensity versus frequency spectrum). This transformation is performed by the computer which then supplies the user with the desired spectral information for analysis. To account for the spectral composition of the light source a background spectrum must also be measured. This is normally a measurement with no sample in the beam. The background measurement is then compared to the measurement with the sample in the beam to determine an absorption spectrum. This technique results in a spectrum which has all of the instrumental characteristics (e.g. absorption from optical components of the instrument) removed. Thus, all spectral features which are present are strictly due to the sample. An IR absorption spectrum is traditionally plotted with Y-axis units as absorbance or transmittance and the X- axis as wavenumber units. For quantitative applications it is necessary to plot the spectrum in absorbance units (Smith, 1999).

Absorbance is a quantitative measure expressed as a logarithmic ratio between the radiation falling upon a material and the radiation transmitted through a material:

$$A_\lambda = \log_{10} (I_0/I_1)$$

where A_λ is the absorbance at a certain wavelength of light (λ), I_1 is the intensity of the radiation (light) that has passed through the material (transmitted radiation), and I_0 is the intensity of the radiation before it passes through the material (incident radiation). The FT-IR absorbance spectra follow Beer‘s law, which relates concentration to absorbance by this equation:

$$A_\lambda = l\, \varepsilon_\lambda\, c$$

Where A_λ= Absorbance, l = Path length, ε_λ = Absorptivity, c = molar concentration. Transmittance is not directly proportional to the concentration and is defined as follow:

$$\%T = I_S / I_R$$

Where I_S = Intensity of IR beam after passing through the sample, I_R = Intensity of IR beam before passing through the sample.

In biological materials, the standard building blocks such as proteins, lipids, nucleic acids, and carbohydrates have unique chemical structures corresponding to distinctive infrared spectra (Fig. 10). Functional groups present in a molecule tend to absorb IR radiation in the same wave number range with limited influence from other structures in the molecule (Table 2). Thus there is a correlation between IR band positions and chemical structures in the molecule.

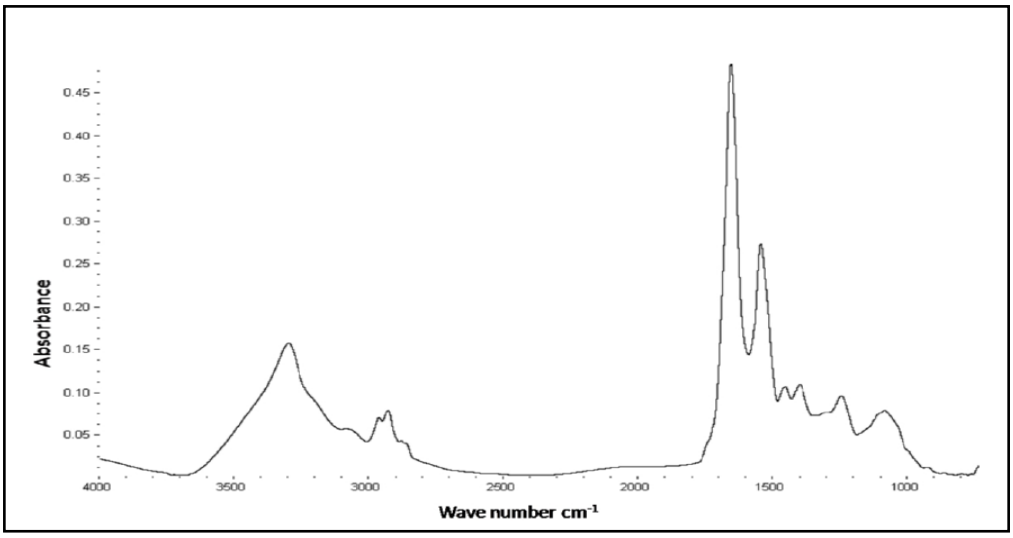

(Fig. 10) A representative FT-IR absorbance spectrum (4000-1000 cm $^{-1}$) of a colony of a Gram-negative bacterium, *Salmonella enterica* (Davis and Mauer, 2010).

Table (2) Assignment of functional groups associated with major vibration bands in mid IR spectra of bacteria (Davis and Mauer, 2010)

Wave number (cm^{-1})	Molecular vibrations of functional groups and the biomolecule contributor
3200	N-H stretching of amide A in proteins
2955	C-H asymmetric stretching of $-CH_3$ in fatty acids
2930	C-H asymmetric stretching of $>CH_2$ in fatty acids
2898	C-H stretching of ≥C-H of aminoacids
2870	C-H symmetric stretching of $-CH_3$ in fatty acids
2850	C-H symmetric stretching of $>CH_2$ in fatty acids
1740	>C=O stretching of lipid esters
1715	>C=O stretching of ester, in nucleic acids and carbonic acids
1695-1675	Amide I band components of proteins
1655	Amide I of α-helical structures of proteins
1637	Amide I of β-pleated sheet structures of proteins
1550-1520	Amide II band of proteins
1515	Tyrosine band
1468	C-H deformation of $>CH_2$ in lipids proteins
1415	C-O-H in-plane bending in Carbohydrates, DNA/RNA backbone, proteins
1400	C=O symmetric stretching of COO- group in aminoacids, fatty acids
1310-1240	Amide III band components of proteins
1240	P=O asymmetric stretching of phosphodiesters in phospholipids
1200-900	C-O-C, C-O dominated by ring vibrations in various polysaccharides
1085	P=O symmetric stretching in DNA, RNA and phospholipids
720	C-H rocking of $>CH_2$ in fatty acids, proteins
900-600	"Fingerprint region"

In colonies of microorganisms, ultrastructure, composition and function of biochemical components can change substantially within a few micrometres. The implementation of FTIR spectroscopy in a microscopy configuration is necessary to appreciate the spatial distribution of these components. FTIR Spectromicroscopy makes it possible to probe these variations, relating composition to location within a colony. FTIR spectromicroscopy involves coupling the infrared spectrometer to an IR microscope. The microscope is used in place of the sample compartment of the interferometer. Microscope optics allows focusing and accurate positioning of the IR beam on the sample, thanks to the parfocality of IR and visible light. This allows identification and targeting of microscopic structures in a sample, confocal apertures are used to restrict the beam to the area of interest within the sample. The transmitted or reflected infrared radiation from that targeted area is then collected and focused onto a detector (Fig. 11). In general, the light from a thermal IR sources can be focused with an infrared microscope to a spot of 75-100 µm in diameter. To measure smaller features, one needs to use an aperture to mask away part of the incoming infrared light. Typical IR microscopes utilize Schwarzschild objectives with a NA of ~ 0.6. Thus for the mid-IR range, the diffraction-limited spatial resolution is (~ 1.7 µm at 4000 cm^{-1} to 13 µm at 500 cm^{-1}) (Miller and Dumas, 2006). Spatial resolution, which determines the measurement area within the biological sample and therefore the length scale of the heterogeneity that can be studied, is often limited by the

brightness of the conventional thermal infrared source found in laboratory FTIR spectrometers (Miller and Dumas, 2010).

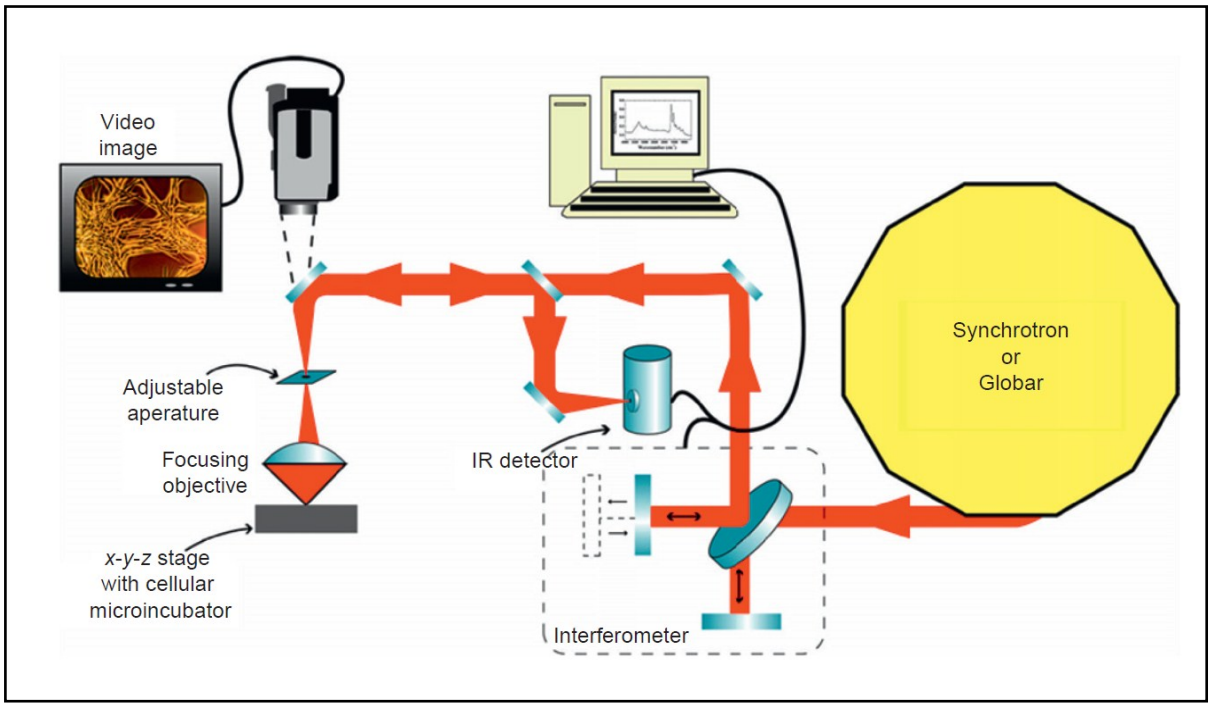

(Fig. 11) Schematic diagram of Fourier transform infrared (FTIR) spectromicroscopy experimental setup. Midinfrared radiation from either a synchrotron or a globar is transported to a FTIR interferometer bench. After modulation by the interferometer, an infrared microscope focuses the beam onto the sample with all-reflecting optics. Microbial or biogeochemical samples can be placed inside an on-stage mini-incubator with environmental controls. The stage is computer controlled and rasters the sample in the x-y-z plane to ~0.1 m precision to obtain spectral maps across the sample. The light reflected from the sample is collected by the same microscope optics and sent to an IR detector. A computer performs a Fourier transform on the measured interferogram to obtain an infrared spectrum (Holman *et al.,* 2010).

2.5.3.2. Synchrotron Radiation FTIR (SR-FTIR)

Replacing the thermal emission source (e.g., a globar) in the conventional FTIR spectromicroscope with a bright synchrotron IR source as shown in figure 12, can significantly improve the spatial resolution, and also the detection sensitivity, which determines the data collection time and therefore time resolution for investigating ongoing biological processes in real time (Dumas *et al.,* 2006). A synchrotron light source is a high-energy electron storage ring optimized for production and collection of the intense light radiated by electrons accelerated to nearly the speed of light. Because the opening angle of radiation emitted from

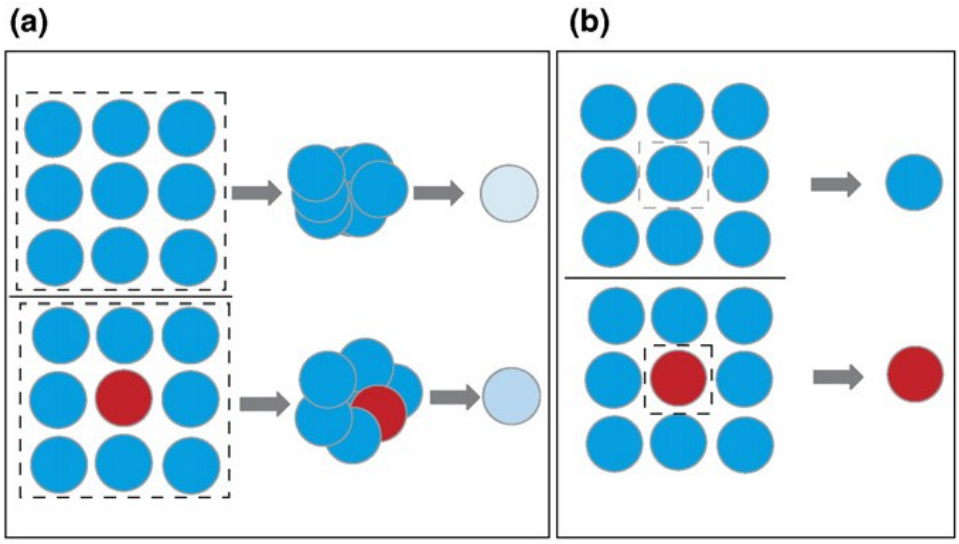

(Fig. 12) Illustration of the advantage provided by using a synchrotron source for infrared microscopy. (a) If the spatial resolution is limited by the photons originating from a low brilliance sources (such as those used in laboratory), the abnormal circle, in red, will be averaged among the eight other blue circles, resulting in an average circle of a different shade of blue. To determine whether an abnormal circle is present in the average result, one might end up with a more uncertain assessment. (b) If the probing toll has a better spatial resolution, then the red circle will be clearly identified and the diagnosis will be straightforward. This is what the synchrotron, thanks to its brilliance, provides to infrared microscopy for diagnostic purposes (Dumas *et al.,* 2006).

relativistic electrons in a synchrotron storage ring is very small, the effective source size of infrared radiation source is dominated by diffraction, due to the nature by which waves propagate; and thus can be considered as a nearly ideal point source (Sham and Rivers, 2002). The high brightness synchrotron infrared source allows smaller regions to be probed with acceptable signal-noise ratio. Unlike the conventional source, a synchrotron infrared source enables one to obtain spectra from targeted areas whose size approaches the diffraction limit (Carr, 1999). Thus for SR-FTIR spectromicroscopy, the infrared beam can be focused to a spot with a diameter of its wavelength, which yields a spatial resolution at the diffraction limit (Levenson *et al.,* 2006, 2008). For mid-IR wavelengths of 2.5-25 μm, SR-FTIR spectromicroscopy enables one to obtain spectra on targeted areas of ~2-20 μm in diameters.

2.5.3.3. Limitations

Water strongly absorbs mid-IR light and even the absorption due to a thin layer of water can completely dominate the spectrum. However, water is necessary for life and is the most common ingredient (>70%) in living cells. So it is essential to get the optical thickness of water “just right”: enough to support life and ensure the validity of model systems, but not so

much that it masks the molecular signatures of interest. Typically, <10 μm of bulk water is preferred to exploit the molecular information across most of the mid-IR spectral range (Holman *et al.,* 2010). A traditional approach to minimize water absorption during living cell experiments is attenuated total reflectance (ATR) FTIR equipped with a flow chamber. In ATR-FTIR, the IR beam internally reflects off a high index crystal (e.g., diamond or germanium), and the attenuation of the IR beam caused by the absorption of the evanescent wave is measured and analyzed (Iwamoto and Ohta, 1984) For living cell experiments, cells are cultured on ATR crystals in a specially designed flow chamber that can carefully control the culturing/experimental conditions (pH, temperature, ionic strength, flow shear stress, and delivery of materials such as nutrients and drugs) for hours (Suci *et al.,* 1998). The evanescent field formed at the cell/ATR crystal interface has a typical penetration depth of <1 μm, thereby reducing the optical path length in water. However, this small penetration depth, though important in reducing the path length through water, will allow capturing information only from molecules at or near the interface, while prevent examining chemical and biological processes in cells within biological systems with an extensive extracellular matrix. Another important consideration is the effect of growing the cells on the ATR crystal. Many cells require a substratum for normal growth, and the use of an ATR crystal may affect extracellular matrix properties that are important in cellular phenotype. Another common approach to decrease the spectral contribution of water is to replace it with large concentrations of heavy water, D_2O, in the preparation of media and buffers. The stretching modes of D_2O, $\upsilon_{s\ D2O}$ and υ_{as} D_2O appear around 2500 cm^{-1}, where few chromophores of biological interest absorb (Venyaminov and Prendergast, 1997). The main drawback of D_2O addition or dilution when applied to a cellular sample is that, although the structure and the chemical composition of cells are retained, their viability and survival are not guaranteed (Kushner et al, 1999). The different chemical properties of D_2O relative to H_2O imply that the substitution is generally stressful for cells and tissues. The biological effect of D_2O on a sample should be evaluated case by case. The need to control sample thickness, while ensuring the viability of the sample and the possibility to manipulate it, poses several challenges to sample holder design. The simplest configuration to control the sample's thickness is achieved by using standard IR sample holders for solutions (Fig. 13). Such units are based on a sandwich of two optical windows spaced by a thin layer of material of controlled thickness (Tobin *et al.,* 2010; Zhao *et al.,* 2010). The sample holders allow injection of a solution around the perimeter of the windows to reduce water evaporation from the sample itself. Temperature control is via recirculation of the fluid from a thermostatic bath. CaF_2 is the most commonly used material for optical windows, mostly because of its transparency, low cost and refractive index (1.4 at λ

= 5.0) close to that of water - Nonetheless, CaF_2 presents a few disadvantages, namely solubility in acidic solutions, spectral cutoff below 1000 cm^{-1} and considerable brittleness.

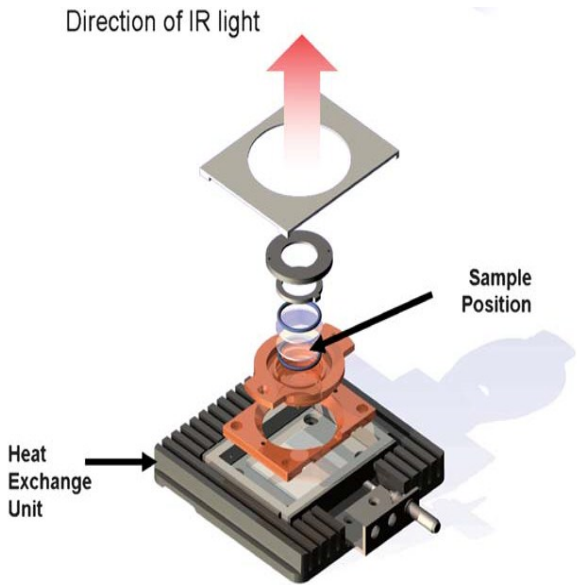

(Fig. 13) Temperature controlled sample holder for aqueous cell suspensions based on compression of a polymeric spacer between two optical windows (Quaroni and Zlateva, 2011).

The latter limitation implies that CaF_2 optical windows are generally thick, ranging from 1 to 3 mm. Only smaller diameter windows are commercially available with a thickness of 0.5 mm. Window thickness leads to chromatic aberration and degradation of visible image quality when visualizing the sample (Quaroni and Zlateva, 2011).

Almost all earth and environmental materials have vibration frequencies in the mid-infrared region, and most minerals do absorb light in the mid-IR region (except for halides and some chalcogenides) of light elements. Nevertheless, and despite the increased availability of synchrotron beam time to environmental scientists, there is only limited research on iron oxides in soils (Singh *et al.,* 2010).

2.5.3.4. Future perspectives

Infrared microscopes are generally equipped with single pixel detectors of high responsitivity, generally liquid nitrogen-cooled, broad-band or narrow-band mercury cadmium telluride (MCT) detectors. However, the most recent development in IR detectors involves the coupling of two-dimensional array detectors to an FTIR microscope. The coupling of an infrared focal-

plane array detector to an interferometer provides an instrumental multiplex/multichannel advantage. Specifically, the multiple detector elements enable spectra at all pixels to be collected simultaneously, while the interferometer portion of the system allows all the spectral frequencies to be measured concurrently. With this method of mid-infrared spectroscopic imaging only several seconds of staring time is required for spectral image acquisition (Lewis *et al.,* 1995). The use of time resolved (TR) FTIR makes it possible to obtain kinetic data on conformational changes in proteins, with a time resolution down to a few nanoseconds in the case of cyclic photo-initiated reactions. In this context it is important to note that kinetic studies have been restricted to reactions which can be initiated by suitable triggering techniques, such as light pulse, temperature jump or pressure jump. This limitation has been partly overcome by the development of solution mixing techniques suitable for TR-FTIR, giving way to a general applicable technique for label-free (bio) chemical reaction monitoring (Kaun *et al.,* 2006).

3. Materials and methods

Liqued culture experiments were performed for studying the effect of two filamentous strains (*S. commune* and *S. acidiscabies*) on two sheet silicates (NAu-2 and CCa-2), and also the effect of these minerals on the two strains. In this case, minerals as a powder material less than 2 µm were added to flasks containing the minimal medium (MM). Moreover, for studying the surface alteration of CCa-2, solid agar plates were prepared, and CCa-2 cut into small polished pieces was added to such plates.

3.1. Liquid culture flask Experiments

3.1.1. Silicate minerals as a powder material

(NAu-2) and (CCa-2) minerals were purchased from the clay mineral society, Purdue University, USA. Minerals were crushed using a hydraulic press (20 KN) until a fraction of 6 µm was obtained by adding deionized water to the slurry in a stirrer. To separate fractions less than 2 µm Atterberg cylinders were used, and fractions at end were freeze dried. Table 3 lists the chemical analyses of the < 2 µm fraction of the two sheet silicates (NAu-2 and CCa-2) measured by x-ray fluorescence (XRF).

Table (3) Major oxide chemistry for the < 0.2 µm size fraction of NAu-2 and CCa-2.

	P_2O_5 (%)	K2O (%)	CaO (%)	MgO (%)	MnO (%)	Fe_2O_3 (%)	Al_2O_3 (%)	TiO_2 (%)	SiO_2 (%)	Total (%)
NAu-2	0,01	0,03	2,78	7,45	0,01	64,44	0,49	0,13	24,17	99,51
CCa-2	0.15	0.12	<Nwg.	52.61	0.07	7.13	16.30	1.09	22.35	99.82

3.1.2. Strains and culture media

Two main microorganisms were used in this study; the filamentous bacterium (*Streptomyces acidiscabies* E13) and the filamentous fungus (*Schizophyllum commune* 12–43). Members of the genus Streptomyces are Gram-positive actinobacteria and the species *S. acidiscabies* is a well-known microorganism for low pH soils. *S. acidiscabies* E13 strain was isolated from soil samples of a heavy metal polluted site at the former uranium mining site, Ronneburg in eastern Thuringia, Germany (Amoroso *et al.,* 2000). The *S. acidiscabies* E13 strain expresses some enzymes like superoxide dismutase for tolerating heavy metals (Schmidt *et al.,* 2007), three different hydroxamate siderophores (Dimkpa *et al.,* 2008), and they also produce "Geosmin", an earthy-smelling substance, which has been isolated from several actinomycetes (Gerber and Lechevalier, 1965). The eukaryotic, basidiomycete fungus *S. commune* is used as a model organism for basidiomycetes and is distributed ubiquitously. *S. commune* is a very successful wood decaying fungus that causes white rot through excreting copper-containing oxidase enzymes called "Lacasses", which are able to degrade lignin (De Vries *et al.*, 1986). They produce in submerged culture medium small cysteine-rich hydrophobic proteins called "Hydrophobins" (Wessels *el al.*, 1991). The strains *S. acidiscabies* E13 and *S. commune* 12–43 used are from the strain collection of Microbial Phythopathology at the University of Jena. Both strains were grown in their MM; which was for the *S. acidiscabies* strain as follow (0.5 g/l L-asparagine, 0.5 g/l K_2HPO_4, 0.2 g/l $MgSO_4$, 0.01 g/l $FeSO_4$, 10 g/l glucose). $FeSO_4$ was not added to the MM of *S. acidiscabies* in order to force the microorganisms to get the amount of iron they need from the clay minerals. The medium is usually neutral after being prepared. The MM of *S. commune* was (20 g/l glucose, 2 g/l aspartat, 1 g/l K_2HPO_4, 0.5 g/l KH_2PO_4, 0.5 g/l $MgSO_4$, 120 mg/100 ml thiaminium chloride), the medium is usually acidic, and the pH have to be adjusted to 6.3 by NaOH. Two fungal strains which produce melanin; *Ceratocystis polonica* and *Alternaria brassicola* were used to test the role of melanin in protecting microorganisms from heavy metals released from the two minerals (CCa-2 and NAu-2).

3.1.3. Sterilization

Gentle sterilizing methods like UV light or Microwave were not effective in sterilizing the mineral material when it was in the powder form, so adding the minerals to the prepared MM to be autoclaved together was the best alternative. XRD was done for clinochlore (CCa-2) and nontronite (NAu-2) after and before autoclaving to see if sterilizing by autoclaving has any effect on the mineral structure or not. 1 g of each mineral (CCa-2) and (NAu-2) was added in 500 ml flask containing 200 ml of the (MM) of the *S. acidiscabies* strain, and another 1 g of each mineral (CCa-2) and (NAu-2) was added to the MM of *S. commune* strain. Both minerals within the MM were sterilized by autoclaving together. It is important to mention that sterilizing the clay mineral alone as a dry powder, then spreading it over a rich medium Luria broth (LB) agar plates to confirm complete sterility by the lack of bacterial growth (Furukawa and O'Reilly, 2007) was not the appropriate method, because it was found that even if the plates were clean and sterile for 10 continuous days, once the sterilized clay mineral is added to the liquid medium culture, spore forming organisms start to flourish and grow, which was also the case by (Perdrial *et al.,* 2009). However, when clay mineral was added after preparing the medium and autoclaved together, no contamination was detected.

3.1.4. Inoculate preparation

After growing the *S. acidiscabies* on minimal medium solid agar plates with vents for aeration as the microorganisms grow aerobically, a loop was taken and immersed in 20 ml minimal medium liquid cultures prepared in 50 ml flasks. The culture was left for three to four days on the shaker at 28°C incubation room to make sure that there is no contamination, by checking the turbidity of the culture. After four days, the culture was pure, then 2 to 3 ml of the culture were added to each of the 200 ml MM (*S. acidiscabies* E13) liquid culture flasks which contains the minerals (CCa-2) and (NAu-2) separately. For the *S. commune* 12-43 strain which was grown on an old plate, then was cut into small pieces which were ground in a sterilized blender with a little amount of the MM. The grounded mixture was poured back to the sterilized flask and left for three to four days also for checking contamination, 2 to 3 ml of the culture were added to MM (*S.commune*) culture mediums which contains the minerals (CCa-2) and (NAu-2) separately. The rest of the inoculum was kept at the -20ºC freezer after mixing cultures with 60%glycerol.

3.1.5. Sampling

For measuring the release of elements during the incubation period, Inductively Coupled Plasma Optical Emission Spectrometry (ICP-OES) was used. Before adding the inoculums to the MM containing the minerals, sample zero was taken to determine the initial concentration of the elements. After adding the inoculums, samples were taken periodically each week and for two continuous months as following: aliquot of 10 ml were sampled from different minerals (NAu-2 & CCa-2) in the MM. The extracted liquid aliquots were centrifuged at 4000 rpm at 4°C for 45 min. to settle down the mineral particles, then filtered through 0.2 mm sterile (Sartorius) filter, the supernatant was finally acidified with 100 ml HNO_3 (65%) to stabilize the dissolved ions. The prepared samples were restored in a refrigerator (4–6°C) and the concentration of different elements was then measured by ICP-OES all on one day to minimize instrumental variations. The dissolved Si and other elements in the aqueous phase were used to monitor the dissolution of the mineral. At the same time pH was measured weekly after sampling before acidifying the samples. Same sampling steps were done for the control flasks which contain only autoclaved minerals without incubation with any microorganisms. Microbial pellets which were formed during the incubation period were fixed and scanned by SEM. The pellet of the samples which was taken at the end of the experiment, was dried in an oven at 37°C, and then grounded to be tested with different analytical technique like XRD, Raman spectroscopy, and SEM to compare the change of the powder material of the sheet silicates after and before incubation.

3.1.6. XRD

The evolution of clay mineral structure and the formation of secondary phases were monitored by XRD. The dried material was resuspended five times for 1 min in an ultrasonic bath in 150 mL of a 1 M $SrCl_2$ solution. Saturation with Sr^{2+} was used to ensure the presence of two water layers in the expandable layers under XRD data collection conditions. To promote complete cation exchange, the suspensions were stored after the ultrasonic treatment for 4 h at 50°C. After this procedure, the sample was washed five times with 150 mL of deionized water. After washing the samples, the solid material was used to prepare the XRD slide. Oriented slides were prepared by pipetting a slurry of Sr-saturated samples on a glass slide and drying it at room temperature for a few hours to obtain an air-dried preparation. Ethylene glycol solvation was achieved by exposing the oriented clay slides to ethylene glycol vapor at 60°C for 12 h. XRD scans were recorded on a Bruker D8 diffractometer (Cu radiation at 40 kV and 40 mA).

The measuring range was from 2° to 60° 2θ with a step size of 0.04° and 6 s counting time. The divergence slit, the two Soller slits, the antiscatter slit, and the resolution slit were 0.5°, 2.3°, 2.3°, 0.5°, and 0.06°, respectively.

3.1.7. Raman spectroscopy

The Raman scattering was excited by a frequency doubled Nd: YAG laser at a wavelength of 532 nm with a laser power between 0.5 and 1 mW incident on the sample. The laser beam was focused on the sample by means of a Leica PLFluotar 100X/0.75 microscope objective down to a spot diameter of approximately 0.7 µm. The Raman scattered light was detected by a Peltier-cooled charge coupled device (CCD) detector. The integration time for one Raman spectrum ranged from 100 to 300 s. The low values for the laser power and the relatively short acquisition times were chosen to avoid any possible changes in the samples. Scans were taken by 6 cm^{-1} spectral resolution.

3.1.8. SEM of microbial pellets

The mycelial growth of filamentous microorganisms under submerged conditions in liquid medium with agitation leads to the formation of microbial pellets. These pellets formed by the filamentous microorganisms are usually spherical or ellipsoidal masses of hyphae with a variable internal structure. This structure might be loosely packed hyphae, forming fluffy pellets, to tightly packed, compact, dense pellets (Yanagita and Kogane 1963). It is true that submerged conditions of microorganisms are quit far from their growth in the natural soils, spherical pellet could be regarded to some extent as three dimensional version of fungal colony grown on the surface of solid medium (Fomina and Gadd, 2002). The importance of studying the morphology of the microbial pellets and the effect of minerals on its morphology is that they can be used for biosorptive detoxification of heavy metal and radionuclide-containing industrial effluents (Gadd, 2000; Abd El-Rahim and Moawad, 2003). Microbial pellets which were formed with both minerals (NAu-2 & CCa-2) were washed with phosphate buffered saline (PBS) pH 7.4, and slightly centrifuged at 100 g for 2-3 times. For chemical fixation of pellets, 2% glutaraldehyde in PBS was used for 1 h., then washed with PBS for 3 times, then pellets were left to sediment on a glass holder. A series of ascending ethanol concentration from 30% up to 100% was then used, after that critical point drying using liquid CO_2 was used to remove all the ethanol, microbial pellets were sputtered with gold, and were ready for SEM.

3.1.9. Bradford protein assay

To test whether the two strains have produced enzymes or extracellular proteins, which might play a role in mineral dissolution or if they are assisting in the precipitation of new mineral (Chan *et al.,* 2004), the Bradford protein assay was done by taking 25 ml from each different sample; *S. acidiscabies* strain inoculated with both NAu-2 and CCa-2 and *S. commune* strain incubated with both minerals. Samples were centrifuged for 20 min., then the supernatant was transferred to a certain white centrifuge tubes, and equal volume of (20% trichloroacetic acid (TCA) / 50% Acetone - 20 Mm dithiothreitol (DTT)) was added to the centrifuge tubes, and kept in the –20°C for 20 min. then for 2 h at 4°C. Samples were centrifuged after that for 20 min. at 11000 rpm at 4–20°C. Supernatant was discarded, and the pellets were redissolved in 1 ml cooled acetone (kept at -20°C). Pellets washed with acetone were centrifuged at 1400 rpm at 4°C. The last step was repeated from three to five times. After the last time of washing, pellets were resuspended in 50 Mm NaH_2PO_4 buffer. Bradford protein assay was conducted using concentrations of 0, 2, 4, 6, 8, 10 µl of the sample + 200 µl of the Bradfold dye. Mixture was incubated with each other for 10 min., and then measured by a spectrophotometer at wavelength 595 nm. Same steps were done also on pure *S. acidiscabies* and pure *S. commune* grown alone in MM to be used as a control.

3.1.10. FTIR

3.1.10.1. FTIR spectromicroscopy

FTIR experiments were carried out using the endstation of beamline X01DC at the Swiss Light Source. The endstation comprises a Bruker (Bruker Optics, Billerica, MA) Vertex 70/v interferometer coupled to a Hyperion 3000 IR microscope. A 15 x magnification Schwarzschild objective was used to focus IR light on the sample and collect the reflected beam. A KBr supported Ge-multilayer beam splitter and a single element MCT detector were used to measure spectra in the mid-infrared spectral region. Very small parts of the pellets of *S. acidiscabies* and sometimes complete small pellets were added between two (1 mm thick) CaF_2 optical windows separated by a polytetrafluoroideethylene (PTFE) spacer with a nominal thickness of 15 µm. The aqueous phase was transferred to the holder together with the pellet fragments. The absorbance spectra were measured between 4000 and 400 cm^{-1} at a spectral resolution of 4 cm^{-1} with 128 scans. Measurements were performed in transmission Spectral maps were obtained using 15 x objective and a 50 μm^2 aperture with a step length of 25 µm,

using the corresponding electrolyte solution as background to eliminate IR peaks arising from the medium and non organic components. Data were analyzed after converting absorption spectra to their second derivatives to allow for more accurate comparison by reducing baseline effects. Graphs were prepared using OPUS 6.5.

3.1.10.2. Attenuated Total Reflectance (ATR-FTIR)

ATR-FTIR at the Karlsruhe Institute of Technology (KIT), Institute for Nuclear Waste Disposal was used to get information about structural changes which might occur to the minerals by the effect of the *S. acdicscabies* and *S. commune* strains. A Bruker Tensor 27 spectrometer, equipped with a DLaTGS (deuterated lanthanum triglycine sulphate) detector was employed to obtain the IR-spectra. 64 scans in the 4000 – 400 cm^{-1} spectral range were recorded with a scanner velocity of 10 kHz and a resolution of 4 cm^{-1}. For the ATR measurements a Platinum ATR single reflection diamond cell (Bruker Optics) equipped with gold mirrors was used. The sample preparation was very easy. For the measurements a small amount of powder was pressed on the diamond surface by a sapphire tipped anvil. No further treatment was applied to the samples before measurement.

3.2. Solid agar plate experiments

3.2.1. Polished minerals

CCa-2 was cut into small pieces with DISCOPLAN TS supplied by a diamond saw blade. Sanding was done on three stages using silicon carbide slices with different mesh sizes (starting by 65 µm and ending by 5 µm for fine sanding). High quality polished surfaces were achieved by using Microtex 550 HC PSA supplied by a polished cloth for diamond polishing. Polished pieces were masked by (permatex blue), which has no effect on minerals surfaces and was very stable when the mineral pieces were autoclaved. Masking was performed to be able to compare between surfaces exposed to microbial or chemical treatments and the masked surfaces. The NAu-2 was too fragile to be cut into small pieces, and that is why the solid agar plate experiments were only performed using the CCa-2 mineral.

3.2.2. Sterilization

Polished pieces were added to small eppendorf tubes to be sterilized by autoclaving. Sterilized pieces were added to the MM solid agar plate for *S. acidiscabies* strain and to the MM of *S. commune* strain Pieces were left in the agar plates for two days without adding any strains for checking contamination. Plates were clean and ready to be inoculated.

3.2.3. Adding inoculants

Few drops from the liquid culture of the *S. acidiscabies* strain were added over each polished CCa-2 pieces. For the *S. commune* the strain which was grown on an old plate were cut into small pieces and added around the polished sterilized CCa-2 pieces in the MM, however the growth of *S. commune* strain was very weak on its MM, that is why the strain was added to complex yeast medium (CYM) solid agar plates composed of (2 g/l trypticase peptone, 2 g/l yeast extract, 20 g/l glucose, 0.5 g/l $MgSO_4$, 0.5 g/l KH_2PO_4, 1 g/l k_2HPO_4, 18 g/l agar) to enhance the strain's growth. The two strains were left for incubation at 28°C for two months (Fig. 14).

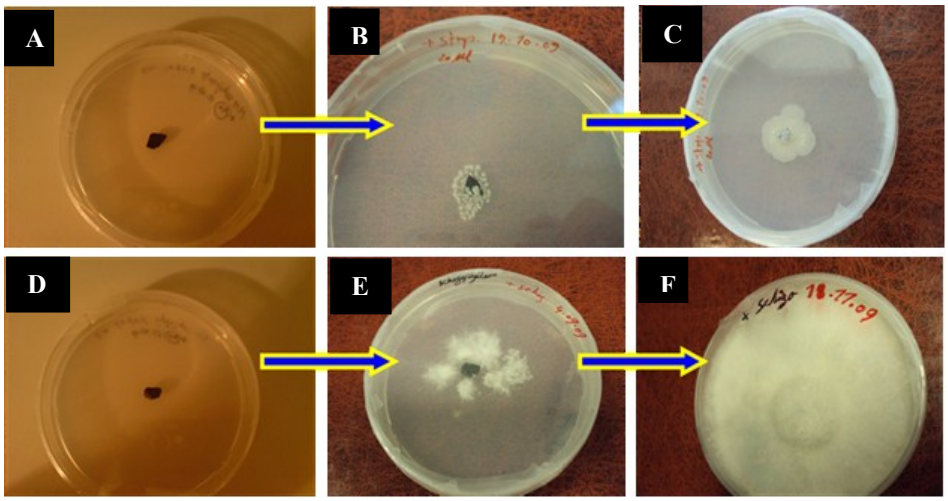

(Fig. 14) CCa-2 polished sterilized pieces on solid agar plates incubated with both strains; *S. acidiscabies* (A, B, C) and *S. commune* (D, E, F).

3.2.4. Addition of organic and inorganic acids

Nitric (HNO_3 -65%) and sulphuric acid (H_2SO_4- 96%) were used as inorganic acids, while 0.1 M of oxalic ($H_2C_2O_4$) and citric acid ($C_6H_8O_7$) were used as organic acids for their chelating

properties, which are similar to what is produced by microorganisms. Several drops of each acid were added regularly over the polished sterilized pieces for two continuous months.

3.2.5. Removal of microorganisms

In order to study biosignatures on mineral surfaces, safe removal of microbial matter must be guaranteed without causing any chemical or physical change to the surface. Buss *et al.,* 2003 have tried four different detergents, which were chosen according to their previous use as bactericides followed by acetone; 2% (v/v) sodium dodecyl sulfate (SDS), 1% (v/v) Triton X-100, 5mM sodium pyrophosphate (SPP) ($Na_4P_2O_7$. 10 H_2O), and 5 mM sodium tetraborate (borax, $Na_2B_4O_7$. 10 H_2O), in addition to CO_2 snow cleaning method where a flow of CO_2 snow particles moves in a high velocity CO_2 gas. They found that the four detergents tested can be a viable option for bacterial removal, but for surface chemistry analysis, they recommended the pH-neutral, anionic detergent SDS. Lysozyme was also tried before, however, residual matter was observed when lysozyme treated surfaces were analyzed in nanoscale by AFM. So after the end of the incubation period, polished pieces were removed by a forceps and submerged in 2% SDS solution and were left on a shaker for two continuous days, then washed with acetone and finally with distilled water before being analyzed by SEM, AFM and VSI.

4. Results

4.1. Liquid culture flask Experiments

4.1.1. ICP-OES

Elements measured by ICP-OES (Fig. 15), showed rapid release of Mg from the interlayer sites of CCa-2 and Ca from NAu-2 in the inoculated and non-inoculated. The solution chemistry of Mg and Ca from both minerals by both microorganisms had varied over the incubation time. The release of Mg for example from CCa-2 had decreased at the end of the incubation with *S. acidiscabies* strain then increased again (Fig. 15 A). Ca released from NAu-2 had also decreased then increased but at the beginning of the incubation with both microorganisms (Fig. 15; E&G). The Si released from CCa-2 and NAu-2 by *S. acidiscabies* strain was almost double the amount released from non-inoculated minerals (control), and was more than the amount of Si released by the *S.commune* strain.

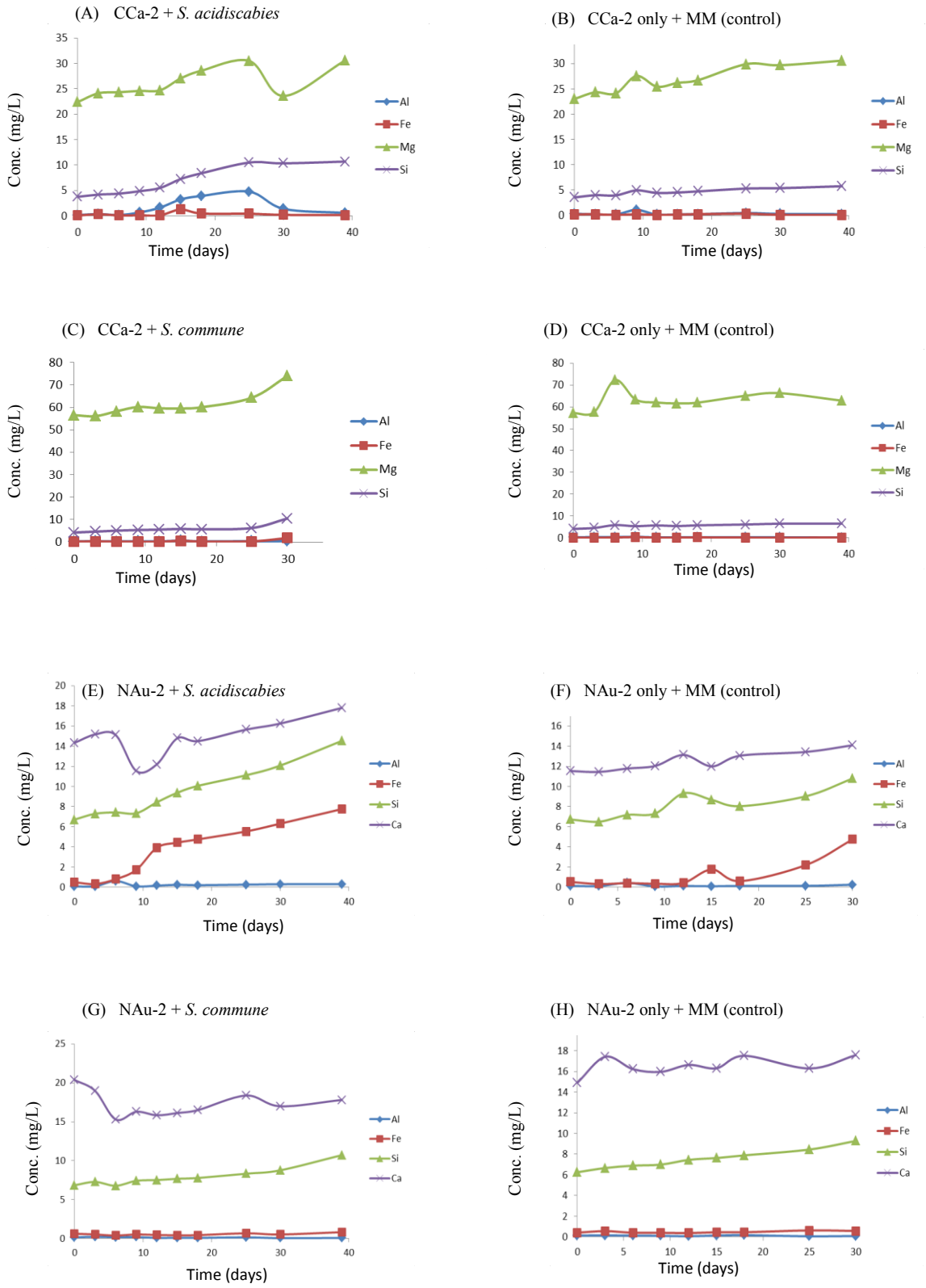

(Fig. 15) ICP-OES measurements of samples taken from flasks containing CCa-2 inoculated with both strains *S. acidiscabies* and *S. commune* (A & C) and the non-inoculated CCa-2 (B & D); and from flasks containing NAu-2 inoculated with the same two strains (E & G) and the non-inoculated NAu-2 (F & H).

The release of Fe from NAu-2 by *S. acidiscabies* strain was higher than the non-inoculated mineral and higher than the Fe released by *S. commune* strain. However, the amount of Fe released from CCa-2 by both microorganisms was very low. The release of Al by S. *acidiscabies* strain from CCa-2 (Fig. 15 A) was more than from NAu-2 (Fig. 15 E), however its concentration decreased again in the solution. The release of Al from the two minerals by the *S. commune* strain was very low.

4.1.2. pH measurements

S. acidiscabies strain produced some acids which might have lowered the pH while incubated with CCa-2 and NAu-2, and even when they were grown alone in the MM (Fig. 16; A, B, C). The pH of CCa-2 incubated with *S. acidiscabies* strain was neutral at the beginning (pH 6.5), then decreased to (pH 4.7), and finally increased again to (pH 7.7). For NAu-2 incubated with *S. acidiscabies* strain, the pH was also neutral at the beginning, then decreased to (pH 4.2), and stayed constant ~ (pH 4) to the end of the experiment. Negative controls, where CCa-2 and NAu-2 added to the MM without any inoculum had neutral pH during the whole time of the experiment (Fig. 16; D & E). The pH of *S. commune* strain with both minerals in addition to the negative controls was always neutral too.

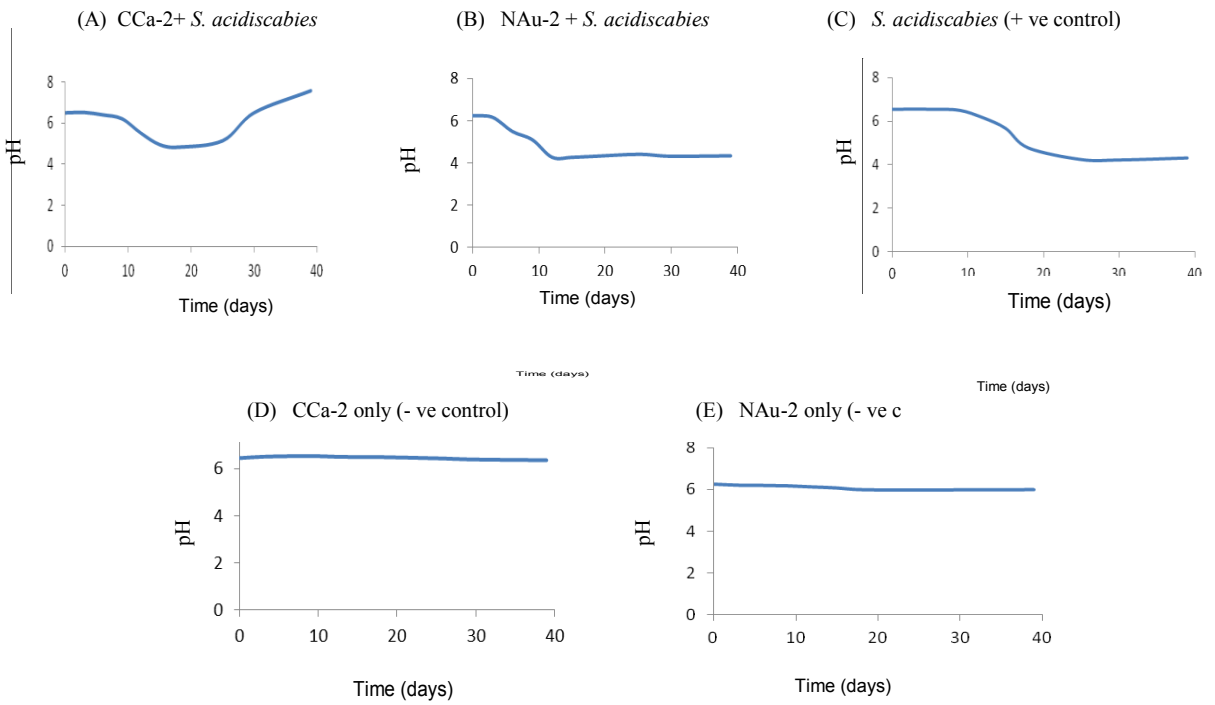

(Fig. 16) pH of *S. acic* Time (days) (A), with NAu-2 (I Time (days) in MM (C). pH of negative controls; CCa-2 (D), a

4.1.3. XRD analysis

XRD spectrum showed no difference between the original and the autoclaved CCa-2 whether air dried or glycolated. The same result obtained with NAu-2. The d spacing of the NAu-2 (air dried) for the 001 peak around 6.46º (2θ) was ~14 Å, and hasn't changed when NAu-2 was autoclaved. When both (original and autoclaved) NAu-2 were glycolated, the 001 peak was shifted to the left at 5.2 º (2θ), and the d spacing expanded to ~ 17 Å (Fig. 17). In case of air dried NAu-2 incubated with *S. commune* strain, the 001 peak was shifted to the right and the d spacing collapsed from 13.7 Å to 12.6 Å (with *S. commune*) and to 11.9 Å for the control (without schizo.), in addition to that, the intensity of the 001 peak decreased and its width has broadened and become asymmetric (Fig. 18).

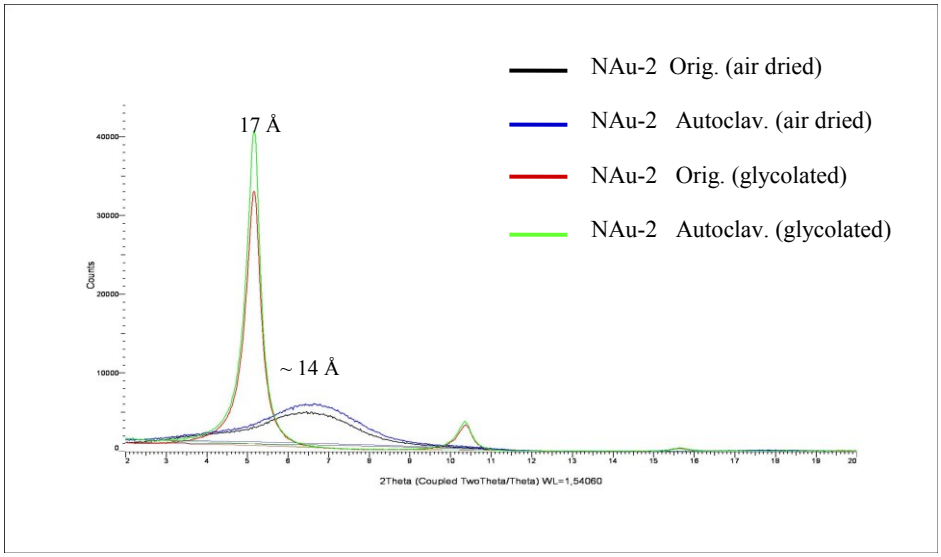

(Fig. 17) XRD for autoclaved and non-autoclaved NAu-2 (air dried and glycolated).

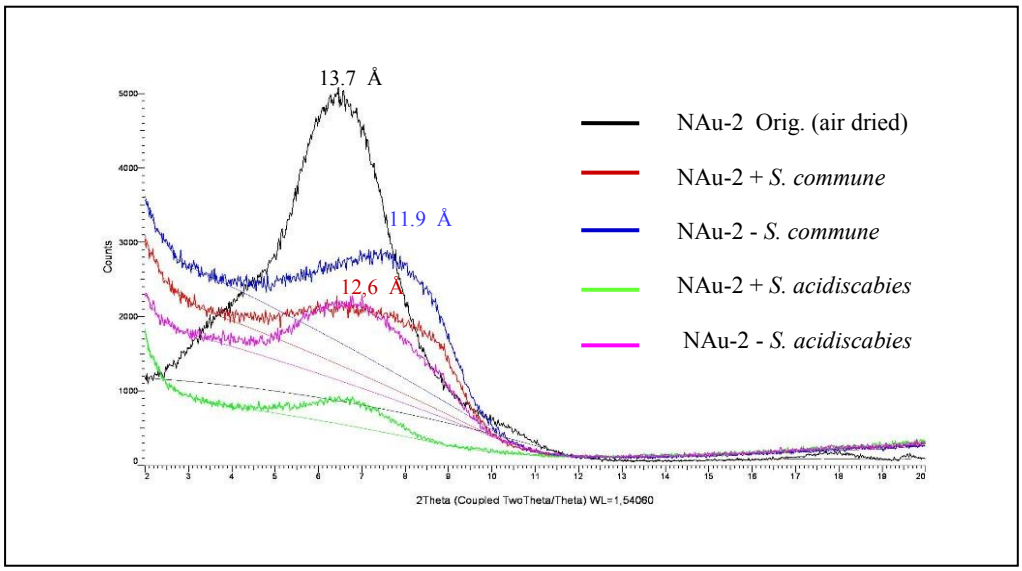

(Fig. 18) XRD for air dried NAu-2 incubated with both strains *S. commune* and *S. acidiscabies* and NAu-2 alone in both MM without inoculum.

In case of NAu-2 incubated with *S. acidiscabies*, there was no shift in the 001 peak, however the intensity decreased for the control (without inoculum), and decreased more and was almost flat for the inoculated sample. It is important to note that the scattered intensity primarily depends on the amount of scattering material, which was not controlled. The glycolated NAu-2 with both strains and their control had also expanded and the d spacing of the 001 peak increased to 17 Å. However, the intensity of the peak decreased in the following order, NAu-2 - *S. commune*, NAu-2 + *S. commune*, NAu-2 - *S. acidiscabies*, then finally NAu-2 + *S. acidiscabies* (Fig. 19).

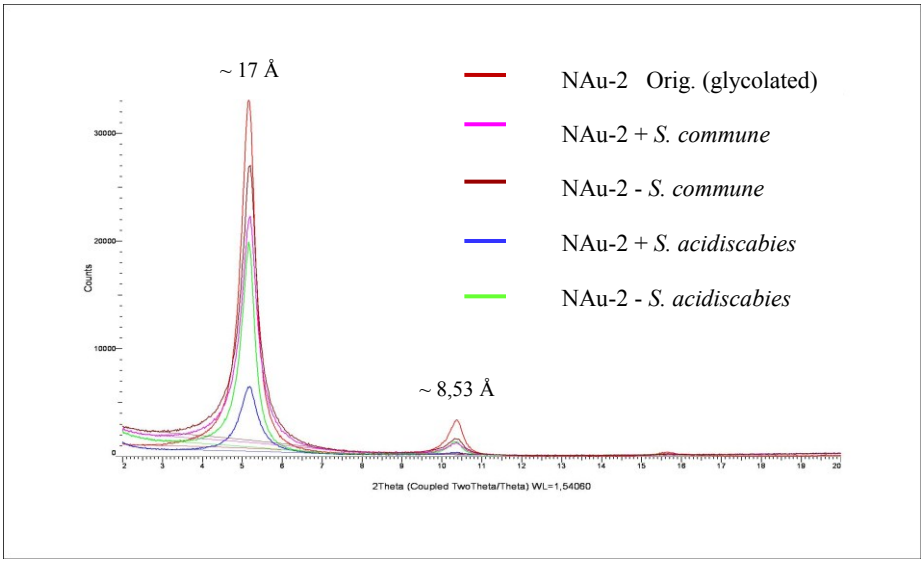

(Fig. 19) XRD for glycolated NAu-2 incubated with both strains *S. commune* and *S. acidiscabies*

There was no difference between XRD spectra of CCa-2 (air dried and glycolated) after and before incubation with both strains (*S. acidiscabies* and *S. commune*) as shown in (Fig. 20).

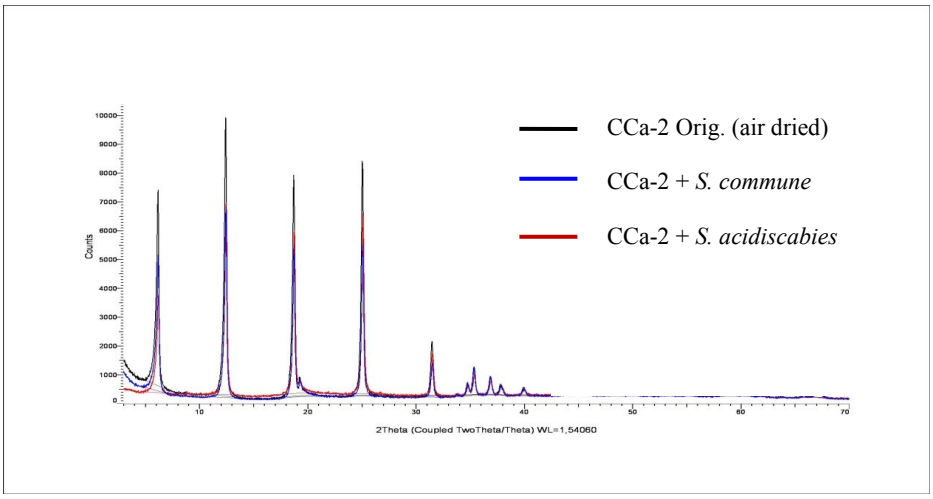

(Fig. 20) XRD spectrum of CCa-2 (air dried) before and after incubation with both strains (*S. acidiscabies* and *S. commune*).

4.1.4. Raman spectroscopy

Raman spectroscopy is good tool for mineral identification and its transformation to another mineral. Raman spectroscopy was able to detect NAu-2 after its incubation with both microbial strains, indicating that NAu-2 hasn't transformed to another mineral by the effect of microorganisms. The Raman images of the NAu-2 incubated with the *S. acidiscabies* strain showed the presence of flocs and big particulates (Fig. 21 A) which was not the case with the *S. commune* (Fig. 21 B)

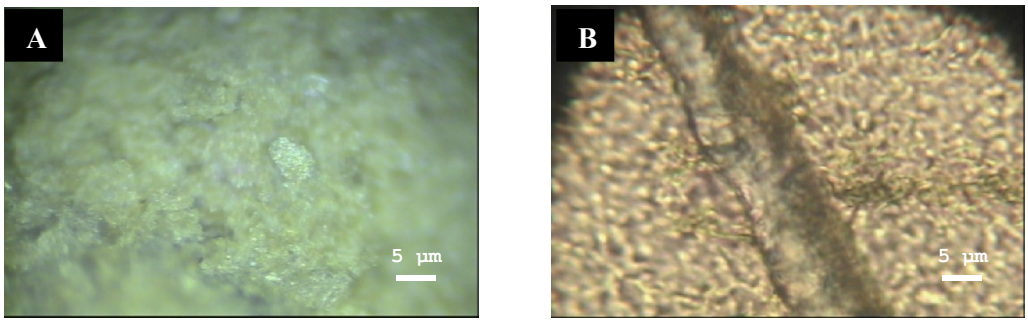

(Fig. 21) Raman images showing NAu-2 flocs when incubated with; *S. acidiscabies* (A), but no NAu-2 flocs with *S. commune* (B).

Only the NAu-2 could be characterized using Raman spectroscopy. In case of CCa-2 (whitish material), the fluorescence of the sample covered completely the weaker Raman signal. However, a rough powder material for CCa-2 incubated with the *S. acidiscabies* was also noticed when the powder was spreaded over one of the XRD holders (Fig. 22 A). When CCa-2 was incubated with the *S. commune*, the powder mineral was very fine like the original material without any microorganisms (Fig. 22 B).

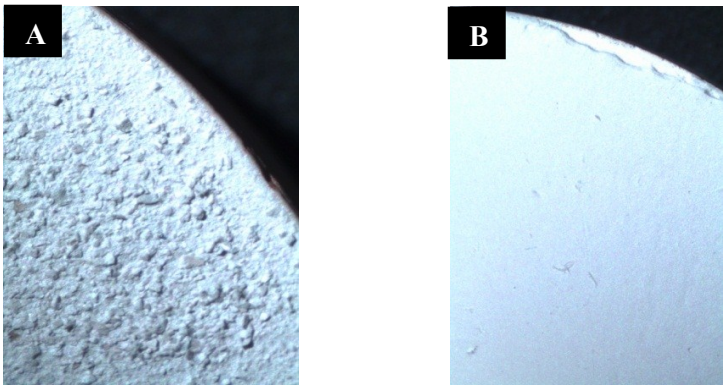

(Fig. 22) Rough CCa-2 particles spread over XRD holder when incubated with; *S. acidiscabies* (A) and the original material without treatment (B).

4.1.5. SEM of microbial pellets

The filamentous hyphae of the *S. acidiscabies* strain incubated with CCa-2 formed at the beginning irregular pellets (Fig. 23 A), but turned roundish after shaking for two months (Fig. 23 B), many mineral flakes were still present but burried under new precipitates (Fig. 23 C), while the hyphae were smooth (Fig. 23 D). Formed pellets of the same strain with NAu-2 were irregular at the beginning (Fig. 23 E) , then turned round (Fig. 23 F), but there were not too many mineral flakes present (Fig. 23 G) as if they were dissolved to a large extent, and the hyphae were encrusted (Fig. 23 H).

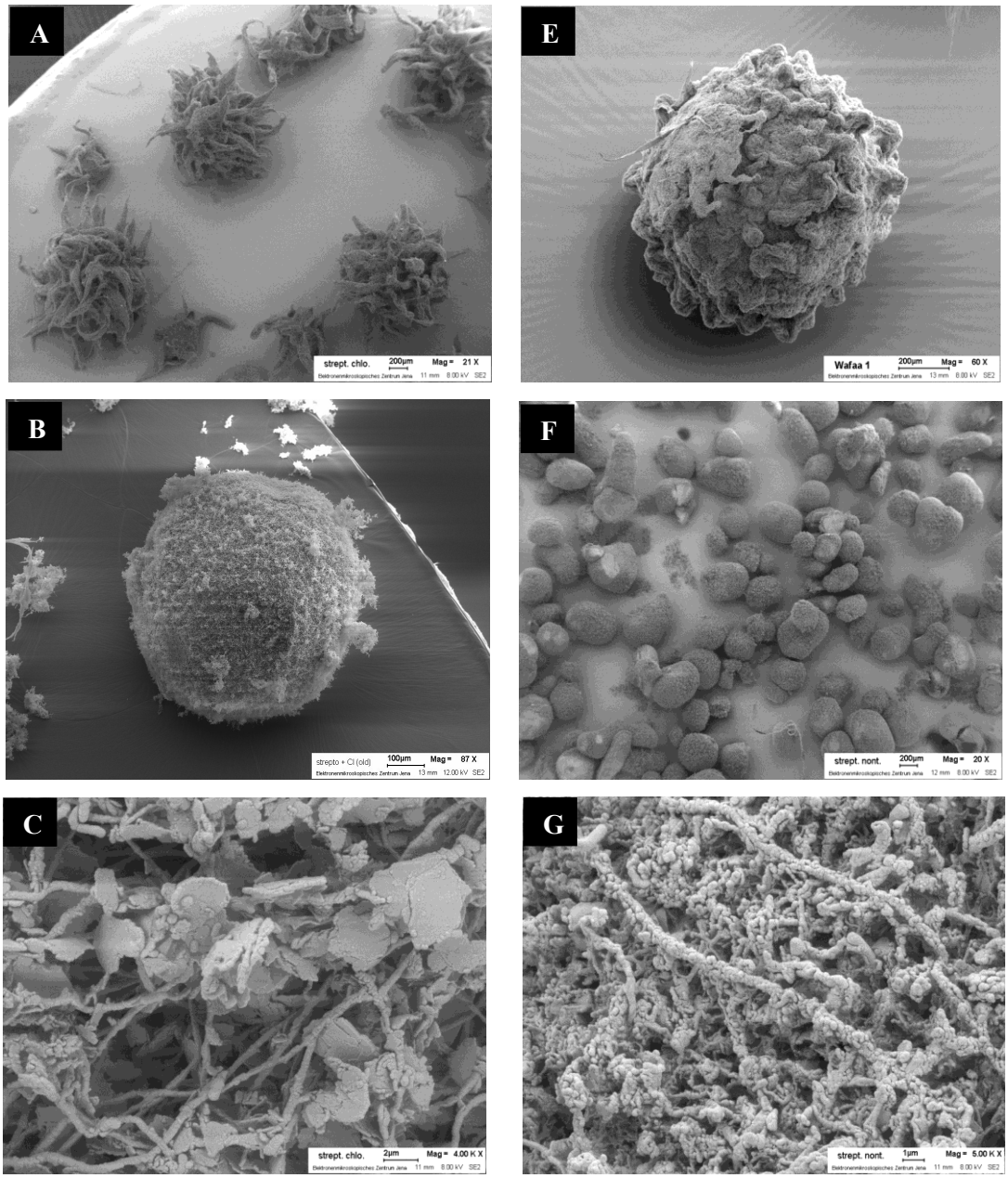

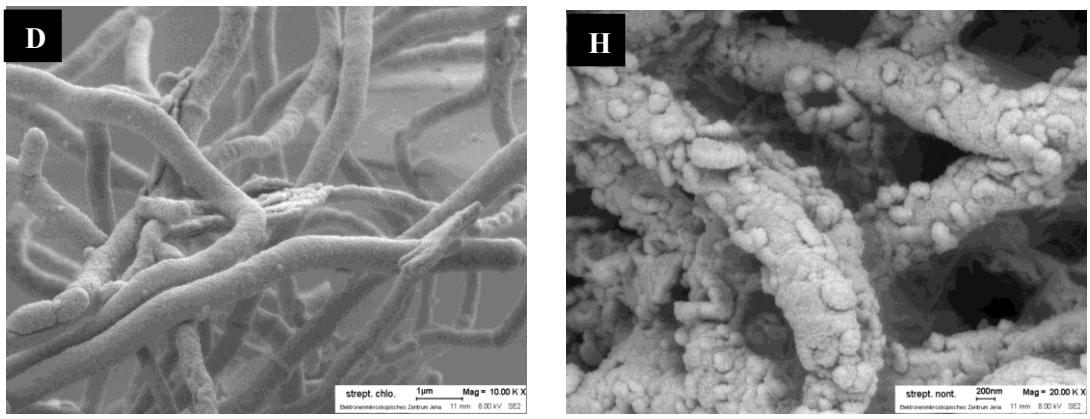

(Fig. 23) Microbial pellets of *S. acidiscabies* incubated with CCa-2 (A, B), mineral flakes are present (C) and the hyphae are smooth (D) and microbial pellets of *S. acidiscabies* incubated with with NAu-2 (E, F), no mineral flakes are present (G), and the hyphae are encrusted (H)

The *S. commune* strain hasn't formed any pellets when it was incubated with 1 g of each mineral, so we tried with less amounts of both minerals. With any amount of CCa-2 no pellets were formed, while with NAu-2 (0.25 g) only the mineral appeared as clay leaflets perpendicular to the hyphae, which were not really encrusted (Fig. 24 A & B).

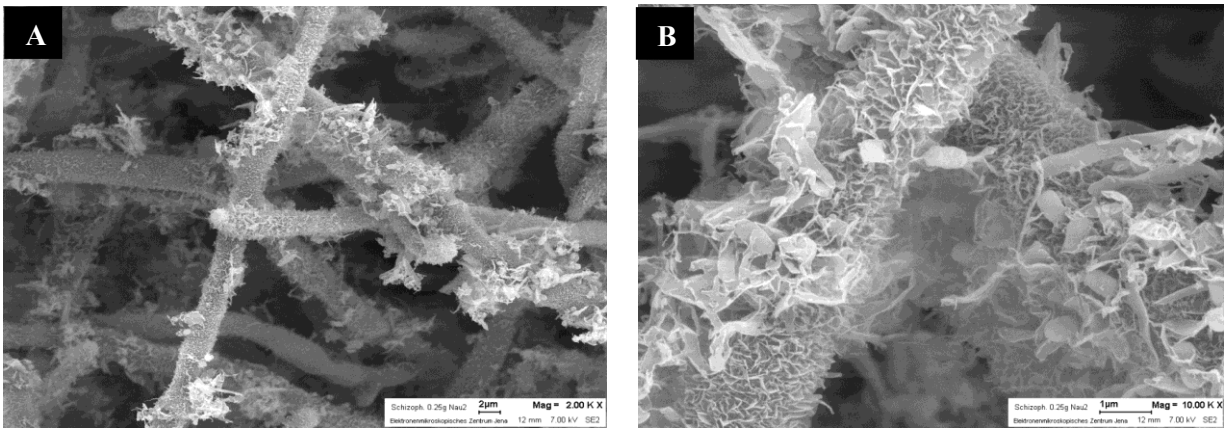

(Fig. 24) *S. commune* with 0.25 g NAu-2 (A), mineral flakes appearing perpendicular to the hyphae (B)

4.1.6. Bradford protein assay

Both strains (*S. commune* and *S. acidiscabies*) incubated with NAu-2 turned the color of the dye to blue indicating high amount of protein produced in the medium solution. While in case of both strains when incubated with CCa-2, the color of the dye hasn't changed (Fig. 25 A & B). Pure strains growing alone in the MM haven't also changed the color of the dye.

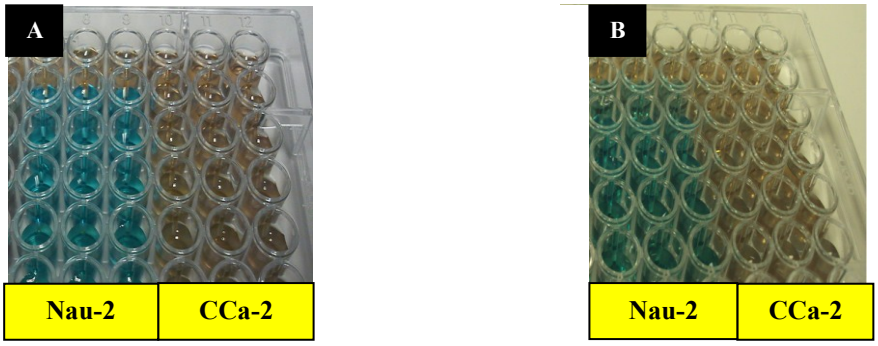

(Fig. 25) Color of the dye has changed with NAu-2 only and not with CCA-2 when both minerals were inocubated with *S. commune* (A), and with *S. acidiscabies* (B).

4.1.7. FTIR spectromicroscopy

FT-IR spectromicroscopy was used as a tool to detect some of the chemical changes induced by microorganisms when exposed to the sheet silicates CCa-2 and NAu-2. Because the *S. commune* strain couldn't form any pellets with 1 g of both minerals, it was excluded form this analysis. Samples of the *S. acidiscabies* strain cultures were collected at different intervals during their incubation and growth with the minerals for 2 months. Aliquots obtained from cultures at the early stages of growth were transferred to the sample holder. Aliquots obtained from cultures at later stages, containing large clay aggregates were first prepared by cutting the aggregates into smaller fragments, about 10-100 µm in size. By this way they could be pressed between the optical windows of the sample holder down to the nominal thickness of the spacer. It is worthwhile to notice that, due to the thickness of the residual particles of aggregates and the difficulty in compressing them, the effective sample thickness was often a few micrometers larger than the thickness of the spacer. The average spectra collected on samples from consecutive stages of culture growth are shown in (Fig. 26). The strong complex band between 900 and 1200 cm^{-1} is dominated by absorption bands assigned to the silicate groups (Si-O), which is present in the two sheet silicate minerals. Clay mineral bands overlap with the bands in this region due to C-O bonds absorption from polysaccharides (900-1200 cm^{-1}) and to symmetric stretching of P=O absorption bands (~ 1085 cm^{-1}) in DNA, RNA, and phospholipids giving rise to a complex multiplet. While the band at 1245 cm^{-1} refers to the asymmetric stretching of phosphodiester in phospholipids and nucleic acids. The absorption bands at 1380 and 1499 cm^{-1} are due to bending vibrations of the methylene groups.

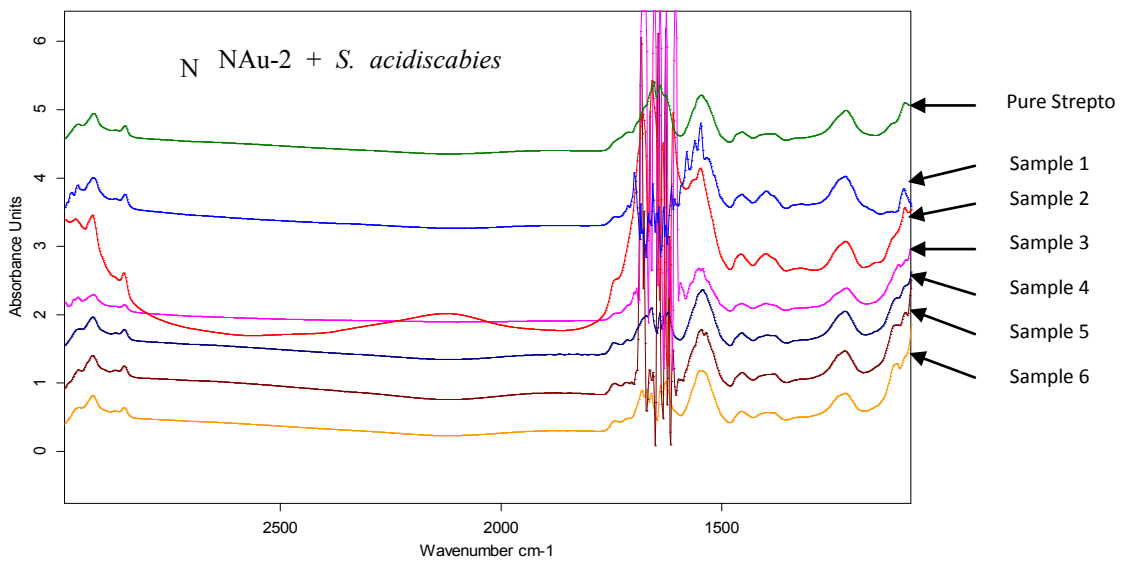

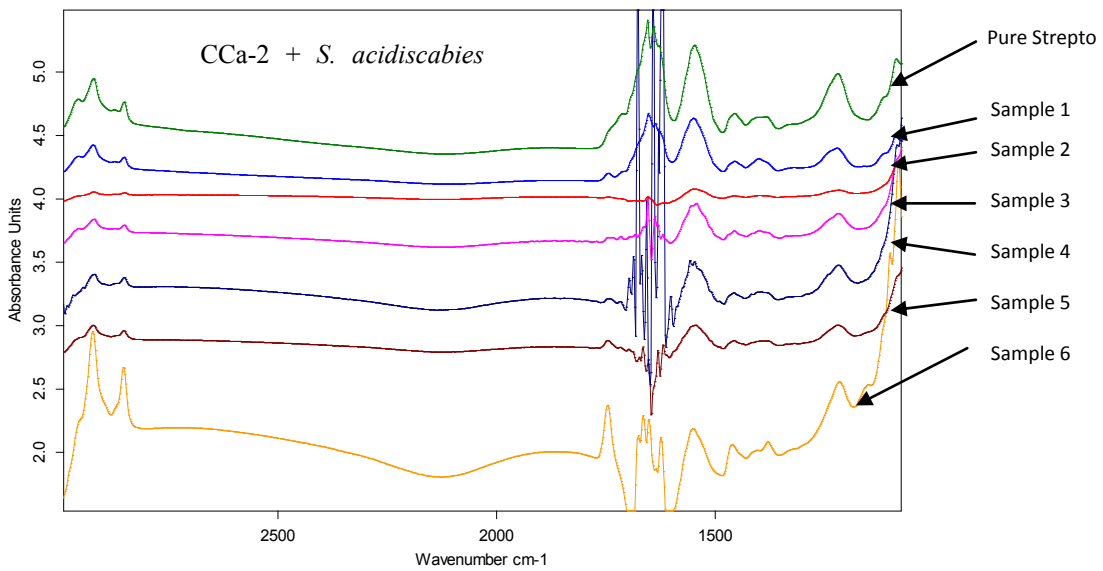

(Fig. 26) FT-IR spectra of samples collected from consecutive stages of *S. acidicscabies* growth culture with NAu-2 and CCa-2

The strong band peaking at about 1540-1550 cm^{-1} is due to the Amide II vibration from peptide groups. This is mostly due to a contribution of proteins produced by the organism. The intensity of the band indicates a large protein concentration in the sample and it is roughly correspondent to the mass of organism present. The Amide I band is also due to polypeptide molecules and falls in the region around 1650 cm^{-1}, which is dominated by water absorption. In these samples the contribution from water absorption is too strong and prevents observation of the Amide I. The band at 1744 cm^{-1}, sometimes associated to a weaker band at approximately 1715 cm^{-1} is the characteristic absorption from a carbonyl ester group. Cellular lipids showed

intensive duplicate absorption bands at 2850 and 2923 cm^{-1} corresponding to the respective symmetric and antisymmetric C-H_2 vibrations

4.1.8. ATR-FTIR

ATR-FTIR was used to get information about any structural changes that might have occurred to the NAu-2 after incubation with the two microbial strains. In the IR spectrum there are three different regions which are particularly relevant, namely, O-H stretching, O-H deformation, and Si-O stretching in the spectral ranges at 3000–3800, 550–950, and 800-1300 cm^{-1}, respectively. Table 4 shows band assignments for IR spectral features in smectites. The cationic composition of the unaltered NAu-2 octahedral sheet (Fe, Al, and Mg) implies the presence of at least 3 different OH-stretching bands due to FeFeOH, FeAlOH, and FeMgOH environments. The weak band at ~ 3638 cm^{-1} which is attributed to AlAlOH environment

Table (4) band assignments (cm^{-1}) for IR spectral features in smectites (Bishop *et al.*, 2002).

JP	Sampor	Rokle	Stebno	SAz-1	SWa-1	SWy-1	Paul	Stein	Goss	Land	App	Gram	Assignment
(426)	430	(427)	(427)	(427)	427	(421)	428	(428)	427	(427)	(426)	(426)	Si-O bend
(443)				(443)				455	(456)				Si-O bend
470	(453)	469	465	469	467	470	469		471	469	470	471	Si-O-Si deformation
	491				(493)			496	495				Fe-O-Si deformation
521	(530)	520	515	520	(520)	525	532		(524)	529	522	522	Al-O-Si deformation
629				628		627				628	627	628	Al-smectite
	678				681			~675′	(687)				Fe-smectite
	(785)				(784)			(759)	(760)				MgFeOH bend
	819		(822)		818			822	820				FeFeOH bend
	845				(844)								FeFeOH deformation
845				841	(844)	(848)				843	841	844	AlMgOH bend
(883)		877	872		875	878	(876)	(875)	873	(877)	880	880	AlFeOH bend
915		916	912	915	(919)	916	914	(915)	(919)	913	916	915	AlAlOH bend (Sm or K)*
1039	1019	1036	1032	1032	1032	1048	1037	1027	1032	1033	1043	1043	Si-O stretch
	3567	~3600	~3600		3570			3546	3567	(3596)			OH stretch in Fe-smectite"
3629				3620		3634	3626			3623	3628	3629	OH stretch in Al-smectite"
	4005				(4005)			4000					Fe-smectite
	4165				(4170)			4200	(4165)				Fe-smectite
4105		4105		4095		4090					4090	4090	Al-smectite
	4380	(4370)	4375		4375			4355	4370				FeFeOH comb.
		4465	4475		4475		4470		(4465)				AlFeOH comb.
4525	(4575)	4530	4530	4520	(4575)	4535	4535		(4555)	4535	4530	4530	AlAlOH comb.
	6980				(6970)			6920	(6960)				FeFeOH overtone
7070		7070	7080	7060	7090	7090	7080		(7080)	7080	7080	7080	AlAlOH overtone

(Fialips *et al.,* 2002 a) appearing in the original NAu-2 (Fig. 27) has vanished in the treated Nau-2 with the two strains as well as the negative control (where minerals were only added to the minimal medium without any microorganism). A very faint band at ~3589 cm^{-1} and refers to Fe^{3+}MgOH (Fialips *et al.,* 2002 a) appeared in the original NAu-2, but has vanished also in the different treatments. In the original mineral, the OH band is relatively at ~3552 cm^{-1} at maximum intensity and was at 3570 cm^{-1} in Fialips *et al.* (2002 b). This position is referred to

the dioctahedral Fe- bearing smectites with $(Fe^{3+})_2$ OH being the predominant OH environment (Russell *et al.* 1979). This band has shifted from 3552 to 3572 cm^{-1} in the treated Nau-2 with the two strains as well as the negative control. Water in high iron bearing smectites has been observed through the stretching mode at 3430 cm^{-1}.

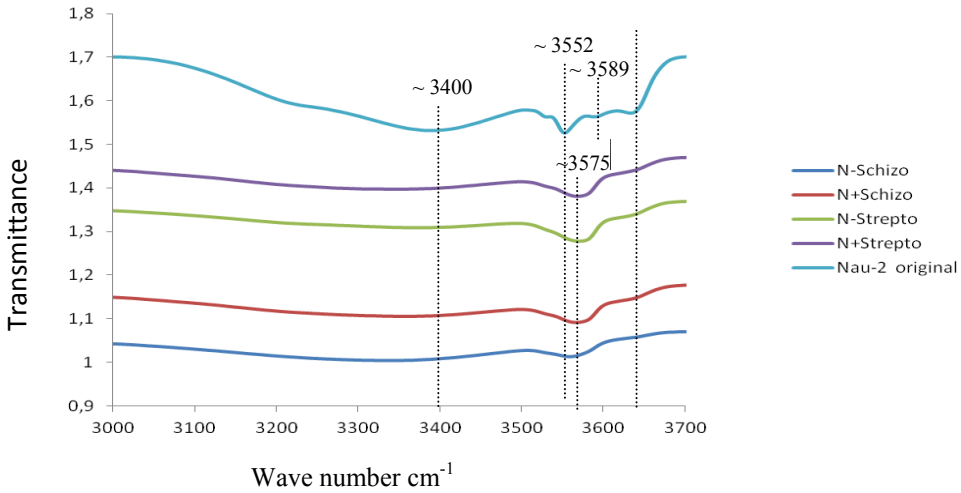

(Fig. 27) ATR-FTIR for the O-H stretching region of the NAu-2 incubated with *S. acidiscabies* and *S. commune* and their negative control.

The strong band appearing in the original NAu-2 at ~1630 cm^{-1} in (Fig. 28) refers to the H-O-H-bending band. This band's width has increased and its intensity has decreased very clearly in the two treatments with the two microorganisms in addition to their control. The Si-O basal and apical stretching modes generated the intense band at 1036 cm^{-1} and the shoulder at 1107 cm^{-1}, respectively. The intensity of the 1107 cm^{-1} band has decreased in the two treatments as well as in their control. Deformation bands belong to M-O-H (with M = Mg, Al, or Fe). The band located at 822 cm^{-1} is assigned to $(Fe^{3+})_2$ OH deformation (Stubican and Roy 1961; Farmer and Russell 1964; Farmer 1974). The 870 cm^{-1} band is attributed to deformation modes of Al Fe^{3+}OH (Russell *et al.* 1970; Farmer 1974). A new band ~850 cm^{-1} has appeared in the four spectra and was not present at the original NAu-2. Farmer (1974) and Goodman *et al.* (1976) suggested that the 790 cm^{-1} band was assigned to Fe^{3+}MgOH deformation, but this assignment is unlikely because NAu-2 contained only 0.05 Mg cations per formula unit (Manceau *et al.* 2000). So an alternative assignment for the 790 cm^{-1} band might be the Si-O vibration of a Si-rich admixture, such as amorphous silica, which absorbs near 790 cm^{-1}. The intensity of this band in the four spectra was higher than in the original NAu-2. According to Farmer (1974) the band at 677 cm^{-1} is attributed to Fe-O out-of-plane vibration. The

assignment of the 589 cm^{-1} band is uncertain but it may be due to a combined Si-O- Fe^{3+}-bending mode (Stubican and Roy 1961).

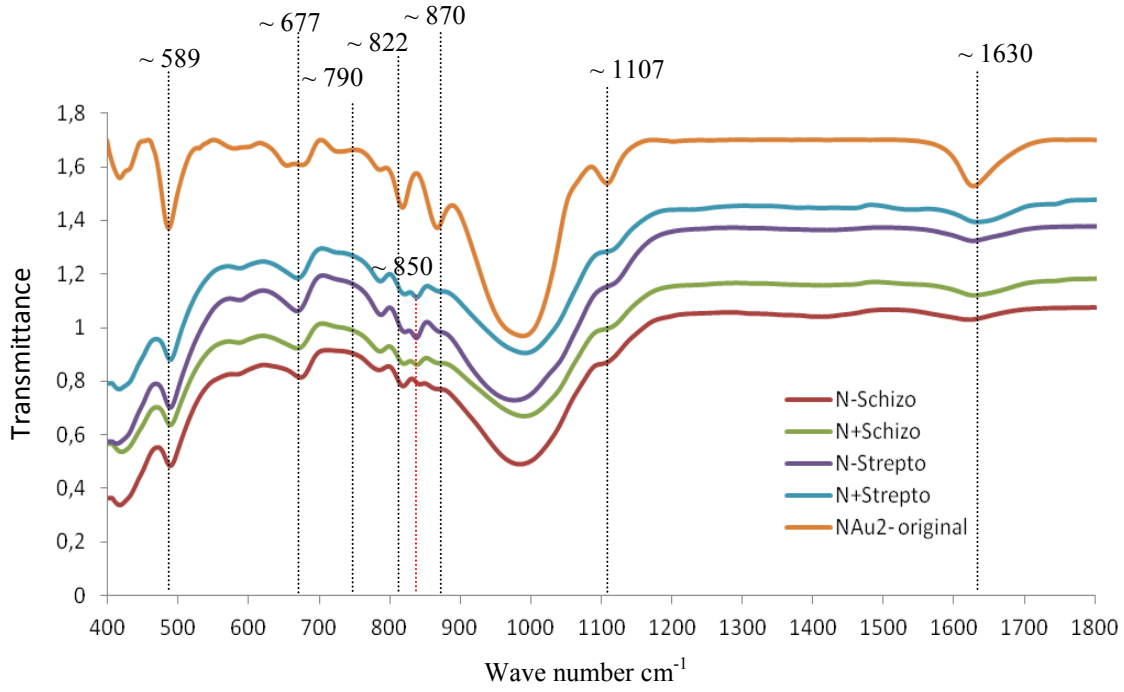

(Fig. 28) ATR-FTIR for the O-H deformation, and Si-O stretching region for NAu-2 incubated with both strains (*S. acidiscabies* and *S. commune*) and their negative control.

4.1.9. SEM of sheet silicates

The SEM images for CCa-2 as a powder material before incubation (Fig. 29 A & B), CCa-2 after incubation with *S. commune* (Fig. 30 A & B), and CCa-2 after incubation with *S. acidiscabies* (Fig. 31 A & B) haven't revealed any differences in the minerals morphology after incubation with both microorganisms. This was also the case for NAu-2 before incubation (Fig. 32 A & B), NAu-2 after incubation with *S. commune* (Fig. 33 A & B), and NAu-2 after incubation with *S. acidiscabies* (Fig. 34 A & B)

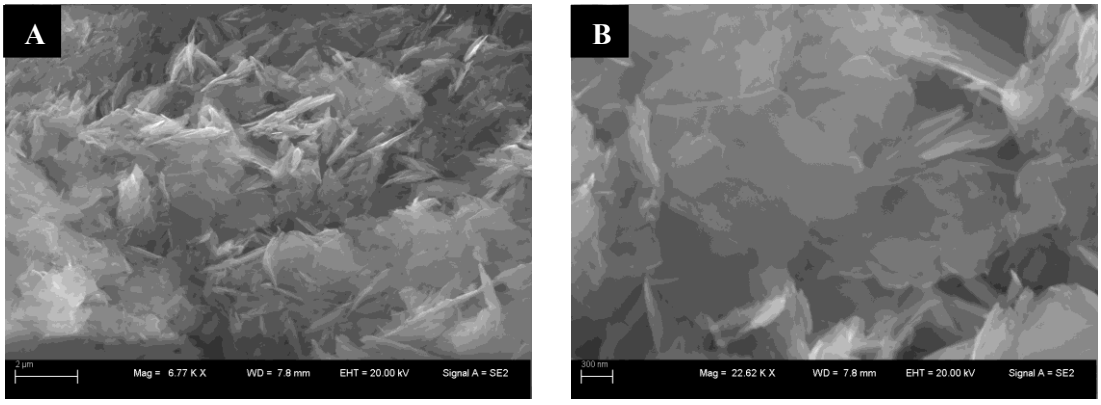

(Fig. 29) CCa-2 before incubation with scale bar; 2 µm (A), and 300 nm (B).

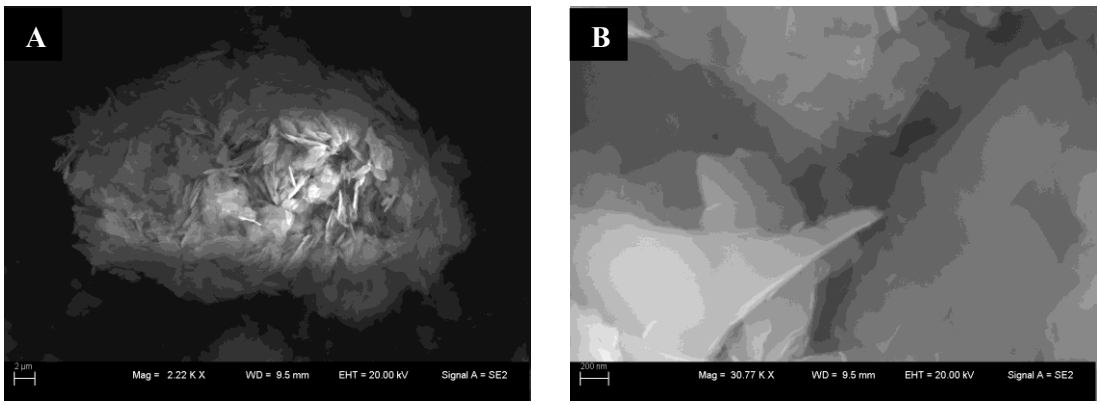

(Fig. 30) CCa-2 after incubation with *S. commune* with scale bar; 2 µm (A), and 200 nm (B).

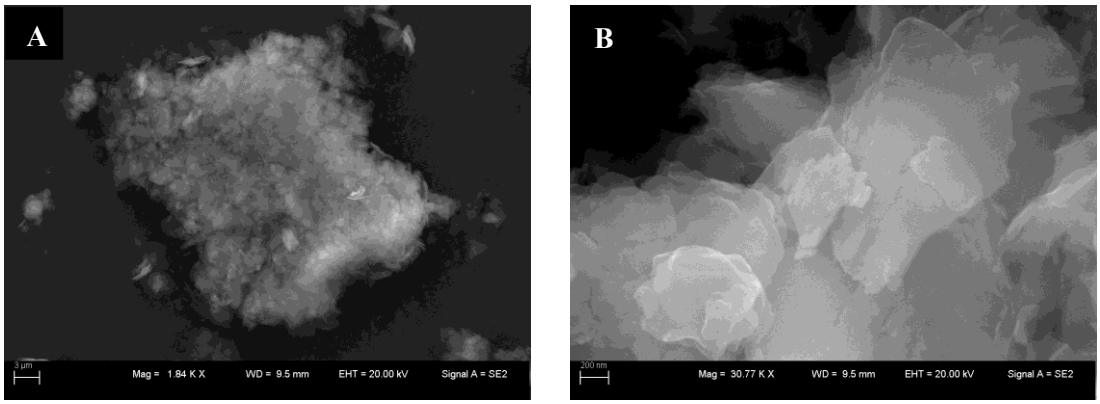

(Fig. 31) CCa-2 after incubation *S. acidiscabies* with scale bar; 3 µm (A) and 200 nm (B).

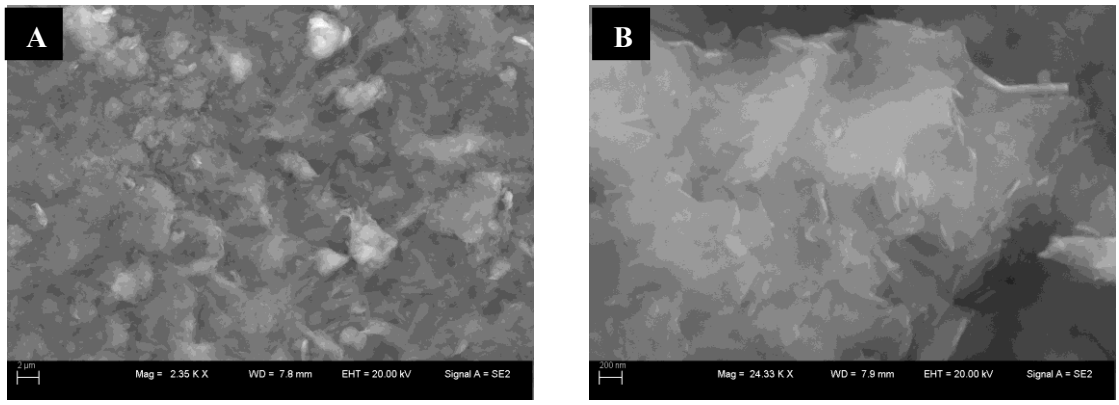

(Fig. 32) NAu-2 before incubation with scale bar; 2 µm (A), and 200 nm (B).

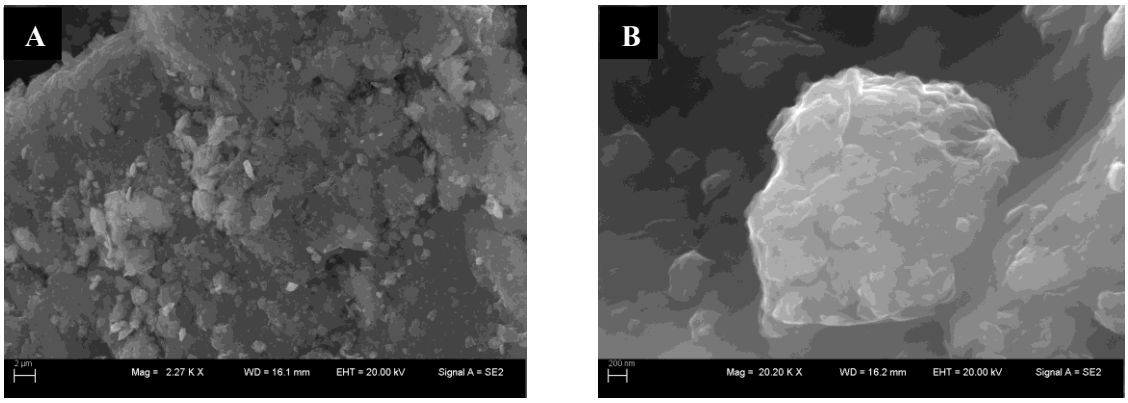

(Fig. 33) NAu-2 after incubation with *S. commune* with scale bar; 2 µm (A), and 200 nm (B).

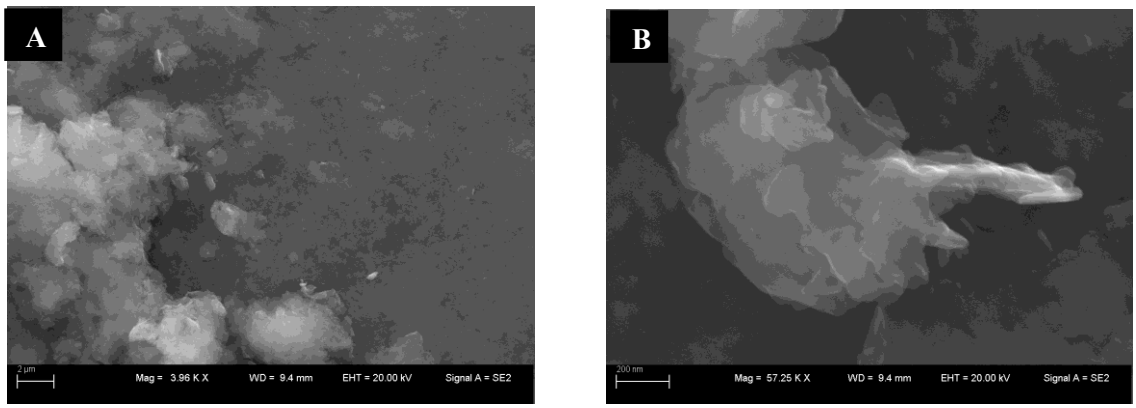

(Fig. 34) NAu-2 after incubation *S. acidiscabies* with scale bar; 2 µm (A), and 200 nm (B).

4.2. Solid agar plate experiments

4.2.1. Atomic force microscopy (AFM)

Scanning the CCa-2 polished pieces before incubation with microorganisms or adding any acid treatment using contact AFM mode revealed very rough surface topography (Fig. 35) within (~ 5 x 5 µm). This surface area is considered very small, in addition that a long time of scan is needed. Therefore, it was concluded that AFM is not the optimum tool for such surface studies.

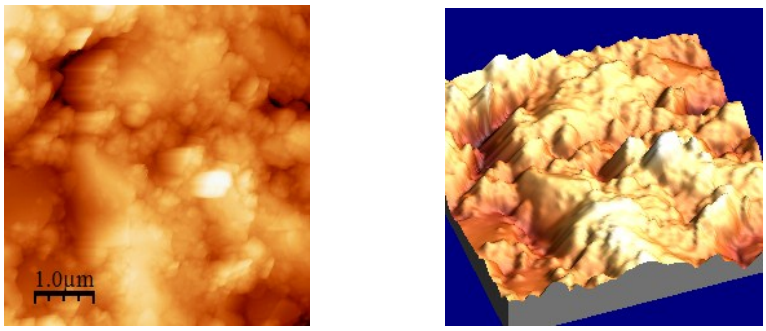

(Fig. 35) AFM images for very rough CCa-2 polished piece before any treatment.

However, when AFM was used with the CCa-2 as a powder material with the *S. acidiscabies*, it was found that sharp edged particles (Fig. 36 A) before incubation, had turned roundish and more smoothly (Fig. 36 B).

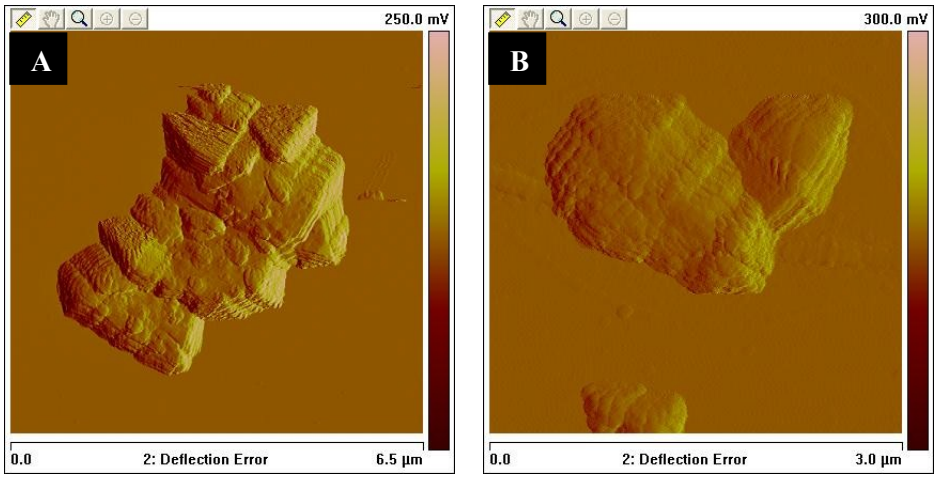

(Fig. 36) AFM images for sharp edged CCa-2 particles before incubation (A) and for roundish edged particles after incubation with *S. acidiscabies* (B).

4.2.2. Vertical scanning interferometry (VSI)

VSI is a nondestructive approach that provides a large field of view (100 µm x 100 µm) with a sufficiently high spatial resolution, high vertical resolution at the Ångstrom to nanometer scale, and fast data acquisition within the order of seconds (Waters *et al.,* 2008). When the *S. commune* was added to CCa-2 polished pieces, the fungi colonized the surface completely within the first four days, but after that by few days the fungus left the surfaces (Fig. 37).

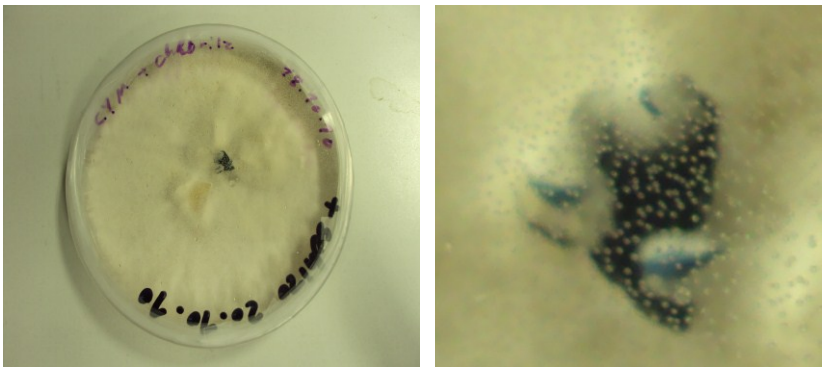

(Fig. 37) *S. commune* left the surface of polished CCa-2 after colonizing it for just few days.

The sample standard deviation (describes the deviation of the measured surface sites from the mean or another reference surface) is called the amplitude parameter (Rq) and defines the average surface roughness. The amplitude parameter (Rq) value for the masked area was 100 nm, which was almost similar to the unmasked (exposed area to the *S. commune*) (Fig. 38;

A&B). Converged surface roughness parameters were used to obtain a deconvolution of surface components of different size scales (Fischer and Lüttge, 2007).

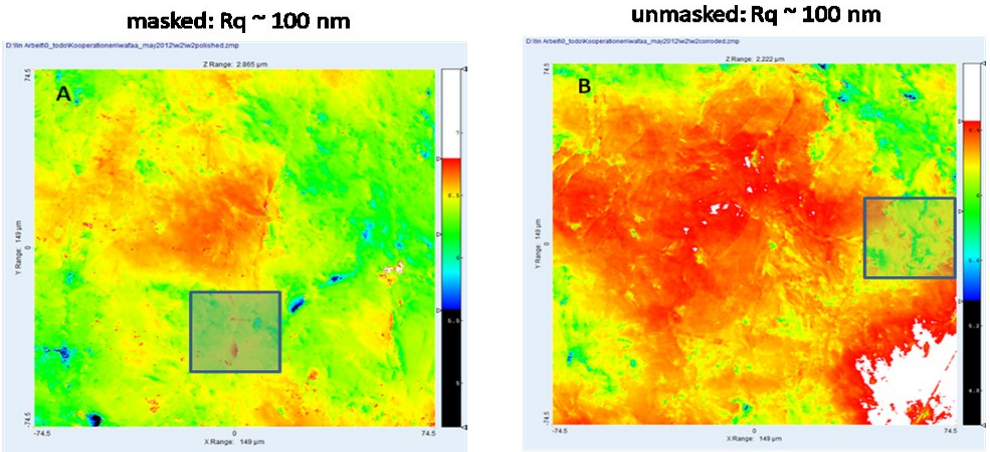

(Fig. 38) VSI image for CCa-2 polished pieces incubated with *S. commune* with equal amplitude parameter (Rq) for the masked part (A) and the unmasked part (B).

CCa-2 incubated *S. acidiscabies* strain showed differences in surface topography between the masked and the unmasked (reacted) part to the bacterial colonization (Fig. 39 A). The relative smoothness of the masked surface is represented by the single red histogram (39 B), while the roughness of the reacted surface is represented by different heights of the blue histogram (39 B). The minimum material loss per unit area (1 μm^2) was 0.35 μm^3, while the maximum material loss per unit area (1 μm^2) was 2.6 μm^3.

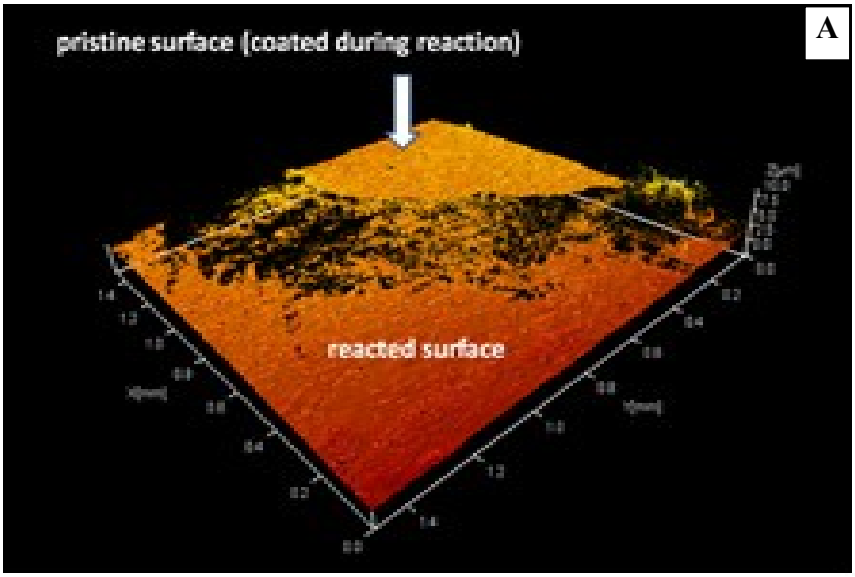

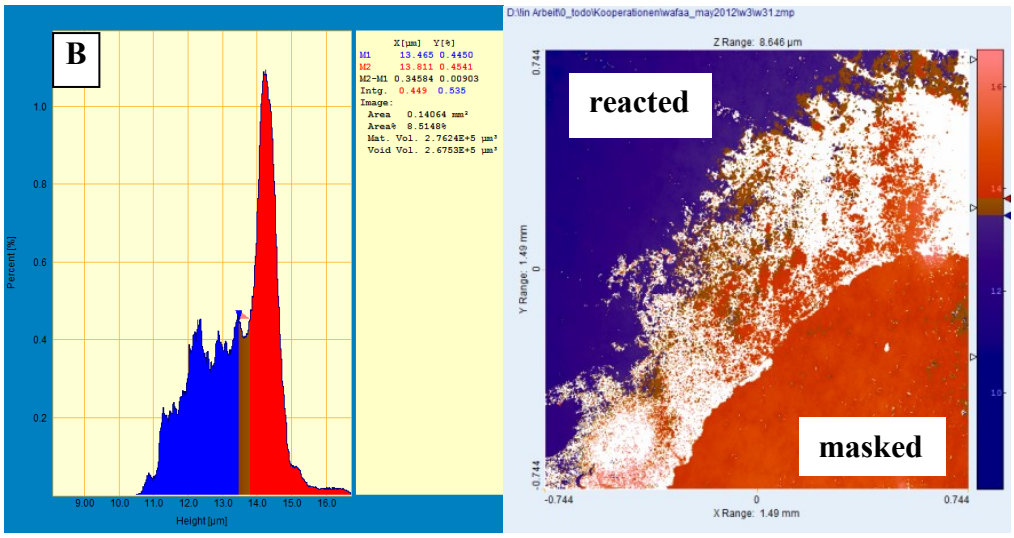

(Fig. 39) 3-D VSI image for surface normal retreat induced by *S. acidiscabies* in the unmasked (reacted) part (A), smoothness and roughness of masked and reacted surfaces are represented by different histogram heights (B).

Acid treatments with H_2SO_4 and HNO_3 showed no change in the surface topography between the masked and the unmasked surfaces. The VSI image for HNO_3 treatment showed no difference between masked and unmasked areas. The histogram analysis showed a single peak without any divergence due to surface retreat (Fig. 40). No change between masked and exposed areas was observed also for polished pieces treated with oxalic acid (Fig. 41) and with citric acid (Fig. 42).

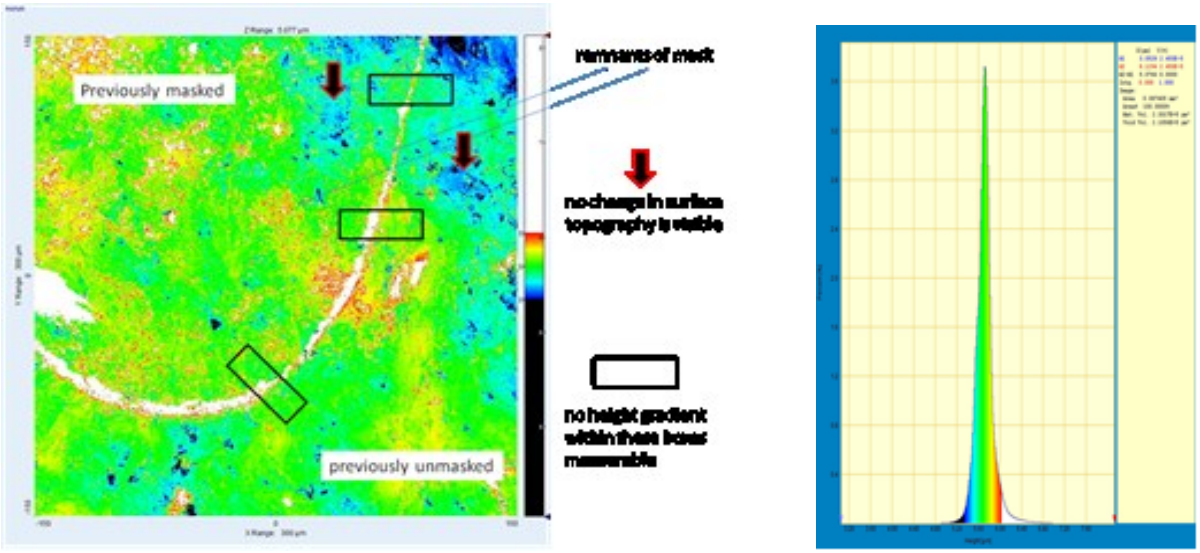

(Fig. 40) VSI image for CCa-2 polished piece treated with HNO_3, the histogram analysis showing a single peak indicating no divergence due to surface retreat.

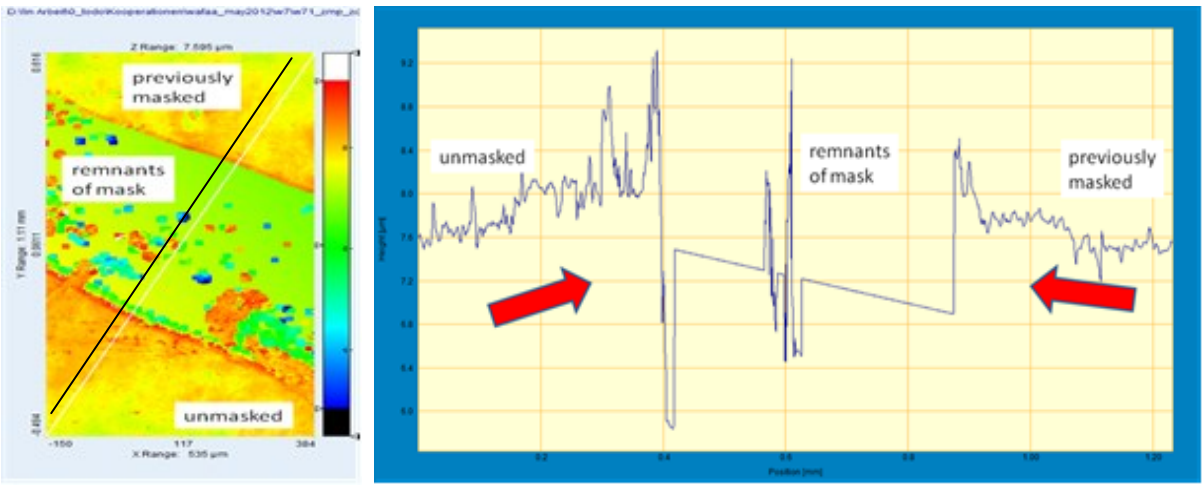

(Fig. 41) VSI image for CCa-2 polished piece treated with oxalic acid, no difference in surface roughness between masked and unmasked surfaces.

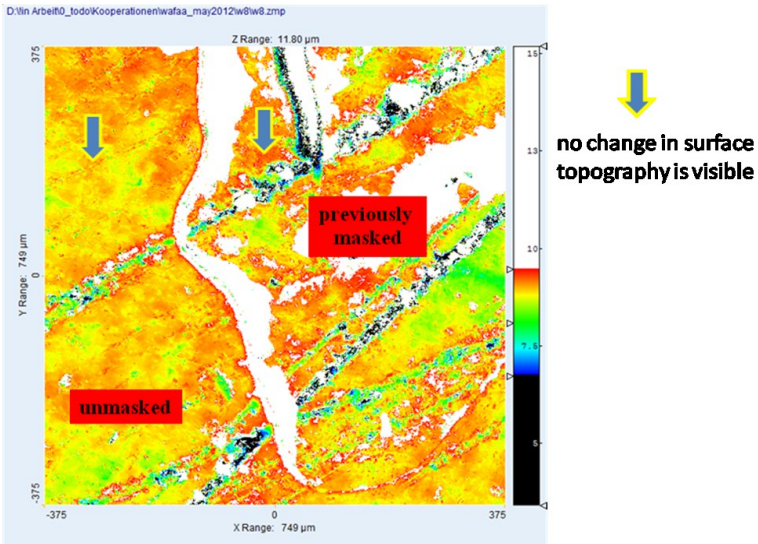

(Fig. 42) VSI image for CCa-2 polished piece treated with citric acid, measured masked and unmasked areas (two blue arrows) indicated no change in surface topography.

4.2.3. SEM of sheet silicates

SEM for polished CCa-2 pieces have showed the extreme anisotropy of phyllosilicate surfaces structures, some surfaces of the polished pieces were somehow smooth (Fig. 43 A) while others were rough and contain some holes (Fig. 43 B). The element mapping of the surfaces showed the presence of Fe and Al, and the deficiency of Mg and Si at the same places in the form of veins (Fig. 43 C) or spots (Fig. 43D).While the distribution of O seemed homogenous.

Surfaces of CCa-2 were disrupted when treated with HNO_3 (Fig. 44 A). The element map distribution showed in addition to the deficiency of Mg and Si, that Al and O were depleted too by adding HNO_3 (Fig. 44 B), while Fe distribution was homogeneous. When surfaces of CCa-2 were treated by H_2SO_4 (Fig. 44 C), the element mapping showed similar Al and O deficiency in addition to slight Fe deficiency (Fig. 44 D).

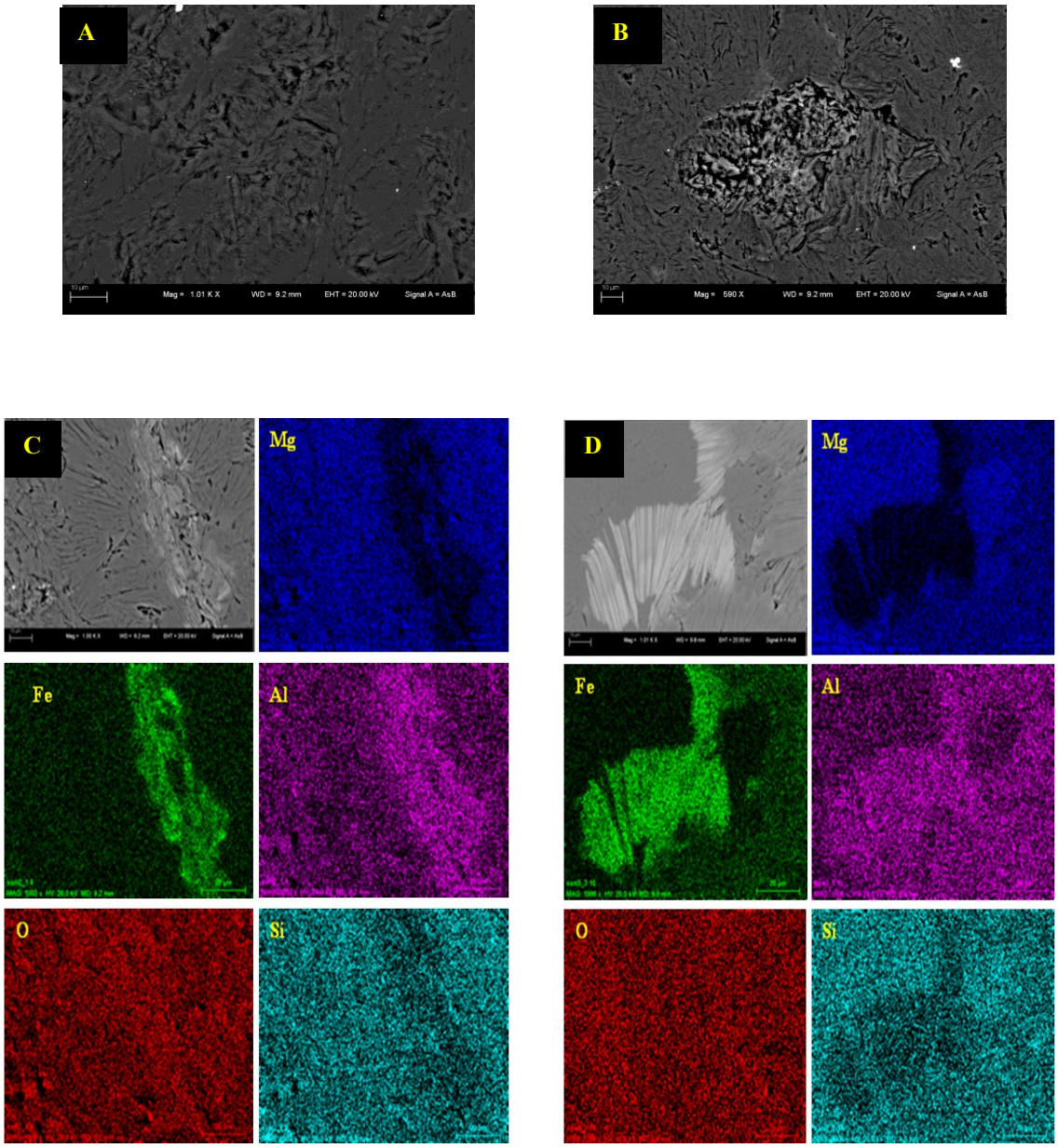

(Fig. 43) SEM images for smooth surfaces (A) and a rough one contains a hole (B), (C) and (D) are element map distribution for Fe, Al, and Mg in the form of veins or spots respectively.

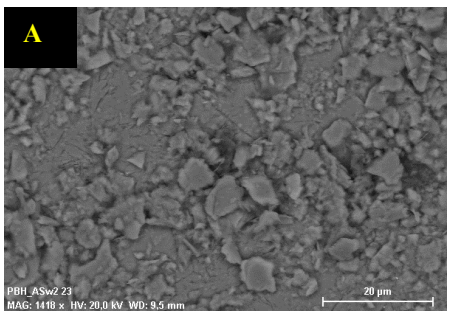

HNO_3 treatment

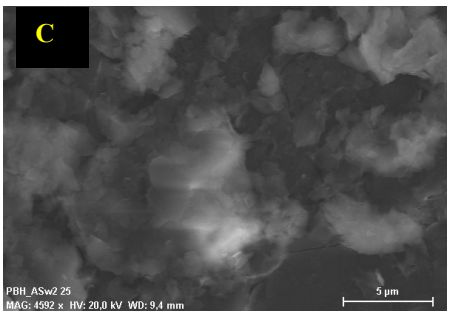

H_2SO_4 treatment

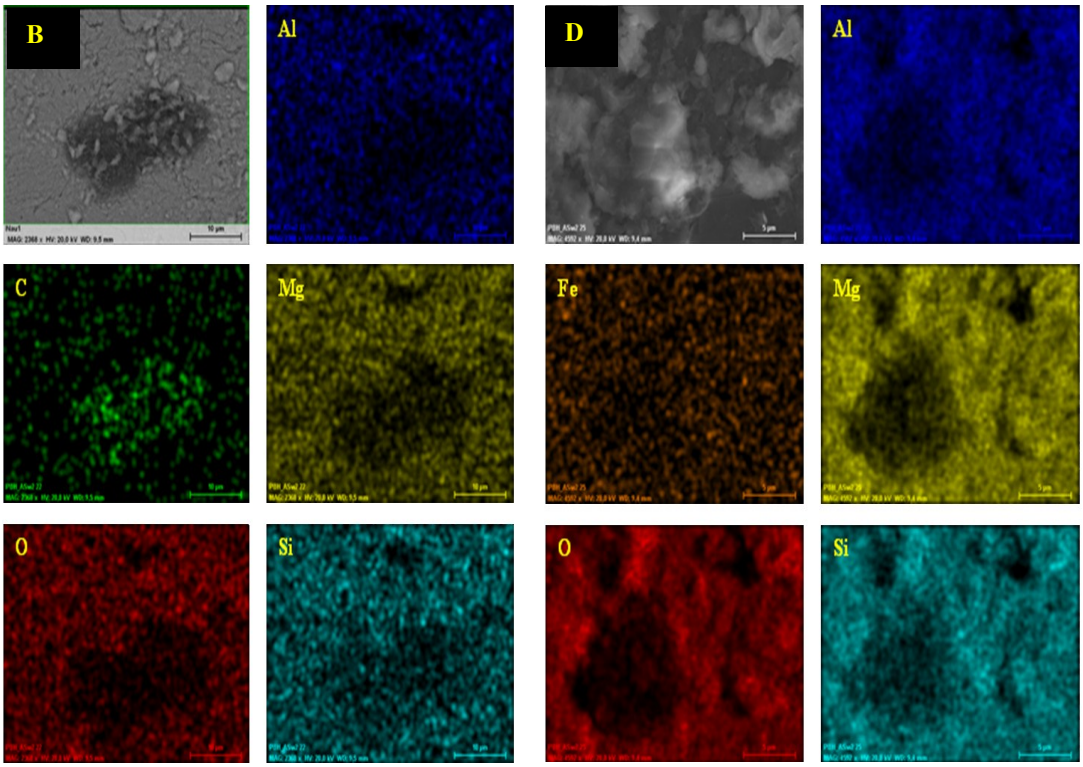

(Fig. 44) CCa-2 surfaces after inorganic acid treatment with; HNO_3 (A), and H_2SO_4 (C) with element mapping for both acids respectively (B &D).

Both citric and oxalic acids haven't showed any change in surface topography or in element distribution. Although the use of 2% SDS was very successful in removing most of the microbial traces from the polished surfaces, however because of the very rough surface topography and the presence of some holes, some hyphae with high C content was detected when CCa-2 was incubated with *S. commune*. Siegel (2010) demonstrated the affinity of the fungus to rough surfaces using SEM. Element mapping for *S. commune* strain incubated with CCa-2 showed less Al, O, and Fe (Fig. 45). Element mapping for *S. acidiscabies* incubated with CCa-2 showed also less Al and O, but homogenous Fe distribution.

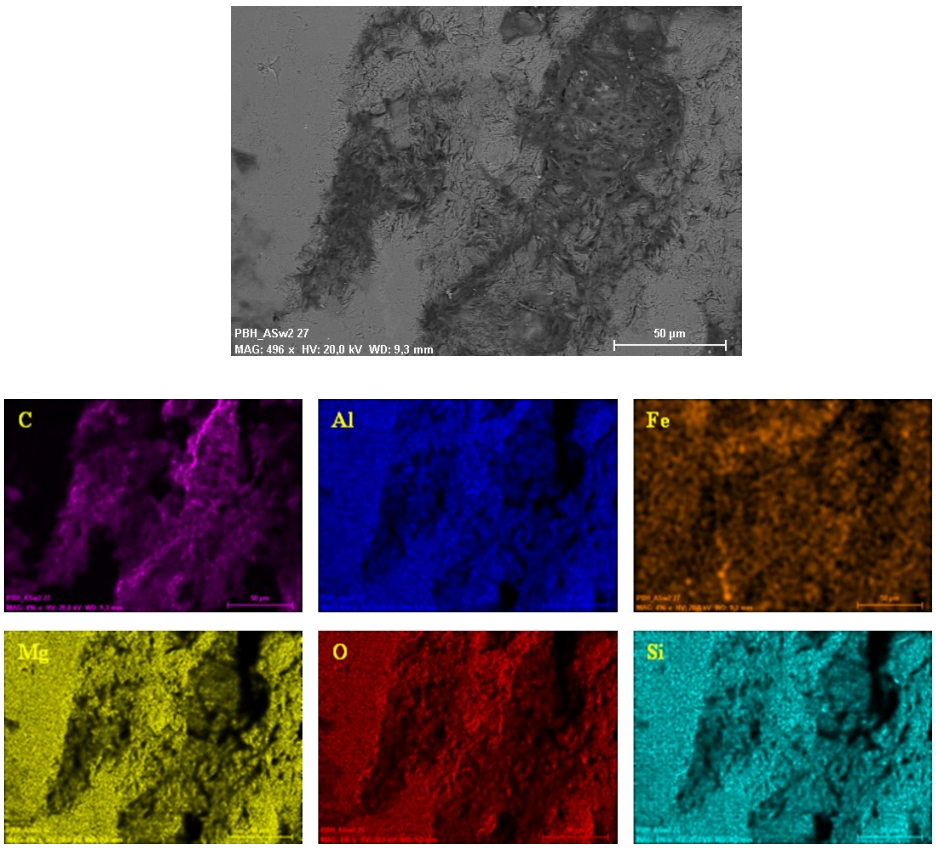

(Fig. 45) Hyphae of *S. commune* appear over a rough surface in addition to the element mapping.

SEM images done for *S. commune* incubated with CCa-2 polished pieces showed that the fungus strain has produced EPS even when grown over the surface of the mineral for a short time (Fig. 46).

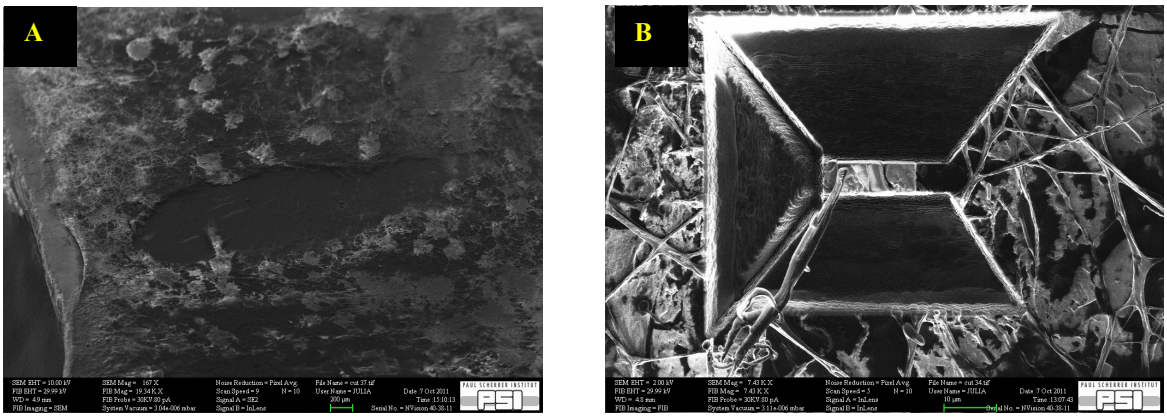

(Fig. 46) SEM images of *S. commune* colonized CCa-2 polished piece, some of the fungal hyphae were removed gently by a tweezer (A); EPS produced around the hyphae are shown while preparing a sample for FIB (Focused Ion Beam) (B).

5. Discussion

5.1. Liquid culture flask Experiments

5.1.1. ICP-OES

As rapid release of Ca from NAu-2, and Mg from the interlayer sites of CCa-2 was detected in the inoculated as well as the non-inoculated minerals, this might be explained by ion-exchange reactions. Variations in solution chemistry (increase/decrease of Ca and Mg) might be due to two possibilities; first is the consumption of those cations by microorganisms like the decrease of Ca during the initial phases of growth, when such nutrients are required most. A second possibility is the temporal storage of cations within biofilm or as secondary phase precipitations. This might explain the decrease of Mg released and its increase again at the end of the experiment when *S. acidiscabies* strain incubated with CCa-2. Most probably the Mg was complexed with the cells then re-released into solution during cell breakdown (lyses). According to the preferred dissolution of NAu-2 tetrahedral edge sites (Bosbach *et al.,* 2000; Bickmore *et al.,* 2001), higher amounts of Si were released by both microorganisms relative to Al indicating dissolution of amorphous silica. Our results showed that *S. acidiscabies* has released (more Fe and Si) from both minerals than *S. commune*. The reason for this is the production of organic acids in addition to siderophores by the *S. acidiscabies*. These results are in agreement with Kostka *et al.* (1999 a). They found that the dissolution of the smectite lattice and associated release of silica within sediments is indirectly coupled to the process of structural iron reduction through the alteration of pore-water pH and the generation of chelating acids from organic matter. They found also that EPS may have a similar function to certain chelators in dissolving the clay mineral structure. While Malinovskaya *et al.* (1990) and Vandevivere *et al.* (1994) found that EPS produced by bacterial cultures, enhanced dissolution of silicate minerals only in combination with low molecular weight metabolites such as organic acids. Buss *et al.* (2007) found that EPS did not enhance release of Fe to solution without the addition of siderophore. The release of Fe from NAu-2 by *S. acidiscabies* might indicate additional dissolution of the octahedral sites. The detection of Al in the solution was very low in all the experiments. Only in the case of *S. acidiscabies* incubated with CCa-2 the concentration of Al in solution has increased then decreased again. Al is a toxic element to most bacteria and it might have been adsorbed to the surfaces of bacterial cells and might even be complexed by bacterial surface's functional groups (Fein *et al.,* 2002) or an another interpretation is that the multi-functional organic acids chelate the aluminum, forming strong, multiply bonded complexes as described by Bennett *et al.* (1988). NAu-2 was more susceptible

to dissolution by *S. acidiscabies* strain than by *S. commune* and by both microorganisms more than CCa-2 as more elements (e.g. Fe & Si) were released into the liquid medium. This is because smectitic clays have a large reactive surface, which is capable of sorbing significant amounts of dissolved organic compounds, in addition to the incorporation of hydrated ions into the smectite interlayer. Consequently NAu-2 structure expands and exposes additional mineral surface to solution and microbial attack, while this is not expected for the chlorite hydroxy-interlayers. The dissolution of CCa-2 was incongruent with a preferential release of Si relative to Fe and Al, and high release of Mg relative to Si.

5.1.2. pH measurements

The pH was neutral (6.5) at the beginning of the incubation period of *S. acidiscabies*, however pH decreased with CCa-2, NAu-2 and even when the strain was growing alone in the MM. This indicates that the *S. acidiscabies* is producing some organic acids as secondary metabolites and not as a response for the exposure of the minerals. The pH stayed low ~ (pH 4) until the end of the experiment when *S. acidiscabies* was incubated with NAu-2, but with CCa-2 had increased again due to the buffer capacity of the mineral. The pH of *S. commune* with both mineral was almost neutral all the time of the experiment. Our results showed that the decrease of the pH might be one of the important factors which results in silicate dissolution. As when both minerals were incubated with *S. acidiscabies*, the release of elements from NAu-2 (pH decreased constantly) was higher than the release of elements from CCa-2 (pH decreased then increased). The release of elements was higher also by *S. acidiscabies* than by *S. commune* (pH was neutral all the time of the experiment). However, protonation is certainly not the only factor for elements release, as the *S. commune* incubated with both minerals (pH neutral) was able to release some elements slightly higher compared by the release of elements from the control flasks (pH neutral), which might be because of the presence of some enzymes (e.g. laccase), proteins or /and EPS produced by the strain, which might have played a role in chelating some required elements.

5.1.3. XRD

XRD peaks for both minerals (NAu-2 & CCa-2) after and before autoclaving were almost similar in the air dried and glycolated samples, which confirmed that autoclaving has no effect on the structures of the two minerals. Well crystallized minerals such as quartz, for which domains are thousands of Ångstroms, produce sharp lines, but as domain size becomes smaller,

noticeable line broadening occurs (Moore and Reynolds, 1997). The broadening of the 001 peak when NAu-2 incubated with both strains as well as their control might be due to the formation of mixed-layer minerals/hydration heterogeneity. However as the ethylene glycolated patterns showed no significant differences on both 001 and 002 peaks, this indicated that no illitization has occured and that the differences observed on air-dried patterns are essentially due to different hydration states (Bauer *et al.,* 2001). The shift in the 001 peak from 13.7 Å for the original NAu-2 to 12.6 Å (NAu-2 with *S. commune*) and to 11.9 Å for the control (NAu-2 without *S. commune*), in addition to the decrease in the intensity of the peaks and the broadening of their width, might be referred to the reduction in the unit cell dimension. In this case the most likely explanation is a change in smectite hydration (increased heterogeneity), and this alteration caused a shift of most reflections toward higher 2θ. Nevertheless, as this shift and decrease in the intensity of the 001 peak was noticed in non inoculated NAu-2 as well as the inoculated mineral, we cannot refer this change to the effect of both strains alone on the sheet silicate mineral. The non-swelling mineral CCa-2 was unaffected at all by the presence of both strains, and XRD spectra for original and inoculated mineral were similar.

5.1.4. Raman spectroscopy

The repackaging of suspended particles into large aggregate particles called flocs (Kranck and Milligan, 1992). Flocs were formed when NAu-2 was incubated with *S. acidiscabies*, which might have produced (EPS), which caused the mineral to aggregate and form these flocs. Flocs speeds up the vertical transfer of incorporated biogenic and lithogenic particles, as well as reactive chemical species (Hill, 1996). Therefore flocculation process is often used in gravitational settling for wastewater treatment in industries (Droppo *et al.,* 2002). According to Kim *et al.* (2005) flocculation might be formed due to clay reduction and consequent change in layer charge. NAu-2 wasn't transformed to another mineral as Raman was able to identify the presence of NAu-2 after incubation with both strains; *S. commune* and *S. acidiscabies*.

5.1.5. SEM of microbial pellets

According to Brandt *el al.* (2003) and Krawczyk-Bärsch *et al.* (2004), the preferential cation release from CCa-2 might lead to a potential precipitation of secondary phases on the primary or altered chlorite phases. The more dominant iron species in CCa-2 is Fe (II), which is stable

only under acidic conditions in the presence of oxygen, and at neutral pH is rapidly oxidized to Fe (III) (Schwertmann and Fitzpatrick, 1992). Microbial pellets formed by different microorganisms play an important role in bioremediation and the adsorbtion of heavy metals on such surfaces. SEM images for *S. acidiscabies* pellets with CCa-2 showed that the hyphae of the *S. acidiscabies* were smooth and non-encrusted, while the mineral flakes were still present, but appeared as if they are deposited under Fe (III) hydroxides. Our interpretation is that the *S. acidiscabies* has lowered the pH by producing some acids, Fe (II) released from CCa-2, and the microorganism took its requirement from iron. When the pH had increased again, the released Fe (II) was quickly oxidized to Fe (III) and precipitated over the CCa-2 flakes. These heavily precipitates over the CCa-2 can be regarded as an extra protection shelf, which made it more difficult for the *S. acidiscabies* strain to attack the burried CCa-2. This result agreed with Santelli *et al.* (2001) where they found that under oxic conditions and over the pH range 2–4, fayalite (Fe_2SiO_4) dissolution sustained the growth of *Acidithiobacillus ferrooxidans* which derive metabolic energy from the oxidation of Fe^{2+}. However, ferric iron released dramatically inhibited dissolution rates by 50–98% compared to the abiotic controls. The *S. acidiscabies* pellets with NAu-2 had, no mineral flakes present as if the mineral was completely dissolved, and the hyphae were completely encrusted. According to Gates *et al.* (2002) most of the iron in Nau-2 is Fe (III). Our interpretation is that under continuous low pH, acids attacked both octahedral and tetrahedral layers resulting in complete dissolution of the mineral. Consequently, Fe (III) precipitated over the hyphae of the *S. acidiscabies*. This is similar to what Konhauser and Ferris (1996) found, that the anionically charged cell wall and extracellular material composed of ionized carboxyl and phosphoryl groups. Such groups were able to bind significant quantities of iron from solution, and because the concentration of silica exceeded that of iron, the dissolved silica bounded to ferrihydrite. The complete encrustation of bacterial cells by a silica-iron combination may be important for the mineral's stability over time, and the microbial mats studied may become future microfossils. Jaisi *et al.* (2005) found that reduction of Fe (III) has resulted in reductive dissolution of NAu-2. The *S. commune* hasn't formed any pellets with any amount of the CCa-2, but formed pellets with 0.25 g of NAu-2. *S. commune* hasn't produced any organic acids as they grow at neutral pH, and that is why the mineral (0.25 g) wasn't dissoluted and appeared as smooth and thin clay leaflets perpendicular to the hyphae, which were not encrusted. ICP-OES measurements showed high release of Cr and Ni from CCa-2 more than NAu-2. The average release of Cr and Ni from CCa-2 was ~ 30 and 103 µg/l, while the average release of the two elements from NAu-2 was 6 and 46 µg/l. This might be a reason why the *S. commune* has grown and formed pellets with 0.25 g only of NAu-2 but not with any amount of CCa-2 at all. Stohs and Bagchi (1995) have

shown that metals such as iron, copper, cadmium, chromium, lead, mercury, nickel, and vanadium exhibit the ability to produce reactive oxygen species, resulting in lipid peroxidation, DNA damage, depletion of sulfhydryls, and altered calcium homeostasis. Toxic metals in general are also potent inhibitors of enzymatic reactions (Baldrian, 2003). According to Mozafar *et al.* (2002), toxic metals (Cd, Cr, Cu, Ni, Pb and Zn) contamination of soil led to a significant decrease in the number of arbuscular mycorrhizal fungi and low colonization of plant roots and, as a result, to changes in species diversity. Many metals are essential for life, e.g.; Na, K, Cu, Zn, Co, Ca, Mg, Mn and Fe, but all can exert toxicity when present above certain threshold concentrations (Gadd, 2010). XRF analysis also showed that CCa-2 is very rich in Mg, and it is possible that its concentration has exceeded the toxic threshold and prevented the *S. commune* from growing with the mineral. Figure 47 shows that melanin is an important fungal pigment which enhance the survival of many species in response to environmental stress (Bell and Wheeler, 1986; Nosanchuk and Casadevall, 2003).

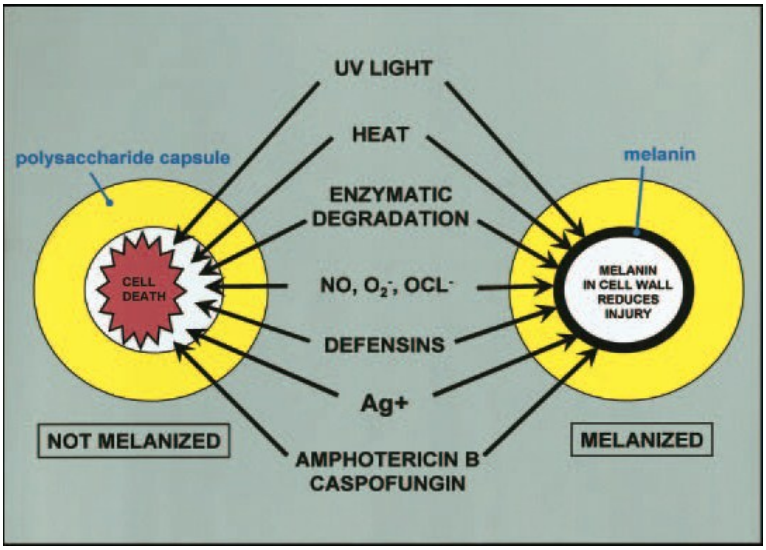

(Fig. 47) Melanin protects fungi from different environmental stress (Nosanchuk and Casadevall, 2003).

Melanins have a strong affinity for metals (Fogarty and Tobin, 1996), and have electron transfer properties (Gan *et al.,* 1976). Nyhus *et al.* (1997) found that melanized stationary-phase of *Cryptococcus neoformans* cells reduced 2 nmol of Fe (III) per 10^6 cells per h—16 times the rate of non-melanized cells - suggesting that this redox polymer participates in reduction of Fe (III). *S. acidiscabies* produced melanin (Fig. 48), which might helped in protecting the strain from the high concentration of heavy metals. To test this hypothesis, two fungal strains *Ceratocystis polonica* and *Alternaria brassicola* (which produce melanin) were inoculated with 1 g of NAu-2, and both strains have grown well and formed microbial pellets.

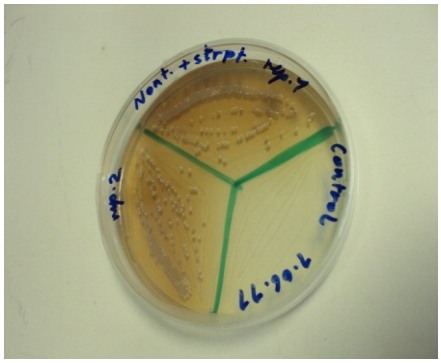

(Fig. 48) Melanin produced by *S. acidiscabies* when inoculated with NAu-2.

5.1.6. FTIR

FTIR spectra for *S. acidiscabies* strain with NAu-2 and CCa-2 showed very strong contribution from a set of bands at 1151, 1118, 1380, 1499, 1550, 1744, 2850, and 2923 cm^{-1}. Although these bands arise from different functional groups, the full set of bands appeared to change in synchrony throughout the samples.This was clear when the intensity of one of these band increasesed, the other bands increased, and when the intensity of one of these bands decreased, the others decreased too, which suggests that they are due to the same molecule. The whole set of these bands indicates the presence of esters of long chain fatty acids in the form of triglycerides, phospholipids and/or exopolysaccharides. The intensity of these bands relative to other cellular bands in some spectra is unusually high compared to the same bands of the spectra of the pure organisms, and suggests that these bands are due to EPS molecules. EPSs compose of polysaccharides and proteins, but include other macro-molecules such as DNA and lipids, and they are important in biofilm formation and cells attachment to surfaces. Most probably EPSs were induced in higher amounts by the strain to be attached to the two sheet silicate minerals. It is well known that the *Streptomyces* differ from many other bacteria in a number of features, like their filamentous nature and their ability to sporulate and to produce a wide range of antibiotics. They produce Triacylglycerol (TAG) which accumulates when they are grown in submerged culture, in addition to the typical membrane phospholipids (Packter and Olukoshi, 1995). Accumulation of TAG may be necessary to maintain cell integrity after glucose becomes exhausted from the medium, and also to provide the C_2 units needed for subsequent biosynthesis of acetate-derived antibiotics in appropriate species (Olukoshi and Packter, 1994). Hu *et al.* (2008) and Griffiths and Harrison (2009) have screened algae for strains that accumulate significant quantities of lipids and have evaluated growth conditions such as nutrient starvation that induce lipid biosynthesis, in particular the

biosynthesis of triacylglycerols. TEM images for *S. acidiscabies* strain with NAu-2 (Fig. 49) showed that the mycelium of the bacteria is full of vacuoles, which are very similar to the accumulation of neutral lipid by *S. lividans* and *S. coelicolor* strains detected by Packter and Olukoshi (1995).

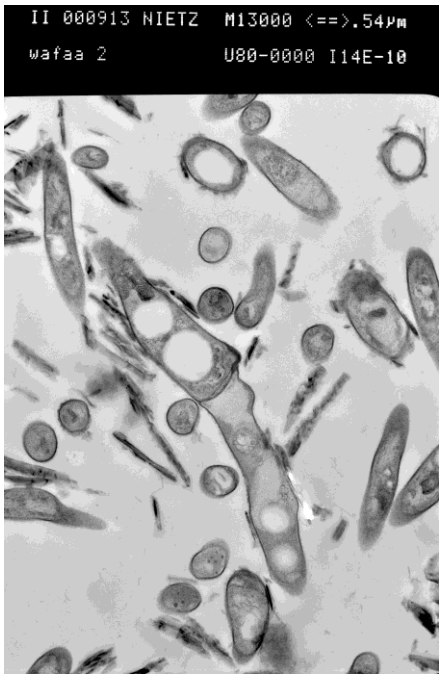

(Fig. 49) TEM image for *S. acidiscabies* with NAu-2, showing many lipid vacuoles among the hyphae.

The spatial distribution of specific absorption bands has been assessed by mapping samples in a confocal configuration. This approach is useful in assessing which absorption bands arise from the same molecule, since bands from the same molecule must have the same distribution in space. The maps show the distribution of some of the characteristic bands detected by the FTIR spectra of the *S. acidiscabies* incubated with NAu-2. The insets in the picture show the location of the mapped positions in a visible light picture of the sample. From the maps shown in (**Fig. 50**) for the *S. acidiscabies* inoculated with NAu-2, it is clear that the absorption bands at 1245 and 2923 cm^{-1} are co-localized, thus confirming that they belong to the same chromophore and that a fatty acid acyl ester is present in solution. The distribution of the Amide II band at 1550 cm^{-1} and the band at 1118 cm^{-1} assigned to polysaccharide vibrations appeared similar but not identical to that of the fatty esters. The four bands are typical for bacterial cellular components with EPS (polysaccharides and proteins), where they are localized inside the pellets for mineral attachment.

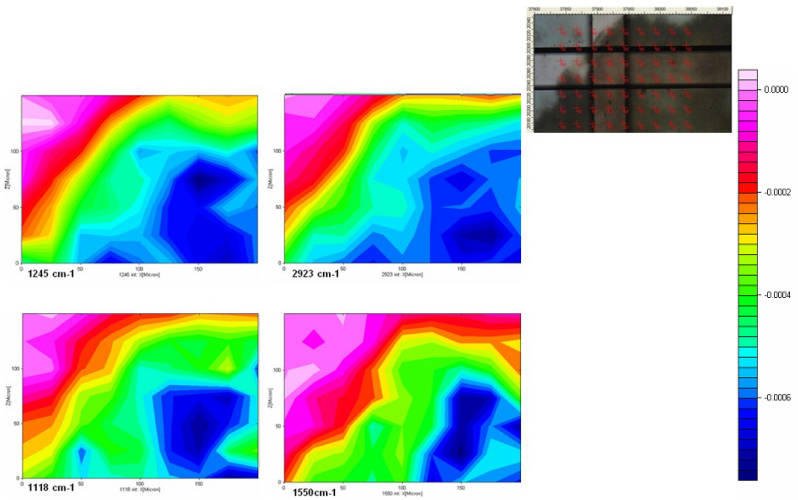

(Fig. 50) Maps acquired at 25 µm intervals across *S. acidiscabies* incubated with NAu-2. A 15 x objective and a 50 µm^2 aperture on the IR microscope was employed to acquire spectra. The images are constructed using the absorbance of the phosphate ester band (1245 cm^{-1}); methylene stretching (2923 cm^{-1}); the amide II band (1550 cm^{-1}); polysaccharides (1118 cm^{-1}).

For samples of *S. acidiscabies* incubated with CCa-2 (Fig. 51), the band at 1245 cm^{-1}, generally assigned to phosphate ester vibrations, shows a different spatial distribution from that of fatty esters. This mismatch in distribution indicates that phosphate groups are not associated to fatty ester groups in these samples and, therefore, phospholipids are not a major component of the sample, however its distribution on the edges of the pellets with the rich Mg CCa-2 mineral, showed that it is a potent magnesium chelator (Lambert *et al.*, 1975). This is a marked difference in behavior associated to the interaction between the two different types of mineral.

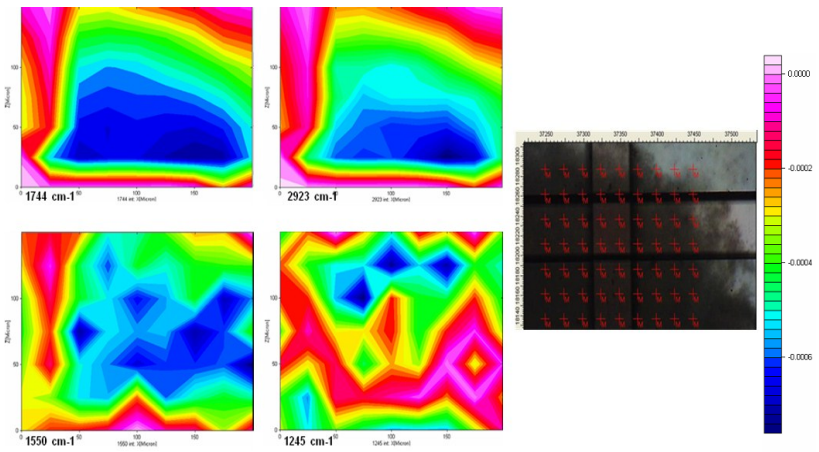

(Fig. 51) Maps acquired at 25 µm intervals across *S. acidiscabies* incubated with CCa-2. A 15 x objective and a 50 µm^2 aperture on the IR microscope was employed to acquire spectra. The images are constructed using the absorbance of the ester carbonyl band (1750–1720 cm^{-1}); methylene stretching (2923 cm^{-1}); the amide II band (1550 cm^{-1}); phosphate ester band (1245 cm^{-1}).

5.1.7. ATR-FTIR

The loss of bands ~ 3638 cm^{-1} (which is attributed to an AlAlOH) , ~3589 cm^{-1} (which refers to $Fe^{3+}MgOH$), as well as ~3552 cm^{-1} (referred to $(Fe^{3+})_2OH$) in the case of NAu-2 incubated with the two strains in addition to their negative control indicated a loss in the OH groups. The stretching water band at 3400 cm^{-1} has also disappeared, while the intensity of the bending water band at 1630 cm^{-1} has decreased and its width has increased indicating that the water molecules become increasingly less strongly hydrogen-bonded to the clay surface. A reason for this might be because all the samples were kept in the oven at 30º C for one week before grinding them. The decrease in the intensity of the bands at 822 cm^{-1} (assigned to $(Fe^{3+})_2$ OH deformation) and 870 cm^{-1} band (attributed to deformation modes of Al $Fe^{3+}OH$) ascertained the loss of OH groups. A new band ~850 cm^{-1} has appeared in the the two inoculated samples and their control and was not present at the original NAu-2 might be assigned to AlMgOH. Several authors (e.g. Petit *et al.,* 1992) suggested that the 840-850 cm^{-1} bands of nontronites is similar to the 839-848 cm^{-1} bands observed by Russell *et al.* (1970) and Cracium (1984) in montmorillonite. The slight increase at the 790 cm^{-1} (referred to amorphous silica) in the four spectra than in the original NAu-2 might be explained due to the immersion in the medium for 2 months in addition to the shaking. In general, there was no difference between the two inoculated NAu-2 minerals and their negative control (without inoculum), which indicated that any structural change that might have happened to the NAu-2 cannot be referred to the effect of microorganisms alone.

5.1.8. SEM of sheet silicates

SEM for both minerals (NAu-2 & CCa-2) in the powder form showed no morphological differences between the original minerals and the inoculated minerals with the two strains. This result is similar to what Golubev *et al.* (2006) reached, as their SEM images of initial and post-experiment for smectite dissolution as a function of pH (1-12) and nine organic ligands were indistinguishable. Biogenic minerals (e.g. siderite, vivianite, and illite) or secondary precipitates were not detected in this study. It was also difficult to see any etch pits caused by microorganisms using SEM.

5.2. Solid agar plate experiments

5.2.1. AFM

AFM was not the appropriate method to detect any etch pits caused by the microorganisms or by any acid treatment which have been applied. This because the surface of the CCa-2 pieces even when polished was still very rough. In addition to the small field of view, it would be almost very difficult to find such etch pits. The presence of roundish and more smoothly CCa-2 particles after incubation with *S. acidiscabies* might indicates the excretion of some immobilized enzymes on the mineral surface, which is similar to the birnesite-protein complex detected by Naidja *et al.* (2002).

5.2.2. VSI

The results of the VSI showed that only the *S. acidiscabies* strain has caused some change in the surface topography when both masked and (exposed) unmasked areas were compared with each other. As we previously know that the *S. acidiscabies* produced some organic acids, however they were not the only reason for changing the surface topography. Otherwise organic acids like oxalate and citrate would have caused some effects in the surface topography, which was not the case. Kodama et al. (1983) suggested that the effect of organic acids on silicate weathering rates in nature is fairly small, as it would have taken from fulvic acid (**FA**) solution 0.025% about 22 yrs to dissolve 1 g of Fe-clinochlore and 7.2 yrs to dissolve 1 g of biotite. In addition that the decrease in the pH wasn't too much. Liermann *et al.* (2000) have found while measuring pH gradients in microbial biofilm–mineral for a streptomyces species using commercial microelectrodes that they were generally beneath detection (differences in pH between silicate–biofilm interfaces and bulk medium (Δ pH) < 0.04). Most probably the presence of different organic acids produced by *S. acidiscabies* strain in addition to the production of siderophore, enzymes, and EPS, all together might have played an effective role. Barker *et al.* (1998) demostratd that microbial colonization of surfaces, production of inorganic and organic acids, and extracellular polymers greatly accelerates mineral weathering reactions and releases up to two orders of magnitude more material to solution than abiotic controls. According to Kostka *et al.* (1999 a) EPS may be functionally similar to certain chelators in dissolving the clay mineral structure. Cheah *et al.* (2003) found that dissolution of goethite in the presence of both siderophore and oxalate was greater than the sum of the dissolution effects

of the two ligands alone. Enzymes, organic acids, siederphores and other ligands become concentrated in EPS. Consequently the viscosity of EPS may restrict their diffusion in a strongly adhering biofilm (Morel and Palenik, 1989; Madigan *et al.*, 2000), and this explains the localization of the surface retreat by the *S. acidiscabies* over the CCa-2 polished pieces. Buss *et al.* (2007) referred the increase in surface roughness and the 'biopits' produced by *Bacillus* sp. on iron-silicate glass planchets chemically similar to hornblende to the siderophores concentrated in biofilms. Because siderophore – Fe complexation releases H^+ from the siderophore ligand, siderophore chemistry may contribute to larger ΔpH (Liermann *et al.* 2000). Siderophores bind Fe (III) in soils more effectively than low molecular weight organic acids. For example, the association constants of oxalic and citric acids with Fe^{3+} are $10^{7.6}$ and $10^{17.3}$ respectively, while the siderophore-Fe complex formation constant is in the range 10^{25} to 10^{35}. In addition, siderophores function from neutral to pH 12, while oxalic and citric acid don't chelate effectively at neutral to alkaline conditions (Kalinowski et al. 2000). The *S. commune* hasn't caused any change in the surface topography, even when the strain produces some enzymes and EPS but have left the surface of the polished pieces. Wether the fungus starin has left the surface because of the heavy metals present in the mineral or because the mineral doesn't really include high amounts of essential required elements, this remains an open question. According to Ernstsen et al. 1998 and Gates et al. 1998, the extent of bioreduction increased with increasing total Fe content of the clay minerals. Bennett *et al.*, 2001, suggested that the progression of mineral weathering may be influenced by a mineral's nutritional potential, with microorganisms destroying only benefecial minerals. As few drops of *S. acidiscabies* were added directly over the CCa-2 pieces, it is important to consider the areal direct contact between the microbial cells and the mineral and the microbial/clay mineral ratio (Dong *et al.*, 2009) as important factors which led to that change in the surface topography.

5.2.3. SEM of Sheet silicates

For the polished CCa-2, element mapping of the surfaces before any treatment showed the presence of Fe and Al in some spots, and the deficiency of Mg and Si in the same spots, while the distribution of O seemed homogenous. After the addition of inorganic acids (HNO_3 & H_2SO_4), the element mapping showed that some spots where Mg and Si are deficient are accompanied by deficiency of Al and O also. Fe was deficient also in the case of H_2SO_4 while with HNO_3 was homogeneously distributed indicating the strong effect of protons released

from diprotic acids. Organic acids haven't altered the surface's topography and there were no differences between organic and inorganic acid treatments, which disagrees with (Welch and Ullman, 1993), whom found that the rates of plagioclase dissolution in solutions containing organic acids are up to ten times greater than the rates determined in solutions containing inorganic acids at the same acidity. However the VSI results have confirmed the SEM results. The use of 2% SDS was very effective in removing most of the microbial traces from the surface of the mineral gently without disturbing the surface itself, however some fungal hyphae were detected by SEM. Therefore, it is necessary to extend the time of the immersed pieces in the SDS whenever there a need for that.

6. Summary and conclusions

Former studies had concentrated on the reduction of iron bearing sheet silicates either chemically like well known reductants (e.g. diothionite and/or hydrazine) or biologically using iron reducing bacteria growing under anaerobic conditions. This work is different as the dissolution of two iron bearing sheet silicates was studied neither by using any chemical reductants nor iron reducing bacteria. But on the contrary, the two used microbial strains were grown under aerobic conditions. In liquid culture flask experiments, two sheet silicates as a powder form less than 2 µm were used; a dioctahedral, swelleing nontronite (NAu-2), and a trioctahedral, non swelling clinochlore (CCa-2). Both minerals were incubated with two filamentous microorganisms; the filamentous bacterium (*Streptomyces acidiscabies*) and the filamentous fungus (*Schizophyllum commune*). The goal was to study the effect of microbes and minerals on each other. The bacterial strain *S. acidiscabies* produces some organic acids, enzymes, siderophores and melanin, while the fungal strain *S. commune* produces the enzyme lacasse. XRD, Raman spectroscopy, SEM, and ATR-FTIR were used for studying any structural or morphological change that might have occurred to the two minerals after the incubation period with the two strains. Release of Si and other elements like Fe and Al in the liquid medium as an indication of mineral dissolution was measured by ICP-OES in the minimal culture medium in addition to the pH measurements. SEM was also used to see the effect of minerals on the microbial pellet's morphology, while FTIR was used to detect any change in microbial expression, which might have been induced as a response to the exposure of the two minerals. Studying the alteration of the mineral's surface, and the changes in its topography and roughness was achieved by using VSI. In this case, the CCa-2 mineral was in the form of small polished pieces, which were added to solid agar plates. These pieces were

incubated with both microorganisms, in addition to their treatment with some acids; two organics (oxalic and citric), and two inorganic (nitric and sulphuric acid). The goal was to compare between etch pits formed biologically and chemically over the CCa-2 mineral's surface. It was clear from the liquid culture experiments that the *S. acidiscabies* was more efficient in releasing more Si and Fe from the NAu-2 than the *S. commune*. Nevertheless both microorganisms have released more elements than their negative control, where only minerals without any microorganisms were present in the liquid flask cultures. The release of elements from the swelling NAu-2 by both microorganisms was higher than from the non-swelling CCa-2. The pH in case of *S. commune* with both minerals was always neutral all the time of the experiment. In case of *S. acidiscabies* with CCa-2, the pH was neutral at the beginning then decreased to (pH ~ 4.7), but then increased to be neutral again. While in case of *S. acidiscabies* with NAu-2, the pH decreased from neutrality to (pH~ 4.3), and remained acidic till the end of the experiment. Protonation enhances the hydroylsis of X-O (X=Si, Al, Fe, Mg) bonds, and might have played a role in the dissolution of NAu-2 more than CCa-2. However, VSI showed that acid treatments alone whether organic or inorganic over the CCa-2 polished pieces haven't revealed any change in the topography of the surface or caused any surface roughness. VSI results showed that *S. acidiscabies* was capable of altering the surface topography, as there was a maximum material lost around 2.6 μm^3 per 1 μm^2 and 0.35 μm^3 minimum material lost per same area. Most probably the production of siderophores in addition to organic acids together were the most effective factors for causing such surface normal retreats. When *S. commune* was added to the polished CCa-2, the fungus strain has grown and spread over the whole plate and over the surface of the polished piece, but hasn't stayed over the surface for a long time. This indicated the importance of the areal contact between the microorganism and the mineral, and that is why no effect on the CCa-2 surface was detected by the VSI in the case of *S. commune*. VSI results have shown also that inorganic acids (HNO_3 & H_2SO_4) as well as organic acids (oxalic and citric) haven't caused any change in the surfaces of CCa-2. The small field of view of the AFM, in addition to the long time of scan needed have demonstrated that it is not the appropriate technique for studying such surface alteration. SEM of the two minerals in the powder form haven't showed any difference in morphology and neither bio-etch pits nor biogenic minerals were detected. SEM of the CCa-2 polished pieces hasn't revealed any significant differences between the surfaces before and after biological and chemical treatments. However, the element mapping showed that protons in the (HNO_3 & H_2SO_4) might have led to the break of the Al-O bond and the deficiency of both elements. After using 2 % SDS to remove the microorganisms from the surface of the polished pieces at the end of the incubation period, SEM hasn't detected a lot of microbial traces over the surface except few

fungal hyphae over some rough holes within the mineral's surface. This has proved that 2 % SDS is an effective method to remove microbes from the surfaces safely without disturbing or causing any harm to the surface. SEM images for the microbial pellets showed that *S. acidiscabies* was able to form microbial pellets with 1 g of both minerals (NAu-2 & CCa-2). The microbial pellets of *S. acidiscabies* with CCa-2 were irregular at the beginning then turned roundish in addition that very dense precipitates were obvious over the mineral flakes but most of the hyphae were smooth. As most of the Fe in the CCa-2 mineral is in the Fe (II) form, which is soluble and stable under aerobic and acidic conditions, we assumed that when the pH has decreased, the Fe (II) was chelated out of the mineral by some siderophore, and the microorganisms have taken their need from Fe. Once the pH has increased again the Fe (II) has oxidized to Fe (III) and precipitated over the CCa-2 mineral flakes. Consequently, the CCa-2 mineral was conserved from attacking under these thick heavy precipitates. With the other mineral (NAu-2) the microbial pellets of the *S. acidiscabies* were regular, round, and compact. There were not too many mineral flakes still present as if they were dissolved to a large extent, and the hyphae were completely encrusted. Our interpretation is that *S. acidiscabies* have produced some acids and the pH has decreased and stayed constantly acidic (pH = 4), the acid has attacked both octahedral and tetrahedral layers resulting in complete dissolution of the NAu-2 mineral and the precipitation of Fe (III) over the bacterial hyphae. *S. commune* hasn't formed any pellets when it was incubated with 1 g of both minerals, and formed such pellets with 0.25 g only of NAu-2, but not with any amount of CCa-2. With 0.25 g of NAu-2, the mineral appeared as thin clay leaflets perpendicular to the hyphae which were not really encrusted. Other fungal strains (*Ceratocystis polonica* and *Alternaria brassicola*) which produce melanin have formed microbial pellets with 1 g of NAu-2. Melanin is well known as a protecting biomolecule against toxic heavy metals, and because it was produced by the *S.acidiscabies* only and not by the *S. commune*, this might be a reason for protecting the bacterium strain from toxic metals released from the minerals. FT-IR of *S. acidiscabies* with both minerals indicated the presence of esters of long chain fatty acids in the form of triglycerides, phospholipids and/or exopolysaccharides with much stronger intensities to be due to lipids associated to cellular membranes in the organisms. It was suggested that EPS molecules were excreted by the *S. acidiscabies* to be attached to the two sheet silicate minerals. Triacylglycerol is an another alternative for fatty acids derivatives which might be present in the samples. TEM for *S. acidiscabies* strain with NAu-2 showed that the mycelium of the bacteria is full of such lipid vacuoles, which might be induced by the microorganisms once glucose becomes exhausted from the medium or might be an indication that they were not growing under favourite conditions. The spatial distribution of specific absorption bands has

been assessed by mapping samples in a confocal configuration. This helped in assessing which absorption bands arised from the same molecule, since bands from the same molecule must have the same distribution in space. Maps for *S. acidiscabies* incubated with NAu-2 showed the distribution of bands related to bacterial cellular components with EPS (polysaccharides and proteins), where they are localized inside the pellets for mineral attachment. When *S. acidiscabies* was incubated with CCa-2, the band at 1245 cm^{-1}, (assigned to phosphate ester), showed a different spatial distribution from that of fatty esters. This mismatch in distribution indicated that phosphate groups are not associated to fatty ester groups in these samples and, therefore, phospholipids are not a major component of the sample, however their distribution on the edges of the pellets with the rich Mg CCa-2 mineral, showed that they are a potent magnesium chelator. *S. acidiscabies* and *S. commune* strains have changed the color of the dye in the Bradford assay when both incubated with NAu-2 indicating the production of extracellular proteins or enzymes in the culture medium, while no proteins were estimated in the culture medium when both strains were incubated with the CCa-2. It is still interesting for more future investigation to identify these induced proteins, and to know wether the two strains have induced similar or different extracellular proteins after exposure to the NAu-2. ATR-FTIR though have shown some slight differences in the NAu-2 mineral structure - summed up in loss of OH groups and increase in the amorphous Si- between the original NAu-2 and the inoculated with both strains and even with their control. However, it hasn't revealed any differences between the inoculated NAu-2 and its control, which indicated that any change in the mineral might be referred to its immersion in the medium solution for two months in addition to the shaking during the experiment time. XRD spectra haven't shown any difference between original and autoclaved minerals, which proved that autoclaving is an optimum method for sterilizing minerals without causing any effect on their structure, however this cannot be generalized and it is important to test the effect of autoclaving on other different minerals. XRD of CCa-2 incubated with both strains was similar to the original mineral showing no effect of microorganisms at all on the mineral. When NAu-2 only was immersed in liquid culture without any inoculums while being over the shaker for two months, XRD spectra for non inoculated NAu-2 showed that the intensity of 001 peak has decreased and its width has increased and that this decrease in the intensity was even more obvious when NAu-2 was incubated with both strains. This indicated that chemical and mechanical weathering play the initial role in mineral dissolution, and making it easier for the microorganism to attack the mineral and to lead at the end to the presence of an amorphous material.

7. References

Abd El-Rahim, W. M. and Moawad, H. (2003) Enhancing bioremoval of textile dyes by eight fungal strains from media supplemented with gelatine wastes and sucrose. J. of Basic Microbiology, 43, 367-375.

Amoroso, M. J., Schubert, D., Mitscherlich, P., Schumann, P., and Kothe, E. (2000) Evidence for high affinity nickel transporter genes in heavy metal resistant *Streptomyces* spec. J. Basic Microbiology., 40, 295-301.

Arnold, T., Zorn, T., Bernhard, G., and Nitsche, H. (1998) Sorption of uranium (VI) onto phyllite. Chem. Geol., 151, 129-141.

Baldrian, P. (2003) Interactions of heavy metals with white rot fungi. Enzyme and Microbial Technology, 32, 78-91.

Banfield, J. P., Barker, W. W., Welch, S. A., and Taunton, A. (1999) Biological impact on mineral dissolution: Application of the lichen model to understanding mineral weathering in the rhizosphere. Proceedings of the National Academy of Sciences, USA, 96, 3404-3411.

Barker, W. W., Welch, S. A., Chu, S., and Banfield, J. F. (1998) Experimental observations of the effects of bacteria on aluminosilicate weathering. American Mineralogist, 83, 1551-1563.

Bauer, A., Schäfer, T., Dohrmann, R., Hoffmann, H., and Kim, J. I. (2001) Smectite stability in acid salt solutions and the fate of Eu, Th and U in solution. Clay Minerals, 36, 93-103.

Bayliss, P. (1975) Nomenclature of the trioctahedral chlorites. Can. Miner., 13, 178-180.

Bell, A. A. and Wheeler, M. H. (1986) Biosynthesis and functions of fungal melanins. Annu. Rev. Phytopathol., 24, 411-451.

Bennett, P. C., Melcer, M. E., Siegel, D. I., and Hassett, J. P. (1988) The dissolution of quartz in dilute aqueous solutions of organic acids at 25°C. Geochim. Cosmochim. Acta, 52, 1521-1530.

Bennett, P. C., Hiebert, F. K., and Choi, W. J. (1996) Microbial colonization and weathering of silicates in a petroleum-contaminated groundwater. Chemical Geology, 132, 45-53.

Bennett, P. C., Rogers, J. R., Choi, W. J., and Hiebert, F. K. (2001). Silicates, silicate weathering, and microbial ecology. Geomicrobiological Journal, 18, 3-19.

Benning, L. G., Phoenix, V. R., Yee, N., and Tobin, M. J. (2004) Molecular characterization of cyanobacterial silicification using synchrotron infrared micro-spectroscopy. Geochim. Cosmochim. Acta, 68, 729-741.

Berner, R. A. (1992) Weathering, plants and the long-term carbon cycle. Geochim. Cosmochim. Acta, 56, 3225-3231.

Berner, R. A. (2003) The long-term carbon cycle, fossil fuels and atmospheric composition. Nature, 426, 323-326.

Bickmore, B. R., Bosbach, D., Hochella Jr., M. F., Charlet, L., and Rufe, E. (2001) In situ atomic microscopy study of hectorite and nontronite dissolution: implications for phyllosilicate edge surface structures and dissolution mechanisms. American Mineralogist, 86, 411-423.

Binnig, G., Quate, C. F., and Gerber, Ch. (1986) Atomic force microscope. Phys. Rev. Lett., 56, 930-933.

Bishop, J., Madejová, J., Komadel, P., and Fröschl, H. (2002) The influence of structural Fe, Al, and Mg on the infrared OH bands in spectra of dioctahedral smectites. Clay Minerals, 37, 607-616.

Bosbach, D., Charlet, L., Bickmore, B., Hochella Jr., and M. F. (2000) The dissolution of hectorite: In-situ, real-time observations using atomic force microscopy. American Mineralogist, 85, 1209–1216.

Brady, P. V. and Walther, J. V. (1989) Controls on silicate dissolution rates in neutral and basic pH solutions at 25ºC. Geochim. Cosmochim. Acta, 53, 2823–2830.

Brandt, F., Bosbach, D., Krawczyk-Bärsch, E., Arnold, T., and Berhard, G. (2003) Chlorite dissolution in the acid pH-range: A combined microscopic and macroscopic approach. Geochim. Cosmochim. Acta, 67, 1451–1461.

Burkhardt, E. M., Meisser, S., Merten, D., Büchel, G., and Küsel, K. (2009) Heavy metal retention and microbial activities in geochemical barriers formed in glacial sediments subjacent to a former uranium mining leaching heap. Chemie Der Erde Geochemistry, 69, 21-34.

Buss, H. L., Lüttge, A., and Brantley, S. L. (2007) Etch pit formation on iron silicate surfaces during siderophore-promoted dissolution. Chemical Geology, 240, 326–342.

Canfield, D. E., Jargensen, B. B., Fossing, H., Glud, R., Gundersen, J., Ramsing, N. B., Thamdrup, B., Hansen, J. W., Nielsen, L. P., and Hall, P. O. J. (1993) Pathways of organic carbon oxidation in three continental margin sediments. Mar. Geol., 113, 27-40.

Carr, G. L. (1999) High-resolution microspectroscopy and sub-nanosecond time-resolved spectroscopy with the synchrotron infrared source. Vib. Spectrosc., 19, 53-60.

Cervini-Silva, A., Wu, J., Larson, R. A., and Stucki, J. W. (2000) Transformation of chloropicrin in the presence of iron bearing clay minerals. Environmental Science & Technology, 34, 915-917.

Chan, C. S., De Stasio, G., Welch, S. A., Girasole, M., Frazer, B. H., Nesterova, M. V., Fakra, S., and Banfield, J. F. (2004) Microbial polysaccharides template assembly of nanocrystal fibers. Science, 303, 1656-1658.

Cheah, S. F., Kraemer, S. M., Cervini-Silva, J., and Sposito, G. (2003) Steady-state dissolution kinetics of goethite in the presence of desferrioxamine B and oxalate ligands: implications for the microbial acquisition of iron. Chemical Geology, 198, 63-75.

Cracium, C. (1984) Influence of the Fe^{3+} for Al^{3+} octahedral substitutions on the IR spectra of montmorillonite minerals. Spectroscopy Letters, 17, 579-590.

Davis, K. J. and Lüttge, A. (2005) Quantifying the relationship between microbial attachment and mineral surface dynamics using vertical scanning interferometry (VSI). Am. J. Sci., 305, 727-751.

Davis, R. and Mauer, L. J. (2010) Fourier transform infrared (FT-IR) spectroscopy: A rapid tool for detection and analysis of foodborne pathogenic bacteria. Current Research, Technology and Education Topics in Applied Microbiology and Microbial Biotechnology, 2, 1582-1594.

Dawson, M. P., Humphrey, B., and Marshall, K. C. (1981) Adhesion: A tactic in the survival strategy of a marine vibrio during starvation. Current Microbiology, 6, 195-99.

Dean, A. P., Sigee, D. C., Estrada, B., and Pittman, J. K. (2010) Using FTIR spectroscopy for rapid determination of lipid accumulation in response to nitrogen limitation in freshwater microalgae. Bioresource Technology, 101, 4499-4507.

Deer, W. A., Howie, R. A., and Zussman, J. (2009) Rock forming minerals: layered silicates excluding Micas and clay minerals. The geological society, London.

De Vries, O. M. H., Kooistra, W., and Wessels, J. G. H. (1986) Formation of extracellular laccase by *Schizophyllum commune* dikaryon. Journal of General Microbiology, 132, 2817-2826.

Dimkpa, C., Svatoš, A., Merten, D., Büchel, G., and Kothe, E. (2008) Hydroxamate siderophores produced by *Streptomyces acidiscabies* E13 bind nickel and promote growth in cowpea (*Vigna unguiculata L.*) under nickel stress. Can. J. Microbiol., 54, 163-172.

Devasia, P., Natarajan, K. A., Sathyanarayana, D. N., and Ramananda Rao, G. (1993) Surface chemistry of *Thiobacillus ferrooxidans* relevant to adhesion on mineral surfaces. Appl. Environ. Microbiol., 59, 4051-4055.

Dong, H., Kostka, J. E., and Kim, J. W. (2003) Microscopic evidence for microbial dissolution of smectite. Clays and Clay Minerals, 51, 502-512.

Dong, H., Jaisi, D. P., Kim, J., and Zhang, G. (2009) Microbe clay mineral interactions. American Mineralogist, 94, 1505-1519.

Dong, H. (2012) Clay–microbe interactions and implications for environmental mitigation. Elements, 8, 113-118.

Drief, A., Martinez-Ruiz, F., Nieto, F., and Sanchez, N. V. (2002) Transmission electron microscopy evidence for experimental illization of smectite in K-enriched seawater solution at 50°C and basic pH. Clays and Clay Minerals, 50, 746-756.

Droppo, I. G., Irvine, K. N., and Jaskot, C. (2002) Flocculation/aggregation of cohesive sediments in the urban continuum: Implications for stormwater management. Environmental Technology, 23, 27-41.

Dumas, P., Sockalingum, G. D., and Sule-Suso, J. (2006) Adding synchrotron radiation to infrared microspectroscopy: what's new in biomedical applications? Trends Biotechnol., 25, 40-44.

Eberl, D. D., Velde, B., and McCormick, T. (1993) Synthesis of illite-smectite from smectite at earth surface temperatures and high pH. Clay Minerals, 28, 49-60.

Ehrlich, H. L. (1998) Geomicrobiology: its significance for geology. Earth Sci. Rev., 45, 45-60.

Ehrlich, H. L. and Newman, D. K. (2009). Geomicrobiology, 5th ed. Boca Raton, FL: CRC Press. Taylor & Francis.

Ernstsen, V. (1996) Reduction of nitrate by Fe^{2+} in clay minerals. Clays and Clay Minerals, 44, 599-608.

Farmer, V. C. (1974) The Infrared Spectra of Minerals. Monograph 4, Mineralogical Society, London, p. 344.

Farmer, V. C. and Russell, J. D. (1964) The infrared spectra of layer silicates. Spectrochimica Acta, 20, 1149-1173.

Favre, F., Tessier, D., Abdelmoula, M., Genin, J. M., Gates, W. P., and Boivin, P. (2002) Iron reduction and changes in cation exchange capacity in intermittently waterlogged soil. European Journal of Soil Science, 53, 175-183.

Fein, J. B., Scott, S., and Rivera, N. (2002) The effect of Fe on Si adsorption by Bacillus subtilis cell walls: insights into non-metabolic bacterial precipitation of silicate minerals. Chemical Geology, 182, 265-273.

Ferrage, E., Lanson, B., Sakharov, B. A., Jacquot, E., Geoffroy, N., and Drits, V. A. (2007) Investigation of smectite hydration properties by modeling of X-ray diffraction profiles: Influence of layer charge and charge location. American Mineralogist, 92, 1731-1743.

Fialips, C.-I., Huo, D., Yan, L., Wu, J., and Stucki, J. W. (2002 a) Infrared study of reduced and reduced-reoxidized ferrugious smectite. American Mineralogist, 87, 455-469.

Fialips, C.-I., Huo, D., Yan, L., Wu, J., and Stucki, J. W. (2002 b) Effect of Fe oxidation state on the IR spectra of Garfield nontronite. American Mineralogist, 87, 630-641.

Fischer, C. and Lüttge, A. (2007) Converged surface roughness parameters — a new tool to quantify rock surface morphology and reactivity alteration. American Journal of Science, 307, 955-973.

Fisk, M. R., Giovannoni, S. J., and Thorseth, I. H. (1998) Alteration of oceanic volcanic glass: Textural evidence of microbial activity. Science, 281, 978-980.

Fomina, M. and Gadd, G. M. (2002) Influence of clay minerals on the morphology of fungal pellets. Mycol. Res., 106, 107-117.

Fogarty, R. V. and Tobin, J. M. (1996) Fungal melanins and their interactions with metals. Enzyme and Microbial Technology, 19, 311-317.

Frost, R. L., Kloprogge, J. T., and Ding, Z. (2002) The Garfield and Uley nontronites—An infrared spectroscopic comparison. Spectrochim. Acta, 58, 1881-1894.

Furnes, H., Banerjee, N. R., Muehlenbachs, K., Staudigel, H., and de Wit, M. (2004) Early life recorded in Archean pillow lavas. Science, 304, 578-581.

Furukawa, Y. and O'Reilly, S. E. (2007) Rapid precipitation of amorphous silica in experimental systems with nontronite (NAu-1) and *Shewanella oneidensis* MR-1. Geochim. Cosmochim. Acta, 71, 363-377.

Gadd, G. M. (2000) Bioremedial potential of microbial mechanisms of metal mobilization and immobilization. Current Opinion in Biotechnology, 11, 271-279.

Gadd, G. M. (2010) Metals, minerals and microbes: geomicrobiology and bioremediation. Microbiology, 156, 609-643.

Gan, E. V., Haberman, H. F., and Menon, I. A. (1976) Electron transfer properties of melanin. Arch. Biochem. Biophys., 173, 666–672.

Gates, W. P., Wilkinson, H. T., and Stucki, J. W. (1993) Swelling properties of microbially reduced ferruginous smectite. Clays and Clay Minerals, 41, 360–364.

Gates, W. P., Stucki, J. W., and Kirkpatrick, R. J. (1996) Structural properties of reduced Upton montmorillonite. Physics and Chemistry of Minerals, 23, 535–541.

Gates, W. P., Jaunet, A. M., Tessier, D., Cole, M. A., Wilkinson, H. T., and Stucki, J. W. (1998) Swelling and texture of iron bearing smectites reduced by bacteria. Clays and Clay Minerals, 46, 487-497.

Gates, W. P., Slade, P. G., Manceau, A., and Lanson, B. (2002) Site occupancies by iron in nontronites. Clays and Clay Minerals, 50, 223-239.

Gaupp, R., Matfer, A., Platt, J., Ramseyer, K. and Walzebuck, J. (1993) Diagenesis and fluid evolution of deeply buried Permian (Rotliegende) Gas Reservoirs, Northwest Germany. Am. Assoc. Petrol. Geol. Bull., 77, 1111-1128.

Gazzè, S. A., Saccone, L., Vala Ragnarsdottir, K., Smits, M. M., Duran, A. L., Leake, J. R., Banwart, S. A., *and* McMaster, T. J. (2012) Nanoscale channels on ectomycorrhizal-colonized chlorite: Evidence for plant-driven fungal dissolution, J. Geophys. Res., 117, 2005-2012.

Geletneky, J., Paul, M., Merten, D., and Büchel, G. (2002) Impact of acid rock drainage in a discrete catchment area at the former uranium mining site Ronneburg (Germany). In: Nelson, J. D., Cincilla, W. A., Foulk, C. L., Hinshaw, L. L., Ketellaper, V. (Eds.), Tailings and Mine Waste, Proceedings of the 9th International Conference on Tailings and Mine Waste, Fort Collins, CO, p. 67-74.

Gerber, N. N. and Lechevalier, H.A. (1965) Geosmin, an Earthy-Smelling Substance Isolated from Actinomycetes. Appl. Microbiol., 13, 935-938.

Giordano, M., Kansiz, M., Heraud, P., Beardall, J., Wood, B., and McNaughton, D. (2001) Fourier transform infrared spectroscopy as a novel tool to investigate changes in intracellular macromolecular pools in the marine microalga *Chaetoceros muellerii* (Bacillariophyceae). J. Phycol., 37, 271-279.

Goff, K. L., Quaroni, L., and Wilson, K. E. (2009) Measurement of metabolite formation in single living cells of *Chlamydomonas reinhardtii* using synchrotron Fourier-Transform Infrared spectromicroscopy. Analyst, 134, 2216-2219.

Golubev, S. V., Bauer, A., and Pokrovsky, O. S. (2006) Effect of pH and organic ligands on the kinetics of smectite dissolution at 25°C. Geochim. Cosmochim. Acta, 70, 4436-4451.

Goodman, B. A., Russell, J. D., Fraser, A. R., and Woodhams, F. W. D. (1976) A Mössbauer and IR spectroscopic study of the structure of nontronite. Clays and Clay Minerals, 24, 53-59.

Grantham, M. C. and Dove, P. M. (1996) Investigation of bacterial–mineral interactions using fluid tapping mode atomic force microscopy. Geochim. Cosmochim. Acta, 60, 2473-2480.

Griffiths, M. J. and Harrison, S. T. L. (2009) Lipid productivity as a key characteristic for choosing algal species for biodiesel production. J. Appl. Phycol., 21, 493-507.

Hamer, M., Graham, R. C., Amrhein, C., and Bozhilov, K. N. (2003) Dissolution of ripidolite (Mg, Fe-Chlorite) in organic and inorganic acid solutions. Soil Sci. Soc. Am. J., 67, 654-661.

Harrison, J., Turner, R. J., Marques, L., and Ceri, H. (2005). A new understanding of these mcirobial communities is driving a revolution that may transform the science of microbiology. Am. Sci., 93, 508-515.

Heraud, P., Wood, B. R., Tobin, M. J., Beardall, J., and McNaughton, D. (2005) Mapping of nutrient-induced biochemical changes in living algal cells using synchrotron infrared microspectroscopy. FEMS Microbiology Letters, 249, 219-225.

Hiebert, F. K. and Bennett, P. C. (1992) Microbial control of silicate weathering in organic-rich ground water. Science, 258, 278-281.

Hill, P. S. (1996) Sectional and discrete representations of floc breakage in agitated suspensions. Deep Sea Research I, 43, 679-702.

Hillier, S. (1994) Pore-lining chlorites in siliciclastic reservoir sandstones: Electron microprobe, SEM and XRD data, and implications for their origin. Clay Minerals, 29, 665-680.

Hochella, Jr., M. F., Eggleston, C. M., Elings, V. B., and Thompson, M. S. (1990) Atomic structure and morphology of the albite (010) surface: An atomic-force microscope and electron diffraction study. Am. Mineral., 75, 723-730.

Holman, H.-Y. N., Perry, D. L., Martin, M. C., Lamble, G. M., McKinney, W. R., Hunter-Cevera, J. C. (1999) Real-time characterization of biogeochemical reduction of Cr (VI) on basalt surfaces by SR-FTIR imaging. Geomicrobiol. J., 16, 307-324.

Holman, H.-Y. N., Wozei, E., Lin, Z., Comolli, L. R., Ball, D. A., Borglin, S., Fields, M. W., Hazen, T. C., and Downinga, K. H. (2009) Real-time molecular monitoring of chemical environment in obligate anaerobes during oxygen adaptive response. Proc. Natl. Acad. Sci., 106, 12599-12604.

Holman, H.-Y. N., Bechtel, H. A., Hao, Z., and Martin M. C. (2010) Synchrotron IR spectromicroscopy: Chemistry of living cells, Anal. Chem., 82, 8757-8765.

Hu, Q., Sommerfeld, M., Jarvis, E., Ghirardi, M., Posewitz, M., Seibert, M., and Darzins, A. (2008) Microalgal triacylglycerols as feedstocks for biofuel production: Perspectives and advances. Plant J., 54, 621-639.

Hyacinthe, C., Bonneville, S., and Van Cappellen, P. (2008) Effect of sorbed Fe (II) on initial reduction kinetics of 6-line ferrihydrite and amorphous ferric phosphates by *Shewanella putrefaciens*. Geomicrobiol. J., 25, 181-192.

Isenor, M., Kaminskyj, S. G. W., Rodriguez, R. J., Redman, R.S., and Gough, K. M. (2010) Characterization of mannitol in *Curvularia protuberata* hyphae by FTIR and Raman spectromicroscopy. Analyst, 135, 3249-3254.

Iwamoto R. and Ohta K. (1984) Quantitative surface analysis by fourier transform attenuated total reflection infrared spectroscopy. Appl. Spectrosc., 38, 359-365.

Jaffe, L. A., Peucker-Ehrenbrink, B., and Petsch, S. T. (2002) Mobility of rhenium, platinum group elements and organic carbon during black shale weathering. Earth and Planetary Science Letters, 198, 339-353.

Jaisi, D. P., Kukkadapu, R. K., Eberl, D. D., and Dong, H. L. (2005) Control of Fe (III) site occupancy on the rate and extent of microbial reduction of Fe (III) in nontronite. Geochim. Cosmochim. Acta, 69, 5429-5440.

Jaisi, D. P., Dong, H., and Liu, C. (2007 a) Influence of biogenic Fe (II) on the extent of microbial reduction of Fe(III) in clay minerals nontronite, illite, and chlorite. Geochim. Cosmochim. Acta, 71, 1145-1158.

Jaisi, D. P., Dong, H., and Liu, C. (2007 b) Kinetic analysis of microbial reduction of Fe (III) in nontronite. Environmental Science and Technology, 41, 2437-2444.

Jaisi, D. P., Dong, H., and Morton, J. P. (2008) Partitioning of Fe (II) in reduced nontronite (NAu-2) to reactive sites: Reactivity in terms of Tc (VII) Reduction. Clays and Clay Minerals, 56, 175-189.

Kalinowski, B. E., Liermann, L. J., Brantley, S. L., Barnes, A., and Pantano, C. G. (2000) X-ray photoelectron evidence for bacteria enhanced dissolution of hornblende. Geochim. Cosmochim. Acta, 64, 1331-1343.

Kaun, N., Kulka, S., Frank, J., Schade, U., Vellekoop, M. J., Harasek, M., and Lendl, B. (2006) Towards biochemical reaction monitoring using FT-IR synchrotron radiation. Analyst, 131, 489-494.

Kashefi, K., Shelobolina, E. S., Elliott, W. C., and Lovley, D. R. (2008) Growth of thermophilic and hyperthermophilic Fe (III)-reducing microorganisms on a ferruginous smectite as the sole electron acceptor. Applied and Environmental Microbiology, 74, 251-258.

Keeling, J. L., Raven, M. D., and Gates, W. P. (2000) Geology and characterization of two hydrothermal nontronites from weathered metamorphic rocks at the Uley graphite mine, South Australia. Clays and Clay Minerals, 48, 537-548.

Kim, J. W., Newell, S., Furukawa, Y., Lavoie, D., and Daulton, T. (2003) Characterization of microbially Fe(III)-reduced nontronite: Environmental cell transmission electron microscopy.

Clays and Clay Minerals, 51, 382-389.

Kim, J .W., Dong, H., Seabaugh, J., Newell, S. W., and Eberl, D. D. (2004) Role of microbes in the smectite-to-illite reaction. Science, 303, 830-832.

Kim, J. W., Furukawa, Y., Dong, H., and Newell, S. W. (2005) The role of microbial Fe (III) reduction in the clay flocculation. Clays and Clay Minerals, 53, 572-579.

Kjelleberg, S. and Hermansson, M. (1984) Starvation-induced effects on bacterial surface characteristics. Applied Environtmental Microbiology, 48, 497-503.

Kodama, H., Schnitzer, M., and Jaakkimainen, M. (1983) Chlorite and biotite weathering by fulvic acid solutions in closed and open systems. Can. J. Soil Sci., 63, 619-629.

Komadel, P., Madejova, J., and Stucki, J. W. (1995) Reduction and reoxidation of nontronite: Questions of reversibility. Applied Clay Science, 34, 88-94.

Konhauser, K. O. and Ferris, F. G. (1996) Diversity of iron and silica precipitation by microbial mats in hydrothermal waters, Iceland: Implications for Precambrian iron formations. Geology, 24, 323-326.

Kostka, J. E., Stucki, J. W., Nealson, K. H., and Wu, J. (1996) Reduction of structural Fe (III) in smectite by a pure culture of *Shewanella putrefaciens* strain MR-1. Clays and Clay Minerals, 44, 522-529.

Kostka, J. E., Haefele, E., Viehweger, R., and Stucki, J. W. (1999 a) Respiration and dissolution of iron (III)-containing clay minerals by bacteria. Environmental Science and Technology, 33, 3127-3133.

Kostka, J. E., Wu, J., Nealson, K. H., and Stucki, J. W. (1999 b) The impact of structural Fe (III) reduction by bacteria on the surface chemistry of smectite clay minerals. Geochim. Cosmochim. Acta, 63, 3705-3713.

Kranck, K. and Milligan, T .G. (1992) Characteristics of suspended particles at an 11-hour anchor station in San Francisco Bay, California. Journal of Geophysical Research, 97, 11373-11382.

Krawczyk-Bärscha, E., Arnold, T., Reuther, H., Brandt, F., Bosbach, D., and Bernhard, G. (2004) Formation of secondary Fe-oxyhydroxide phases during the dissolution of chlorite – effects on uranium sorption. Appl. Geochem., 19, 1403-1412.

Kushner, D. J., Baker, A., and Dunstall, T. G. (1999) Pharmacological uses and perspectives of heavy water and deuterated compounds. Can. J. Physiol. Pharmacol., 77, 79-88.

Lambert, P. A., Hancock, I. C., and Baddiley, J. (1975) The interaction of magnesium ions with teichoic acid. Biochem. J., 149, 519-524.

Lee, K., Kostka, J. E., and Stucki, J. W. (2006) Comparisons of structural iron reduction in smectites by bacteria and dithionite: An infrared spectroscopic study. Clays and Clay Minerals, 54, 197-210.

Levenson, E., Lerch, P., and Martin, M. C. (2006). Infrared imaging: synchrotrons vs. arrays, resolution vs. speed. Infrared Phys. Technol., 49, 45-52.

Levenson, E., Lerch, P., and Martin, M. C. (2008). Spatial resolution limits for synchrotron-based spectromicroscopy in the mid- and near-infrared. J. Synchrotron Radiat., 15, 323-328.

Lewis, E. N., Treado, P. J., Reeder, R. C., Story, G. M., Dowrey, A. E., Marcott, C., and Levin, I. W. (1995) Fourier-transform spectroscopic imaging using an infrared focal-plane array detector. Anal. Chem., 67, 3377-3381.

Li, Y. L., Zhang, C. L., Yang, J., Deng, B., and vali, H. (2004) Dissolution of nontronite NAu-2 by a sulfate-reducing bacterium. Geochim. Cosmochim. Acta, 68, 3251-3260.

Liermann L., Barnes A. S., Kalinowski B. E., Zhou X., and Brantley S. L. (2000) Microenvironments of pH in biofilms grown on dissolving silicate surfaces. Chem. Geol., 171, 1-16.

Liu, H. L., Chen, B. Y., Lan, Y. W., and Cheng, Y. C. (2003) SEM and AFM images of pyrite surfaces after bioleaching by the indigenous *Thiobacillus thiooxidans*. Appl. Microbiol. Biotechnol., 62, 414-420.

Lovley, D. R. and Phillips, E. J. P. (1988) Novel mode of microbial energy-metabolism: organic-carbon oxidation coupled to dissimilatory reduction of iron or manganese. Appl. Environ. Microbiol., 54, 1472-1480.

Lovley, D. R., Holmes, D. E., and Nevin, K. P. (2004) Dissimilatory Fe (III) and Mn (IV) reduction. Adv. Microbial Physiol., 49, 219-286.

Lower, S. K., Hochella, Jr., M. F., and Beveridge, T. J. (2001) Bacterial recognition of mineral surfaces: Nanoscale interactions between *Shewanella* and α-FeOOH. Science, 292, 1360-1363.

Lowson, R. T., Comarmond, M.-C. J., Rajaratnam, G., and Brown P. L. (2005) The kinetics of dissolution of chlorite as a function of pH and at 25ºC. Geochim. Cosmochim. Acta, 69, 1687-1699.

Madigan, M. T., Martinko, J. M., and Parker, J. (2000) Brock Biology of Microorganisms. Prentice Hall, New Jersey.

Malinovskaya, I. M., Kosenko, L. V., Votselko, S. K., and Podgorskii, V. S. (1990) Role of *Bacillus mucilaginosus* polysaccharide in degradation of silicate minerals. Mikrobiologiya, 59, 70-78.

Malmström, M., Banwart, S., Lewenhagen, J., Duro, L., and Bruno, J. (1996) The dissolution of biotite and chlorite at 25°C in the near neutral region. J. Contam. Hydrol., 21, 201-213.

Manceau, A., Lanson, B., Drits, V. A., Chateigner, D., Gates, W. P., Wu, J., Huo, D., and Stucki, J. W. (2000) Oxidation reduction mechanism of iron in dioctahedral smectites. 1. Structural chemistry of oxidized reference nontronites. American Mineralogist, 85, 133-152.

Maurice, P., Forsythe, J., Hersman, L., and Sposito, G. (1996) Application of atomic-force microscopy to studies of microbial interactions with hydrous Fe (III)-oxides. Chem. Geol., 132, 33-43.

Maurice, P. A., McKnight, D. M., Leff, L., Fulghum, J. E., and Gooseff, M. N. (2002) Direct observations of aluminosilicate weathering in the hyporheic zone of an Antarctic Dry Valley stream. Geochim. Cosmochim. Acta, 66, 1335-1347.

Miller, L. M. and Dumas, P. (2006) Chemical imaging of biological tissue with synchrotron infrared light. Biochimica et Biophysica Acta, 1758, 846–857.

Miller, L. M. and Dumas, P. (2010) From structure to cellular mechanism with infrared microspectroscopy. Current Opinion in Structural Biology, 20, 649-656.

Moore, D. M. and Reynolds, C. R., Jr. (1989) X-ray diffraction and the identification and analysis of clay minerals. Oxford University Press, New York.

Moreau, J. W., Weber, P. K., Martin, M. C., Gilbert, B., Hutcheon, I. D., and Banfield, J. F. (2007) Extracellular Proteins Limit the Dispersal of Biogenic Nanoparticles. Science, 316, 1600-1603.

Morel, F. M. M. and Palenik, B. (1989). The aquatic chemistry of trace metals in biofilms. In: Characklis,W. G.,Wilderer, P. A. (Eds.), Structure and function of biofilms. pp. 289–300. J. Wiley and Sons, New York.

Mozafar, A., Ruh, R., Klingel, P., Gamper, H., Egli, S., and Frossard, E. (2002) Effect of heavy metal contaminated shooting range soils on mycorrhizal colonization of roots and metal uptake by leek. Environ. Monitoring Assess., 79, 177-191.

Naidja, A., Liu, C., and Huang, P. M. (2002) Formation of protein–birnessite complex: XRD, FTIR, and AFM analysis. J. Colloid. Interface Sci., 251, 46-56.

Nealson, K. H. and Myers, C. R. (1992) Microbial reduction of manganese and iron: New approaches to carbon cycling: Applied and Environmental Microbiology, 58, 439-443.

Nesse, W. D. (2000) Introduction to mineralogy. Oxford University Press, New York.

Newman, D. K. and Banfield, J. F., 2002. Geomicrobiology: how molecular-scale interactions underpin biogeochemical systems. Science, 296, 1071-1077.

Nosanchuk, J. and Casadevall, A. (1997) Cellular charge of *Cryptococcus neoformans*: Contributions from the capsular polysaccharide, melanin, and monoclonal antibody binding. Infect. Immun., 65, 1836-1841.

Nyhus, K. J., Wilborn, A. T., and Jacobson, E. S. (1997) Ferric iron reduction by *Cryptococcus neoformans*. Infect. Immun., 65, 434-438.

Olukoshi, E. R. and Packter, N. M. (1994) Importance of stored triacylglycerols in *Streptomyces*: possible carbon source for antibiotics. Microbiology, 140, 931-943.

O'Reilly, S. E., Watkins, J., and Furukawa, Y. (2005) Secondary mineral formation associated with respiration of nontronite, NAu-1 by iron reducing bacteria. Geochemical Transations, 6, 67–76.

Packter, N. M. and Olukoshi, E. R. (1995) Ultrastructural studies of neutral lipid localisation in Streptomyces. Arch. Microbiol., 164, 420-427.

Palmer, R. J. J., Siebert, J., and Hirsch, P. (1991) Biomass and Organic Acids in Sandstone of a Weathering Building: Production by Bacterial and Fungal Isolates. Micro. Ecol., 21, 253-266.

Parikh, S. J. and Chorover, J. (2006) ATR-FTIR Spectroscopy Reveals Bond Formation During Bacterial Adhesion to Iron Oxide. *Langmuir, 22,* 8492-8500.

Parker, F. S. (1983) Applications of Infrared, Raman, and Resonance Raman Spectroscopy in Biochemistry, Plenum Press, New York & London.

Perdrial, J. N., Warr, L. N., Perdrial, N., Lett, M.-C., and Elsass, F. (2009) Interaction between smectite and bacteria: Implications for bentonite as backfill material in the disposal of nuclear waste. Chem. Geol., 264, 281-294.

Petit, S., Prot, T., Decarreau, A., Mosser, C., and Toledo-Groke, M. C. (1992) Crystallo-chemical study of a population of particles in smectites from a lateritic weathering profile. Clays and Clay Minerals, 40, 436-445.

Petsch, S. T., Edwards, K. J., and Eglinton, T. I. (2005) Microbial transformations of organic matter in black shales and implications for global biogeochemical cycles, Palaeogeography Palaeoclimatology Palaeoecology, 219, 157-170.

Platt, J. D. (1993) Controls on clay mineral distribution and chemistry in the early Permian Rotliegend of Germany. Clay Minerals, 28, 393-416.

Post, J. L. and Plummer, C. C. (1972) The chlorite series of Flagstaff Hill area, California: A preliminary investigation. Clays and Clay Minerals, 20, 271-283.

Quaroni, L. and Zlateva, T. (2011) Infrared spectromicroscopy of biochemistry in functional single cells. Analyst, 136, 3219-3232.

Rogers, J. R. and Bennett, P. C. (2004) Stimulation of subsurface microorganisms by release of limiting nutrients from silicates. Chem. Geol., 203, 91-108.

Rogers, J. R., Bennett, P. C., and Choi, W. J. (1998) Feldspars as a source of nutrients for microorganisms. American Mineralogist, 83, 1532-1540.

Rosso, K. M., Zachara, J. M., Fredrickson, J. K., Gorby, Y. A., and Smith, S. C. (2003) Nonlocal bacterial electron transfer to hematite surfaces. Geochim. Cosmochim. Acta, 67, 1081-1087.

Rothhardt, S. (2012) Influence of white-rot fungus *Schizophyllum commune* on organically coated sand grains and their heavy metal retention (dissertation).

Russell, J. D., Farmer, V. C., and Velde, B. (1970) Replacement of OH by OD in layer silicates and identification of the vibrations of these groups in infrared spectra. Mineralogical Magazine, 37, 869-879.

Russell, J. D., Goodman, B. A., and Fraser, A. R. (1979) Infrared and Mössbauer studies of reduced nontronites. Clays and Clay Minerals, 27, 63-71.

Santelli C. M., Welch S. A., Westrich H. R., and Banfield J. F. (2001) The effect of Fe-oxidizing bacteria on Fe-silicate mineral dissolution. Chem. Geol., 180, 99-115.

Sanz-Montero, M. E., Rodríguez-Aranda, J. P., and Pérez-Soba, C. (2009). Microbial weathering of Fe-rich phyllosilicates and formation of pyrite in the dolomite precipitating environment of a Miocene lacustrine system. European Journal of Mineralogy, 21, 163-175.

Schmidt, A., Schmidt, A., Haferburg, G., and Kothe, E. (2007) Superoxide dismutases of heavy metal resistant *streptomycetes*. J. Basic Microbiol., 47, 56-62.

Schwertmann, U. and Fitzpatrick, R. W. (1992) Iron minerals in surface environments. In: Biomineralization Processes of Iron and Manganese (Skinner, H. C. W. and Fitzpatrick, R. W., Eds.), pp. 7-31. Catena, Cremlingen.

Seabaugh, J. L., Dong, H., Kukkadapu, R. K., Eberl, D., Morton, J. P., and Kim, J. W. (2006) Microbial reduction of Fe (III) in the Fithian and Muloorina illites: contrasting extents and rates of bioreduction. Clays and Clay Minerals, 54, 67-79.

Siegel, D. (2010) Black Slate - Surface Alteration Due to Fungal Activity (dissertation).

Singh, B., Gräfe, M., Kaur, N., and Liese, A. (2010) Chapter 8 – Applications of Synchrotron-Based X-Ray Diffraction and X-Ray Absorption Spectroscopy to the Understanding of Poorly Crystalline and Metal-Substituted Iron Oxides. Developments in Soil Science, 34, 199-254.

Sham, T. K. and Rivers, M. L. (2002) A brief overview of synchrotron radiation. Appl. Synchrotron Radiat. Low Temp. Geochem. Environ. Sci., 49, 117-147.

Smith B. (1996) Fundamentals of Fourier Transform Infrared Spectroscopy. CRC Press, Washington, D.C.

Smith B. (1999) Infrared Spectral Interpretation: A Systematic Approach. CRC Press, Washington, D.C.

Stohs, S. J. and Bagchi, D. (1995) Oxidative mechanisms in the toxicity of metal ions. Free Radical Biology and Medicine, 18, 321-336.

Stubican, V. and Roy, R. (1961) A new approach to assignment of infra-red absorption bands in layer-structure silicates. Zeitschrift für Kristallographie, 15, 200-214.

Stucki, J. W., Lee, K., Zhang, L., and Larson, R. A. (2002) The effects of iron oxidation state on the surface and structural properties of smectites. Pure Applied Chemistry, 74, 2079-2092.

Stucki, J. W. (2006) Properties and behavior of iron in clay minerals. In F. Bergaya, G. Lagaly, and B. G. K. Theng, Eds., Handbook of Clay Science, p. 423-476. Elsevier, Amsterdam.

Stucki, J. W. and Kostka, J. E. (2006) Microbial reduction of iron in smectite. Geoscience, 338, 468-475.

Stumm, W. and Sulzberger, B. (1992) The cycling of iron in natural environments considerations based on laboratory studies of heterogeneous redox processes. Geochim. Cosmochim. Acta, 56, 3233-3257.

Suci, P. A., Vrany, J. D., and Mittelman, M. W. (1998) Investigation of interactions between antimicrobial agents and bacterial biofilms using attenuated total reflection Fourier transform infrared spectroscopy. Biomaterials, 19, 327-39.

Tempest, D. W. and Neijssel, O. M. (1992) Physiological and energetic aspects of bacterial metabolite overproduction. FEMS Microbiol. Lett., 100, 169-176.

Tobin, M. J., Puskar, L., Barber, R. L., Harvey, E. C., Heraud, P., Wood, B. R., Bambery, K. R., Dillon, C. T., and Munro, K. L. (2010) FTIR spectroscopy of single live cells in aqueous media by synchrotron IR microscopy using microfabricated sample holders. Vibrational Spectroscopy, 53, 34-38.

Thorseth, I. H., Furnes, H., and Tumyr, O. (1995) Textural and chemical effects of bacterial activity on basaltic glass: An experimental approach. Chemical Geology, 119, 139-160.

Ueshima, M., Ginn, B. R., Haack, E. A., Szymanowski, J. E. S. and Fein, J. B. (2008) Cd adsorption onto *Pseudomonas putida* in the presence and absence of extracellular polymeric substances. *Geochim. Cosmochim. Acta, 72,* 5885-5895.

Vandevivere, P., Welch, S. A., Ullman, W. J., and Kirchman, D. L. (1994) Enhanced dissolution of silicate minerals by bacteria at near-neutral pH. Microb. Ecol., 27, 241-251.

Van Loosdrecht, M. C., Lyklema, J., Norde, W., and Zehnder A. J. (1990) Influence of interfaces on microbial activity. Microbiol. Rev., 54, 75-87.

Van Schie, P. M. and Fletcher, M. (1999) Adhesion of biodegradative anaerobic bacteria to solid surfaces. Appl. Environ. Microbiol., 65, 5082-5088.

Venyaminov, S. Y. and Prendergast, F. G. (1997) Water (H_2O and D_2O) Molar absorptivity in the 1000-4000 cm^{-1} range and quantitative infrared spectroscopy of aqueous solutions. Anal. Biochem., 248, 234-245.

Vodyanitskii, Y. N. (2007) Reductive biogenic transformation of Fe (III)-containing phyllosilicates (review of publications). Eurasian Soil Science, 40, 1355-1363.

Welch, S. A. and Ullman, W. J. (1993) The effect of organic acids on plagioclase dissolution rates and stoichiometry. Geochim. Cosmochim. Acta, 57, 2725-2736.

Walker, G. F. (1949) The decomposition of biotite in the soil. Mineral Mag., 28, 693-703.

Waters, M. S., Sturm, C. A., El-Naggar, M. Y., Lüttge, A., Udwadia, F. E., Cvitkovitch, D. G., Goodman, S. D., and Nealson, K. H. (2008) In search of the microbe/mineral interface: quantitative analysis of bacteria on metal surfaces using vertical scanning interferometry. Geobiology, 6, 254-262.

Wessels, J. G. H., de Vries, O. M. H., Ásgeirsdóttir, S. A., and Schuren, F. H. J. (1991) Hydrophobin genes involved in forrnation of aerial hyphae and fruit bodies in Schizophyllum. Plant Cell, 3, 793-799.

Xu, J. C., Stucki, J. W., Wu, J., Kostka, J. E., and Sims, G. K. (2001). Fate of atrazine and alachlor in redox-treated ferruginous smectite. Environ. Toxicol. Chem., 20, 2717-2724.

Yanagita, T. and Kogane, F. (1963) Cytochemical and physiological differentiation of mould pellets. Journal of General and Applied Microbiology, 9, 171-187.

Zhang, G., Dong, H., Kim, J. W., and Eberl, D. D. (2007 a) Microbial reduction of structural Fe^{3+} in nontronite by a thermophilic bacterium and its role in promoting the smectite to illite reaction. American Mineralogist, 92, 1411-1419.

Zhang, G., Kim, J. W., Dong, H., and Sommer, A. J. (2007 b) Microbial effects in promoting the smectite to illite reaction: role of organic matter intercalated in the interlayer. Am. Mineral., 92, 1401-1410.

Zhao, R., Quaroni, L. and Casson, A. G. (2010) Fourier transform infrared (FTIR) spectromicroscopic characterization of stem-like cell populations in human esophageal normal and adenocarcinoma cell lines. Analyst, 135, 53-61.

Acknowledgement

Endless thanks for God's Almighty, who have helped, supported and guided me to finish this work by his will.

For the third time and with a broken hand I started my Ph.D. at the Friedrich-Schiller University in Jena after facing a hard time, but never with a broken will to obtain the Ph.D. degree. That is why I am very grateful and I'd like to express my sincere thanks and my deep gratitude to **Prof. Dr. Reinhard Gaupp** and **Prof. Dr. Erika Kothe** for accepting me in their labs., and for giving me the opportunity to do my Ph.D. under their supervision and support.

I'd like to thank also some **external collaborators**; Special thanks for Dr. Luca Quaroni for accepting to host me for three months in his lab. at the Swiss light source in Paul Scherrer Institute (PSI), as well as Dr. Philippe Lerch, Dr. Camelia Borca and Julijana Krbanjevic at the same institute for their kind cooperation. I am very thankful to Dr. Cornelius Fischer (Bremen University) for his effort and kind cooperation with the VSI, Dr. Andreas Bauer (KIT-INE), Dr. Günter Völksch (Otto.schott for glass chemistry), Dr. Gerhard Daut (Institute of Geography- FSU), Dr. Sandor Nietzsche (electron microscopy center at the uni- klinikum in Jena), for the SEM images, Dr. Hans Pöhl (Institute of Systematic Zoology) also for his help with SEM, and Dr. Almuth Hammerbacher (Max Planck Institute for Chemical Ecology) for supplying me with fungal strains.

At the **institute of Microbiology** I'd like to thank Dr. Götz Haferburg and Petra Mitscherlich for supplying me with the microbial strains, for introducing me to the lab., and for their help and guidance during my initial work in the lab. Thanks also for my roommates; Dr. Lars Zeggel**,** Dr. Theodore Asiimwe, Martin Reinicke, Frank Schindler, Francesca Langella. Thanks extend to Andrè Schmidt, Elke-Martina Jung, Eileen Schütze, and Christin Reichmann.

At the **institute of Geosciences;** very special and warm thanks goes to my former wonderful and delicate colleague; Dr. Daniela Siegel for her advices, support and being very nice and helpful to me at the first steps in my Ph.D. work. Special thanks go also to Dr. Karin Eusterhues for her help and patience with me during teaching me the AFM technique, and doing some SEM samples. Xinran Liu was also very helpful and very nice. Thanks for Dr. Dieter Pudlo for supporting me with the minerals, and for my colleagues; Dr. Dirk Merten, Dr.

Michael Abratis, Dr. Michaela Aehnelt, Dr. Jose Baena, Dr. Angela Meier, Dr. Svenja Waldmann, Dr. Anahita Pourjabbar, Azadeh Abdollahi, Susanne Bock, Ulrike Hilse, Martin Klocke, Lailah Akita, Gerardo Herbozo, Rekha Sharma. A lot of thanks go to: Regina Piechnick, Frank Linde, Sigrid Bergmann, Michael Ude, Andreas Hofmann and Volker Schwarz for their valuable help and effort. Special thanks go to my former roommate at the institute of Geosciences: Dr. Ricarda Hanemann, Dr. Walid Salama, Prof. Dr. Abdel-Moneim El Aaraby, Sonia A. Torres Sanchez and to my dear friend Veronika Veselska for all the wonderful time we have spent together.

This Ph.D. project is done for the **research training group (GRK 1257/1) "alteration and element mobility at the microbe-mineral interface"**. I am very thankful to the **DFG** for the financial support, and I'd like to thank all the GRK staff members especially Dr. Katrin Krause for her great effort in arranging everything concerning the GRK, and for the wonderful time we spent every year in storming our brains in Sigmundsburg. Many thanks go to all my colleagues in the GRK especially; Valerian Ciobotã, Matthias Händel, Ralf Bolanz, Soumya Madhaven, Dr. Steffi Rothhardt, Vanessa-Nina Roth, and Felix Yebo Amoako. Thanks also to my two former HIWIs; Rachid and Andreas. Thanks also for Jan findler and Christine for their wonderful supervising during my teaching certificate course.

Many thanks to my friends whom I knew from **outside the work area,** but I have spent with them nice time, and have made life and study abroad somehow happier**:** Lama Rehaibany, Rabab el Mergawy, Nesrine Ryahi, gül kalkan, Fatma Taghreed alsufyani, Tagreed Jazazi, Shayista Amin, Ina Kurtze, Anja Schmotz, Eireen Decker (Farida), Jasmina Djeffal, Khadijah Iderus, Arijana Cajo, Ulrika Killian, Sabine Bohn, Heike Safa, Barno, Joanna Pawlaczek, Vera, Ursula Kai, Sisy Isabell, Elena Dimova. Special thanks also to all my nice neighbors at the "Studentenwohnheim" in the Naumburgerstr. 105.

Special thanks to Dr. Mostafa El- Feqy for helping me to travel to Germany.

I am indepted for my whole life to my school "El –Talaee Al –Islamia" for all the morals and principles which I was taught in this great foundation.

All the thankful words in the world go to the most precious persons in my whole life, and will still never be enough for them; my parents and my three brothers Hassan, Ahmed, and

Mohamed for their warm and true emotional support during the whole time of being abroad doing my Ph.D. work.

I hope I haven't forgot to thank anyone who has helped or contributed in this work to be finished and if this is the case, then I beg their pardon and I hope that my apologize will be accepted.

Finally, at the 25th of January 2010, a peaceful, blessing and wonderful revolution took place at "El-Tahrir square" in Egypt. This is considered one of the most important and historical events I have ever experienced in my whole life, even when I was abroad, but Egypt was never far away from my heart and my mind. This great revolution had ended the old dictator regime by all its disadvantages and gave birth for a new hope to shine for the coming generations to live in a new and a promising future, full of prosperity, dignity and freedom. However, the price wasn't cheap and the liberty wasn't for free, but in return hundreds of the most wonderful and great Egyptian youth have sacrificed by their lives and died for the sake that Egypt and the other millions of Egyptians will live. They preferred to transfer from the heaven of God on the Earth to the heaven of God in the sky to be accounted as martyrs, but alive within their Lord and in our memeories. This thesis is dedicated to their pure souls, to Egypt, as well as to my lovely brothers and my wonderful parents.

Selbständigkeitserklärung

Ich erkläre, dass ich die vorliegende Arbeit selbständig und unter Verwendung der angegebenen Hilfsmittel, persönlichen Mitteilungen und Quellen angefertigt habe.

Curriculum Vitae

Name	Wafaa
Family name	Zidan
Date of birth	15.06.1978
Place of birth	Giza- Egypt
Bachlor	Cairo university- faculty of Agriculture – Soil science dept. (1999)
Diploma	Cairo University – National Institute of Laser Enhanced Sciences (NILES- 2001).
Master	Cairo university- faculty of Agriculture- Agriculture microbiology dept. (2006)
Scientific career	Researcher assistant in the National research centre (2001-2006) –Egypt. Assistant researcher in the National research centre (2006-2007)-Egypt. “Wiss-Mitarbeiterin” Friedrich- Schiller University, Institute of Geosciences (2009-2013).